Colloid Transport, Retention, and Remobilization during Two-phase Flow;

Micro-model Investigation and Modeling

Qiulan Zhang

Colloid Transport, Retention, and Remobilization during Two-phase Flow;

Micro-model Investigation and Modeling

Collo ïden Transport, Retentie, en Remobilisatie tijdens Twee-fase Stroming;

Micro-modellen Onderzoek en Modellering

(met een samenvatting in het Nederlands)

Proefschrift

ter verkrijging van de graad van doctor aan de Universiteit Utrecht
op gezag van de rector magnificus, prof. dr. G.J. van der Zwaan,
ingevolge het besluit van het college voor promoties
in het openbaar te verdedigen
op maandag 25 november 2013 des middags te 4.15 uur

door

Qiulan Zhang

geboren op Weifang te Shan Dong, China

Promoter: Prof.dr.ir. S.M. Hassanizadeh

The Reading and Examing Committee

Prof. M. Celia Princeton University, USA
Prof. J.E. Saiers Yale University, USA
Prof. M. Flury Washington state University, USA
Dr. M. Oostrom Pacific Northwest National Laboratory, USA
Prof. J.F. Schijven Utrecht University,The Netherlands
Prof.M.Th. van Genuchten

ISBN: 978-90-6266-347-7
Title: Colloid Transport, Retention, and Remobilization during Two-phase Flow; Micro-model Investigation and Modeling
NUR-code: 934
NUR-description: Hydrogeology
Number of pages: 168
Cover illustration: Qiulan Zhang
Cover lay-out: Margot Stoete, Faculty of Geosciences, Utrecht University
Printed by: Uitgeverij BOXPress || Proefschriftmaken.nl

This research was supported financially by China Scholarship Coucil and NUPUS international research training group.

Acknowledgements

I would like to extend my thanks to all the people who have helped and supported me in the last four years. Without those people, I couldn't bring this thesis into being.

First of all, I would like to express all my sincere gratitude and respect to my supervisor, Prof. Majid Hassanizadeh. His way of analyzing questions, looking at things, his criticism and together with his enthusiasm has shown us the way how research should be done. His door is always open to me, not only for scientific matters. Majid, it is my great pleasure to have you as my supervisor. I cannot wish for a better one. You introduced me into the complex but fantastic world of flow and transport in porous media. Majid, I will never forget that you helped me to correct my English pronunciations one by one during my first year here. In the first few months, I am not so active to discuss; you always encourage me, pay patience and time to answer my questions (sometimes really stupid ones). Majid, I deeply appreciate the detailed comments and time you devote to my manuscripts. I believe my Chinglish made you 'exciting' and have to work on it till far more midnight. Majid, many thanks for your help during the last four years. I hope to keep learning from you and collaborations with you in my future academic life.

To Pieter J. Kleingeld and Nikos K. Karadimitriou, without your precious suggestion and help, the experimental work could not be successfully done. From Heidelberg University to Debye Institute of Utrecht University, test the possibility of using various microscopes, our way was not straightforward. Dear Pieter, thank you so much for developing the delicate experimental set-up and helping to translate the summary into

Dutch. A special gratitude to Nikos, thank you for being enthusiastic in discussion and helped make fantastic micro-models. You are not only a good friend and colleague, but also a nice “driver” for us during meeting and conferences.

I want to thank Dr. Imhof from Debye Institute of Utrecht University, for giving me the chance to use their confocal microscope, which made the experiments successfully done. To Dr. Bing Liu (刘冰), Bing, thank you for training me how to use the confocal, for making hydrophobic colloids, for answering any of my questions relevant.

To Prof. Amir Raoof and Prof. J.F. Schijven, thank you for your helpful and fruitful discussions, whenever I need discussions, you always came to me as fast as you can. To Prof. van Genuchten, Rien, thank you so much for your discussion, for teaching me things, for editing my papers, and your kindly encouragement.

I also would like to thank Prof. Celia from Princeton University, Prof. Flury from Washington State University, Prof. J.E. Saiers from Yale University, Prof. van Genuchten, Dr. Oostrom from Pacific Ocean lab for their valuable comments on the thesis. Prof. Helming from Stuttgart University, Prof. Flury from Washington State University, and Dr. Bradford from US Salinity Laboratory are greatly appreciate for their helpful discussions through either email or during conferences. I deeply appreciate for the experimental data provided by Dr. Torkzaban from CSIRO and his fruitful discussion.

In my daily work I have the good chance to work with a friendly and cheerful group of colleagues. First of all I should thank Margreet, for her kindly help in administrative tasks, and reminding me about lunch time. Margreet, I enjoy our short but nice chats during coffee break. Thank you Prof. Ruud Scotting for the big bus ticket you gave to me (on my first working day), for the delicious dinner at your place, for showing us your beautiful garden, and for the high rock concerts in Rotterdam. Many thanks to my former and current officemates, Imran and Elaheh, we really had nice time together. I would also like to thank my friends and colleagues, Mojtaba and Reza, every time I need

syringes, sample bottles, and so son, they were always there for help, and also thanks for the delicious BBQ that you prepared for us. Thank you very much, Thomas, for kindly help to translate the summary and title into Dutch. Many thanks to the other friends and colleagues: Vahid, Brijesh, Eric, Hamid, Wouter, Manuel and Philipp (our visitor from Stuttgart University), Seetha (visitor from India), Bruno (visitor from France) and Emilio (visitor from Spain), thanks for providing the productive working atmosphere; I enjoy our wonderful group meeting, helpful discussions, and nice lunch time.

I would like to thank the Chinese friends and colleagues in the group, Chaozhong (朝中), it is really nice to have someone in the group to discuss research in Chinese; Shuai (帅), deeply appreciate the delicious food you prepared for me, also whenever I need labor, you are there; Luwen (鲁文), thank you for your company during the most difficult time of my research; Xiaoguang (晓光), you are fresh in the group, but you are so friendly, good luck for your research.

To Foroz (my dear supervisor's wife), thank you so much for your support on the scientific discussions during weekends/holiday at your house, for the nice dinner that you prepared for us, for kindly gave me your daughter's bike at the beginning of my arrival.

Here, I wish to thank all the Chinese friends outside of Environmental Hydrogeology group but in Utrecht for the nice time we shared together: Yinghuan (迎焕), Jingwei (璟玮) and Jinfeng (金峰), Hong (胡宏), Ao (傲), Junting (俊婷) and Meng (蒙), Chenjuan (蒋陈娟), Bo (博), Xin (鑫), Zhixiang (志祥), Anqi (安琪), Xiaoli (晓丽) and Bert, Haifan (海帆), Hao (浩), Shiyang (石洋) and his beautiful wife, Juan (娟) and Ran (冉), Shaoyu (邵宇), Jianxi (建喜), and VK(维开).

Special thanks the support and encouragement I got from Yinghuan (迎焕) and Jingwei (璟玮) during the process of writing my thesis. It's great to have you both around.

The encouragement and care from outside Utrecht are also deeply appreciate: my

dear fellow-brother Tao (李涛) from Finland, Chun (礼春) and Zhi (荔枝) from US, and many others. Deeply appreciate Prof. J. Shao, Prof.Y.Cui and Prof. L.Wan from China University of Geosciences (Beijing) kindly offering me a job there. Especially Prof. Shao, you always encouraged me and gave me a lot of suggestions and kindly help, I will never forget about that.

最后，我想感谢我亲爱的爸爸和妈妈，感谢您们的养育之恩以及多年来的爱护，信任，支持，和鼓励！爸爸，谢谢您对我学习和工作的鼓励和认可。另外，还要谢谢我的 uncles， 舅舅是我人生和科研道路上永远的榜样。谢谢我亲爱的大姐，谢谢您无私的关爱。

Qiulan Zhang

Utrecht

October 2013.

Contents

Chapter 1

Introduction

1.1 Motivations and background

Colloids are particles with effective diameters less than 10μm. A large variety of organic, inorganic, and micro-biology colloids can be found in the subsurface (McCarthy and Zacchara, 1989).

Viruses, bacteria, and protozoan pathogens from contaminated water, e.g. from septic tanks or leaking sewage pipes, can contaminate groundwater. These pathogens can cause some severe illnesses. Soil can serve as a natural filter to protect the groundwater from being polluted. Considerable research has been carried out for understanding processes that govern the removal of microbial colloids by soil passage (see e.g. the review by Schijven and Hassanizadeh, 2000).

Furthermore, mineral colloids in the soil water and groundwater can adsorb dissolved contaminants and carry them further into the subsurface; a process that is known as "Colloids-facilitated/enhanced contaminant transport" (Sprague et al., 2000; Grolimund et al., 2005; Saiers and Ryan, 2006; Cheng and Saiers, 2010).

The majority of studies have focused on colloids transport in saturated porous media and retention of colloids in unsaturated porous media during steady-state flow. However, in practice, we encounter transient flow conditions, where colloids could behave differently. For example, in the vadose zone, attached colloids can be remobilized during imbibition events, induced by rainfall or irrigation (DeNovio et al., 2004; Zhuang et al., 2007; Shang et al., 2008; Cheng and Saiers., 2009; Zhuang et al., 2009), or during drainage events induced by evaporation (Zhuang et al., 2009; Cheng and Saiers., 2009) or sudden drop of water levels. Once remobilized, colloids can pass through the vadose zone with the infiltrating water and transport contaminants to the saturated strata.

As the first line of defense in protecting groundwater from viruses and contaminants, unsaturated zone plays an important role. So, it is of great significance to study colloids transport, retention, and remobilization under unsaturated flow conditions.

1.2 Research objectives

The goal of this thesis is to identify the mechanisms that control colloids transport through unsaturated porous media, especially colloids remobilization under transient partially-saturated flow. To achieve this goal, by using a confocal laser microscope, we measured colloids concentration breakthrough curves and co-currently we conducted pore-scale visualization experiments in PDMS micro-models.

The specific objectives of this thesis are as follows:

(1) Investigate the role of flow rate and its changes on colloids retention and remobilization by experimental observations and pore-network modeling; and develop a model that can describe colloid detachment from collectors.

(2) Conduct concentration breakthrough measurement and numerical simulation to study how saturation change affects colloids remobilization.

(3) Study the role of moving fluid-fluid interfaces on colloids remobilization by conducting pore-scale visualization experiments in a micro-model.

(4) Study the colloids surface property on their transport.

(5) Study the role of capillary forces on retention and remobilization of colloids.

1.3 Thesis outline

This thesis is organized as follows.

Chapter 1 gives a brief introduction and the main objectives of this thesis.

In **Chapter 2**, an overview of visualization methods and findings on colloids transport through unsaturated conditions are presented. In addition, we discuss the variety of forces that play a role in controlling the behaviors of colloids.

In **Chapter3**, results of column experiments performed by Torkzaban et al. on the transport of viruses under unsaturated conditions and their remobilization are modeled numerically. Virus remobilization had been observed during draining or imbibing the column. Three approaches were employed to simulate the transport and the release of attached viruses. An existing model was modified remobilization of colloids attached to

the solid-water interface (SWI) was assumed to be proportional to temporal change of saturation. Colloids detachment from fluid-fluid interface (FWI) was modeled as desorption from the FWI interfacial area.

In our own experimental work, we performed in the micro-model under confocal microscope during steady-state and transient two phase flow. In **Chapter 4**, the design and construction of a novel PDMS micro-model used in these experiments are described. The experimental set-up, materials and procedures are also presented. Some visualization results and measured breakthrough curves confirmed the utility of the micro-model and confocal microscopy for the study of colloids transport, retention, and remobilization during two-phase flow.

In **Chapter 5**, results of flow rate effect on colloids transport in single-phase flow are presented. These include measured concentration breakthrough curves at various flow rates during steady-state flow. Colloids remobilization due to a sudden flow rate increase was observed in the breakthrough curves and pore-scale images. These experiments were also simulated by pore-network modeling.

In **Chapter 6,** results of colloids remobilization under transient two-phase flow experiments are presented and discussed. The experiments were performed at steady-state flow with different saturations. Pore scale images that provide visual information on the interaction of colloids with the moving fluid-fluid interfaces/contact lines are presented. Also, the concentration breakthrough curves from each experiment are given. They are simulated numerically using the remobilization model presented in Chapter 3.

Studies mentioned above were carried out with hydrophilic colloids. But, in practice, we encounter both hydrophilic and hydrophobic colloids. To investigate the role of particles surface property on colloids transport, performed experiments with two different kinds of colloids: microspheres that could be suspended in water and microspheres that could be dispersed in fluorinert. We conducted visualization and breakthrough experiments under both saturated and unsaturated flow conditions. We also performed the theoretical calculations of the interaction energies of two types of colloids associated with the solid-fluid interface, fluid-fluid interface, fluid-fluid-solid contact lines, as well as interactions among colloids themselves. All these results are presented in **Chapter 7**.

In **Chapter 8**, concluding remarks about experimental work and numerical analysis are given.

References

(1) **Cheng** T., and J.E. Saiers (2009), Mobilization and transport of in situ colloids during drainage and imbibition of partially saturated porous media. Water Resour. Res. 45, W08414, doi: 10.1029/2008WR007494.

(2) **Cheng**, T., and J.E. Saiers (2010), Colloid-Facilitated Transport of Cesium in Vadose Zone Sediments: The Importance of Flow Transients. Environ. Sci. Technol., 44, 7443–7449.

(3) **DeNovio**, N. M., J. E. Saiers, and J. N. Ryan (2004), Colloid movement in unsaturated porous media: Recent advances and future directions, Vadose Zone J., 3, 338– 351, doi:10.2113/3.2.338.

(4) **Grolimund**, D.; Borkovec (2005), M. Colloid-facilitated transport of strongly sorbing contaminants in natural porous media: Mathematical modeling and laboratory column experiments. Environ. Sci. Technol., 39, 6378–6386.

(5) **MacCarthy**, J. F., and J. M. Zachara (1989), Subsurface transport of contaminants, Environ. Sci. Technol., 23, 496– 502.

(6) **Saiers**, J.E., and J.N. Ryan (2006), Introduction to special section on colloid transport in subsurface environments. Water Resour. Res. 42:W12S01. doi: 10.1029/2006WR005620.

(7) **Schijven**, J.F., and S.M. Hassanizadeh (2000), removal of viruses by soil passage: overview of modeling, processes, and parameter. Crit. Rev. Environ. Sci. Technol. 30:49–127.

(8) **Sprague**, L. A.; Herman, J. S.; Hornberger, G. M.; Mills (2000), A. L. Atrazine adsorption and colloid-facilitated transport through the unsaturated zone. J. Environ. Qual., 29, 1632–1641.

(9) **Zhuang**, J., J.F. McCarthy, J.S. Tyner, E. Perfect, and M. Flury (2007), In situ colloid mobilization in Hanford sediments under unsaturated transient flow conditions: Effect of irrigation pattern. Environ. Sci. Technol., 41: 3199- 3204, doi: 10.1021/es062757h.

(10) **Zhuang**, J., J.S. Tyner, E. Perfect (2009), Colloid transport and remobilization in porous media during infiltration and drainage. J. Hydrol. 377:112-119.

(11) **Shang**, J., M. Flury, G. Chen, and J. Zhuang (2008), Impact of flow rate, water content, and capillary forces on in situ colloid mobilization during infiltration in unsaturated sediments, Water Resour. Res., 44, W06411, doi: 10.1029/2007WR006516.

Chapter 2

Visualization of Pore-scale Processes for Colloid Transport and Forces Determine Attachment and Detachment of Colloid: an Overview

Abstract

The understanding of colloid transport processes at the pore scale in the vadose zone is limited. In this literature study, we discuss our current knowledge on colloids transport through a porous medium under both steady-state and transient unsaturated flow conditions. The study of forces acting on colloids is needed in order to explain the interaction among colloids as well as colloids interactions with interfaces. Major relevant forces are Derjaguin–Landau–Verwey–Overbeek (DLVO) forces, hydrodynamic forces, and capillary forces.

Over the past decade, visualization, which can provide direct observation of pore-scale processes governing colloids transport, has been increasingly employed to study colloids transport at the pore scale,. We first discuss various carriers of porous media using in the visualization experiments. Then imaging set-ups are briefly discussed. Finally, the observations of colloids distribution during steady-state and transient flow are presented.

Prepared for submission to Vadose Zone Journal, Zhang Q.L. and S.M. Hassanizadeh.

2.1 Introduction

Colloids are generally defined as suspended matter with an average diameter less than 10μm (Stumm, 1977). The colloids in the natural subsurface include silicate clays, Fe and Al oxides, mineral precipitates, humic materials, and micro-organisms (e.g. bacteria and viruses) (McCarthy and Zachara, 1989). There are a number of practical situations where colloids transport is very important. This includes the removal of pathogenic microorganism during subsurface passage; release of colloids into soil solution and groundwater; enhanced contaminant transport through the vadose zone to groundwater when colloids serve as carriers (Saiers and Hornberger, 1996; Saiers, 2002; de Jonge et al., 2004a, b).

The classic DLVO theory has been used to describe colloids attachment to the solid surfaces (SWI). However, researchers found that it difficult to use classic DLVO only to explain colloids attachment to the air-water interface (AWI) or air-water-solid (AWS) contact lines (Crist et al., 2005). In fact, one must take into account an additional force retaining colloids at AWS, namely capillary forces, which may be several orders of magnitude greater than DLVO forces (Gao et al., 2008; Shang et al., 2008). The capillary force can be decomposed into two components perpendicular and tangential to the grain surface. The normal force component can result in an increase of the resistance to sliding of colloids attachment to an interface (Gao et al., 2008; Shang et al., 2008, 2009). More recently, Sharma et al. (2008), Shang et al. (2009) and Aramrak et al. (2011) reported that capillary forces generated with the moving contact line can help remobilize the deposited colloids from the solid surface.

Another force can cause colloids detachment from interfaces is the drag force exerted by a moving fluid. If the drag force, or its corresponding torque, exceeds the adhesive force, or resisting torque, then colloids are detached (Ryan et al., 1998).

Concentration breakthrough curves of colloids transport through column experiments have been often employed to investigate colloid retention under various water saturations [Wan and Wilson, 1994a; Keller et al., 2004; Torkzaban et al., 2006a, b]; transient flow effects on colloids remobilization (Saiers et al., 2003; Lenhart and Saiers, 2002, 2003; Torkzaban et al., 2006a, b; Zhuang et al., 2007, 2009, 2010; Shang et al., 2008); and effect of chemical conditions on colloids/virus transport (Zevi et al., 2009; Sadeghi et al., 2011, 2013). However, breakthrough curves represent a combined response of various mechanisms affecting colloids transport in the column. Given the limitation of breakthrough curves, pore-scale visualization has been increasingly

employed in order to "see" effects of different mechansims in the last decade. Visualization of colloids transport at the pore scale enables researchers to directly observe colloids interactions with each other, with SWI, AWI, and AWS. Visualization in natural porous media poses few problems to overcome. Therefore, 'ideal' media like single capillary channels (Gómez et al., 1999a, b; Sharma et al., 2008; Aramrak et al., 2011), media-packed flow cells (Huang et al., 1992; Crist et al., 2004, 2005; Gao et al., 2006; Ochiai et al., 2005; Zevi et al., 2005, 2009), and micro-models have been used as representations of porous medium. Especially micro-models have been increasing employed, e.g. glass micro-models (Wan and Wilson, 1994a; Lanning et al., 2002); silicon micro-models (Baumann et al., 2004); and PDMS micro-models (Auset and Keller, 2004; Zhang et al., 2013).

Here we provide a review of various setups used for the visualization of colloids behavior in porous media. Also, the visualization methods and main findings of the visualization results are presented. The detailed experimental results can be found in the original papers as referred. We also discuss forces acting on colloids in the direct vicinity of interfaces and surfaces. Through theoretically calculation of force balances or torque balances, one can predict whenever particles will be released from the surface or remain deposited on the interface. Here, we mainly consider water-air porous media systems. The discussion of forces needs to be adapted for other fluids.

2.2 Forces acting on colloids

2.2.1 DLVO forces

Generally, colloid-interface interaction energies have been calculated using DLVO theory. The total energy ΔG_{tot} is the sum of electrostatic energies, ΔG_{el}, and van der Waals interaction energies ΔG_{vdw} (Derjaguin and Landau, 1941; Verwey and Overbeek, 1948), all as a function of the colloid-interface separation distance, h:

$$\Delta G_{tot}(h) = \Delta G_{el}(h) + \Delta G_{vdw}(h) \tag{2.1}$$

The electrostatic energies can be calculated as (Gregory, 1975):

$$\Delta G_{el} = 64\pi\varepsilon R\left(\frac{kT}{ze}\right)^2 \times \left[\tanh\left(\frac{ze\psi_{0,1}}{4kT}\right)\right]\left[\tanh\left(\frac{ze\psi_{0,2}}{4kT}\right)\right]\exp(-\kappa h) \tag{2.2}$$

and the van der Waals interaction energies are given by (Gregory, 1981):

$$\Delta G_{vdw} = -\frac{AR}{6h}\left[1-\frac{5.32h}{\lambda_0}\ln(1+\frac{\lambda_0}{5.32h})\right] \tag{2.3}$$

where ε is the permeability of water; R is radius of the colloid; kT is the thermal energy; z is the ion valence; e is the electron charge; $\Psi_{0,i}$ is the surface potential for the colloid and the interfaces of interest; κ is the inverse Debye-Hückel length; A is the effective Hameker constant of colloid-water-interface system, λ_0 is a characteristic length of 100nm.

The net classic DLVO force was then obtained as the derivative of the total energy:

$$F_{DLVO} = \frac{d}{dh}(\Delta G_{tot}) = \frac{d}{dh}(\Delta G_{el} + \Delta G_{vdw}) \tag{2.4}$$

The adhesive resisting torque for colloids is expressed as:

$$T_{resist} = F_{DLVO}\, l_x \tag{2.5}$$

Where the lever arm l_x can be represented as (Israelachvili, 1992; Bradford et al., 2008):

$$l_x = (\frac{F_A r_c}{4K})^{1/3}$$

where K [M L^{-1} T^{-2}] is the composite Young's modulus (Johnson et al., 1971).

2.2.2 Hydrodynamic forces

When a fluid moves over a colloid adhering to a surface, the drag force F_D and lift force F_L, and a torque T_{hydro} are generated (shown in Fig.2.1a). The forces help to remove the colloid off the surface. As mentioned above, the detachment mechanisms that happen to the colloid could be sliding, lifting and rolling.

The drag force, acts in the direction of flow and is affected by the flow velocity and flow path tortuosity (Simons et al., 1992). It can be calculated as (Goldman et al., 1967; O'Neill, 1968; Sharma et al., 1992; Burdick et al., 2005; Bradford et al., 2008):

$$F_D = 10.205\pi\mu(\frac{\partial V}{\partial r})R^2 \tag{2.6}$$

Where μ is the water dynamic viscosity, $\partial V / \partial r$ is the shear rate to be calculated at a distance of r from the surface, if the colloid is totally covered with water, then $r = R$. (R is the radius of the colloid). Under laminar flow conditions, shear is considered of greatest importance (Soltani and Ahmadi, 1994; Bergendahl and Grasso, 1998, 1999, 2000).

The hydrodynamic torque caused by drag force is given as (Goldman et al., 1967; O'Neill, 1968):

$$T_{hydro} = 1.4RF_D \tag{2.7}$$

The lift force can be expressed as (Busnaina et al., 1993):

$$F_L = 1.615 \cdot 4\mu R^2 \left(\frac{\rho}{\mu}\frac{du}{dr}\bigg|_{r=R}\right)^{\frac{1}{2}} V \tag{2.8}$$

r is the vertical direction. When the water flow is laminar, the lift force acting on the colloid perpendicular to the interface is negligible.

2.2.3 Capillary forces

The capillary force between a spherical colloid and a flat solid surface in contact with an AWI can be calculated as (Zhang et al., 1996; Veerapaneni et al., 2000; Shang et al., 2008, 2009):

$$F_{cap} = 2\pi R\gamma \sin(\phi)\sin(\theta+\phi) + \Delta p \pi R^2 \sin^2\phi \tag{2.9}$$

where γ is the air-water surface tension; θ is the contact angle between colloid and air-water interface; ϕ is the filling angle between the center of the colloid and the colloid-water contact line; Δp is the capillary pressure across the air-water interface.

(a)

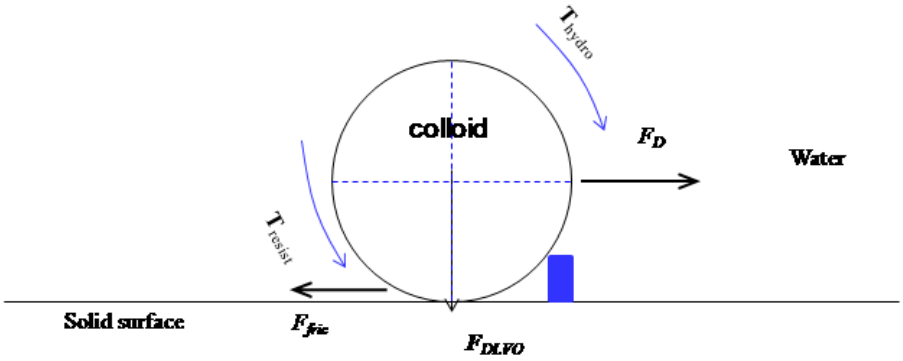

(b)

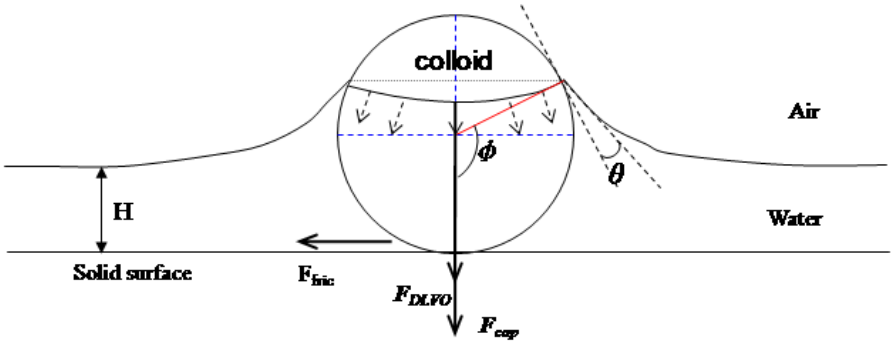

Fig. 2.1 *(a) Schematic of torques acting on colloid; (b) schematic of capillary force at the contact line.*

Fig. 2.2 shows the calculation of capillary force as a function of filling angle. As can be seen, for given contact angle, the direction of the capillary force depends on the value of filling angle.

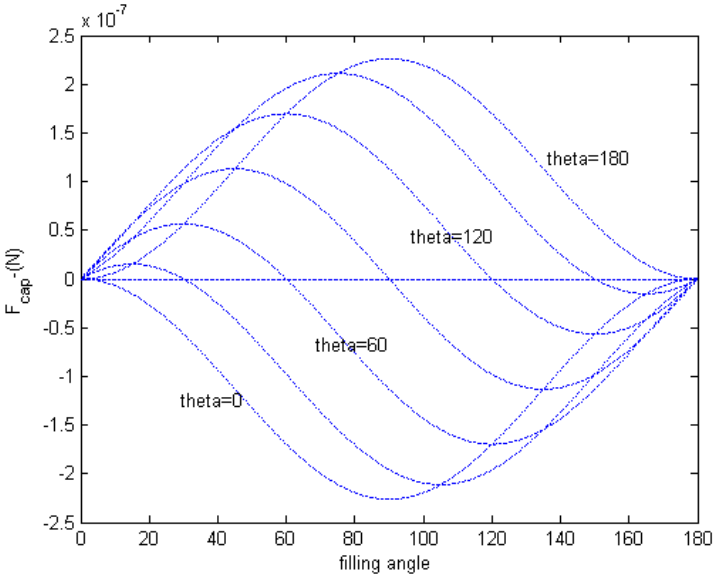

Fig. 2.2 *Calculation of capillary forces as a function of filling angle at various contact angles. In this figure positive values represent repulsive forces opposing attachment; negative values stand for forces that help the colloid attach to the solid surface.*

The maximum values of capillary forces parallel and perpendicular to the solid surface depend on the contact angle α between the solid surface and air-water interface. These can be expressed as (Leenaars and O'Brien, 1989; Boks et al., 2008):

$$F_x^{max} = 2\pi R\gamma \sin^2(\frac{\theta}{2})\sin(\alpha) \qquad \alpha < 90^\circ \tag{2.10}$$

$$F_y^{max} = 2\pi R\gamma \sin^2(\frac{\theta}{2})\cos(\alpha) \qquad \alpha < 90^\circ \tag{2.11}$$

$$F_x^{max} = -2\pi R\gamma \sin^2(\frac{\pi+\theta}{2})\sin(\alpha) \qquad \alpha > 90^\circ \tag{2.12}$$

$$F_y^{max} = -2\pi R\gamma \sin^2(\frac{\pi+\theta}{2})\cos(\alpha) \qquad \alpha > 90^\circ \tag{2.13}$$

Where α is the contact angle between the solid surface and air-water interface.

Fig. 2.3 shows the maximum repulsive forces acting on colloids as a function of surface water contact angle at different colloid contact angles. It can seen that， at contact angle values smaller than 90°, the detachment forces increase with the increase of colloid contact angle. An opposite trend is found when the surface contact angle is larger than 90°.

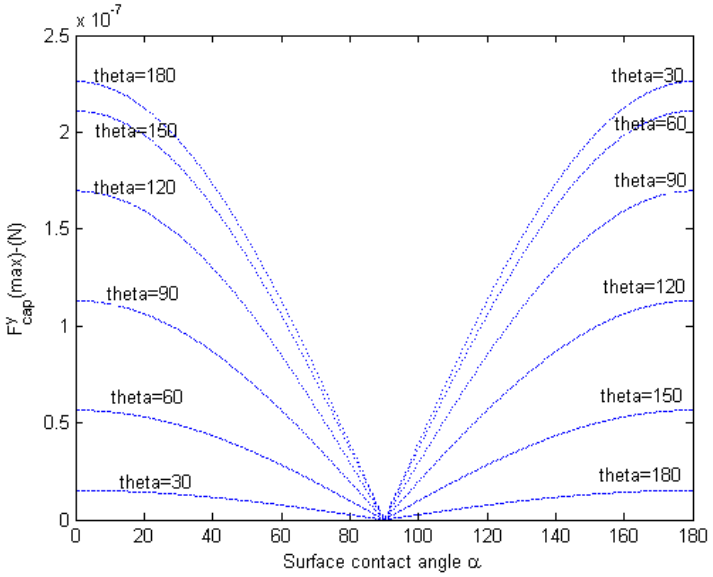

Fig. 2.3 *Theoretical calculations of maximum detachment forces perpendicular to the solid surface obtained from Equations (2.12) and (2.14).*

2.2.4 Forces causing colloid remobilization

It is known that both drainage and imbibition processes may cause the remobilization of attached colloids. In Fig. 2.4, three stages of passage of an air-water interface during imbibition (figures on the left) and drainage (figures on the right) are shown. The three stages are described below.

(A) In the first set of figures (during imbibition or drainage), the moving air-water interface has not reached the colloid yet. The colloid is seen to be thoroughly immersed in one fluid (air or water). Only drag force and net classic DLVO force are present. For detachment to occur (due to rolling), the hydrodynamic torque (T_{hydro} must overcome the adhesive resisting torque (T_{resist}), otherwise the colloid would remain deposited on the solid surface.

(B) In the second stage, the air-water interface is passing over the colloid. Thus, in addition to drag force and DLVO force, capillary forces are generated as well. Depending on the balance of forces, one of the following situations may occur: if $F_{cap}^{y} > F_{DLVO}$, the colloid can be lifted and remobilized; if $F_{cap}^{x} \neq F_S$, the colloid removing will be due to sliding. These figures, as well as electrostatic and DLVO forces are computed (using equation 2.10-2.13) and plotted in Fig. 2.5. We clearly see that the magnitude of capillary forces is almost always much larger than drag forces (normally in the order of 10^{-13} to 10^{-12}N) and DLVO forces (attractive force in the order of 10^{-9}N). Thus, with the moving wetting and drying fronts, capillary forces play the primary role in the remobilization of colloids.

Once again if rolling occurs, the torque balance should include capillary force torque, hydrodynamic torque and resisting torque. The torque balance can be written as:

$$F_{DLVO} l_x = 1.4RF_D + F_{cap} R\cos(\phi) \tag{2.14}$$

If the right hand side is larger than the left hand side, then the colloid will be released from the solid surface.

(C) After the passage of an AWI, if the colloid is not carried away, it will remain attached in the case of drainage. This is because a film of water will remain (see Fig. 2.5 right graphs) and both the DLVO force and capillary force act to pin the colloid to the solid surface. During imbibition, the colloid will become fully immersed in water, and its force depends on the flow velocity. If the drag force large enough to overcome

electrostatic and DLVO forces, the colloid may become remobilized.

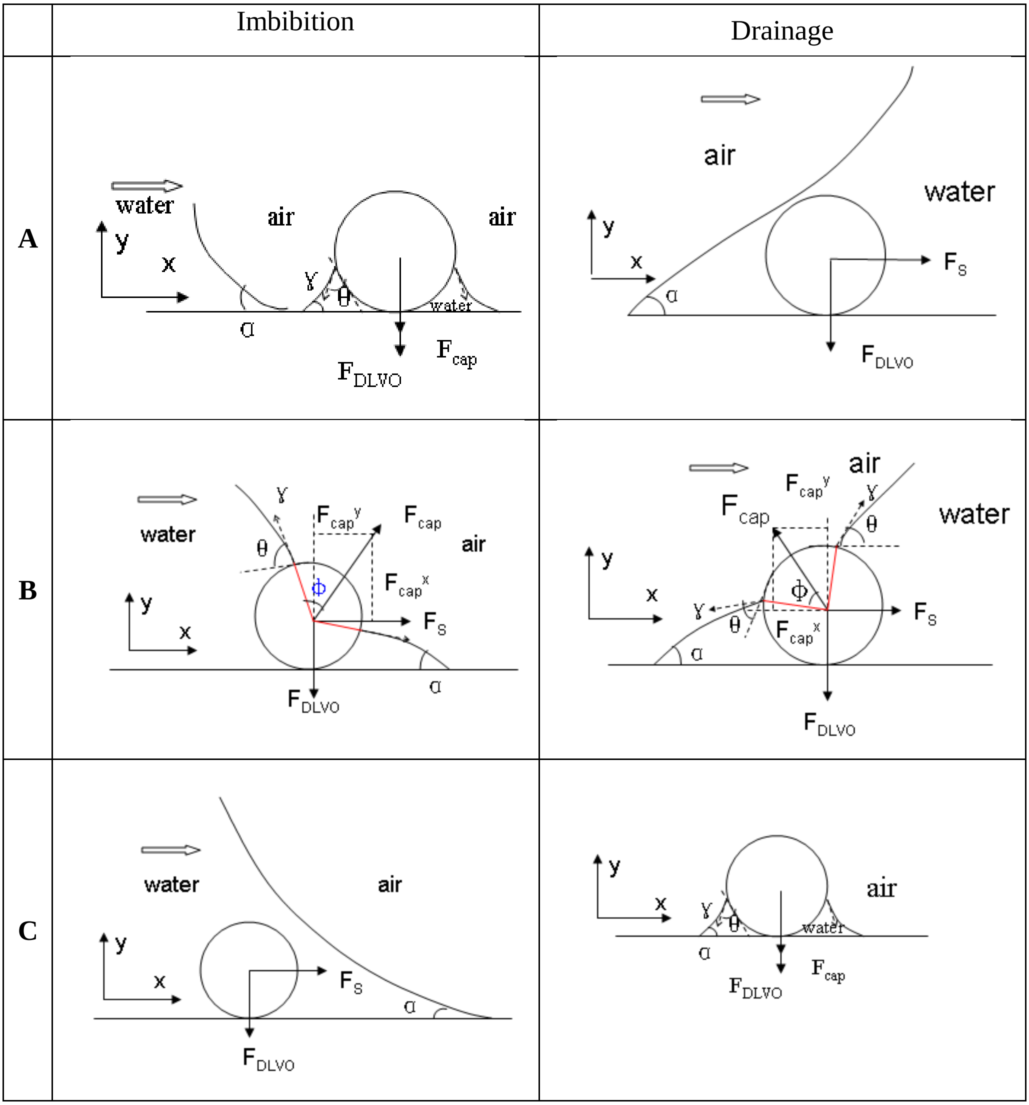

Fig. 2.4 *Conceptual of forces exerted on colloid with the moving wetting front and drying front.*

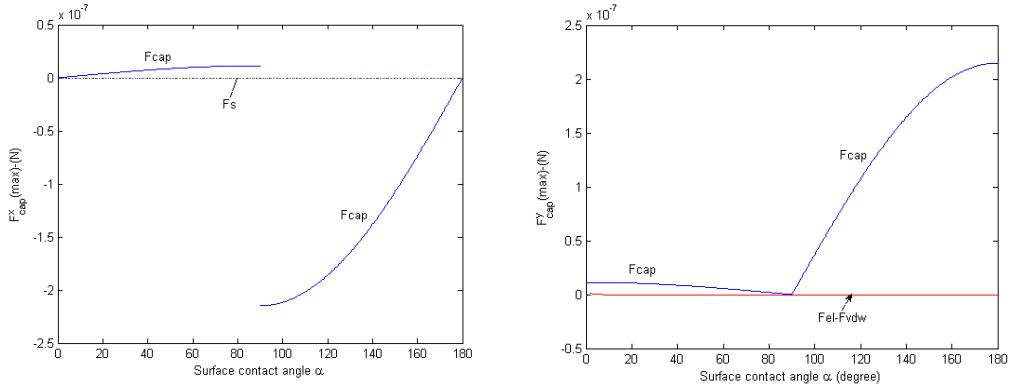

Fig. 2.5 *Maximum detaching capillary forces compared with shear force (left) and DLVO attractive forces (right). The colloid has a radius of 300nm.*

2.3 Visualization of colloid transport in pore networks

Concentration breakthrough curves have the following limitations: 1) they show the combined effects of all relevant mechanisms; 2) they cannot give information about colloids interactions with the SWIs, AWIs, and AWS; 3) direct observations are not allowed. Visualization experiments are valuable tools to complement breakthrough measurements, as they allow direct observation of interactions of colloids with the interfaces under the hydro-chemical conditions (ionic strength, PH) and hydraulic conditions (flow rates, saturations).

Visualization systems mainly include three components: (1) pump to inject fluids or colloids suspension into the medium; (2) porous network; (3) imaging system, usually consisting of a camera or epifluorecent or confocal microscope, coupled with a device that can capture still or video images. Generally, the porous medium cell is put horizontally on the stage of the microscope. The flow of fluid(s) is established by a syringe connected to the inlet or outlet. Summary of the colloids visualization experiments are shown in Table 2.1.

2.3.1 Visualization systems

In this section, we discuss a number of visualization systems that have been used to

study pore-scale behavior of colloids. We shall mainly focus on the porous media type, colloids, and the visualization tools used in those studies.

As a representation of a porous medium, three types of flow-through systems have been mainly employed: single pore channel; media-packed flow cells; and micro-models.

Single pore channel

The simplest system has been either an open or closed single micro-fluidic channel, used as a surrogate of a pore. A number of examples are described below.

Sharma et al. (2008) employed an open channel, made of Plexiglas, having a rectangular cross section with dimensions of 16 cm×2.7 cm×1 cm. They performed experiments on colloids deposition and the role of moving air-water interface on the detachment of colloids. Aramrak et al. (2011) used a glass cylindrical channel with inner diameter of 3.7mm and length of 7.5cm (as shown in Fig. 2.6) was employed by Aramrak et al. (2011). Two rectangular shaped (25 mm-10 mm) microscopy glass slides were glued to both ends of the channel to provide a support platform. Then they used confocal microscope to visualize the colloids deposited inside the channel.

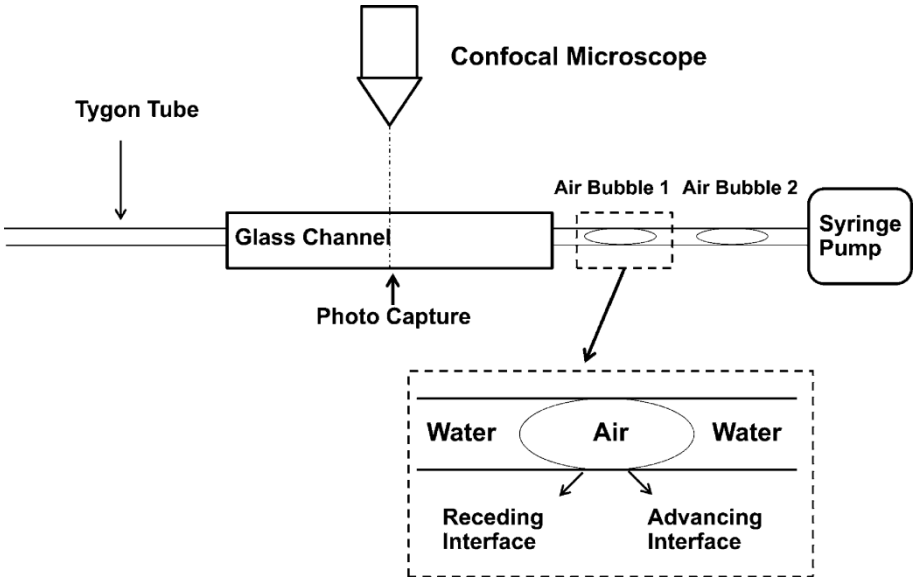

Fig. 2.6 *Schematic of confocal microscope visualization colloids transport in a glass capillary channel (Aramrak et al., 2011).*

Lazouskaya et al. (2008) used an open glass capillary channel with rectangular section and dimensions of 0.4mm×0.4mm×54mm. Then they employed a confocal microscope to observe the positions of colloids relative to the AWI. The disadvantage of this system was that first only static experiments can be done. Also, there was the problem evaporation and they found it difficult to identify the exact position of colloids relative to the AWI. So, later Lazouskaya et al. (2011) employed a closed micro-fluidic channel to replace the open capillary channel. The micro-fluidic channels were made of PMMA and had a trapezoid cross-section (as shown in Fig. 2.7) with bases of 42μm and 70μm; the depth and the length of the channels were 20μm and 85mm, respectively. They also used confocal microscope to observe the effect of moving contact line on colloid remobilization and transport.

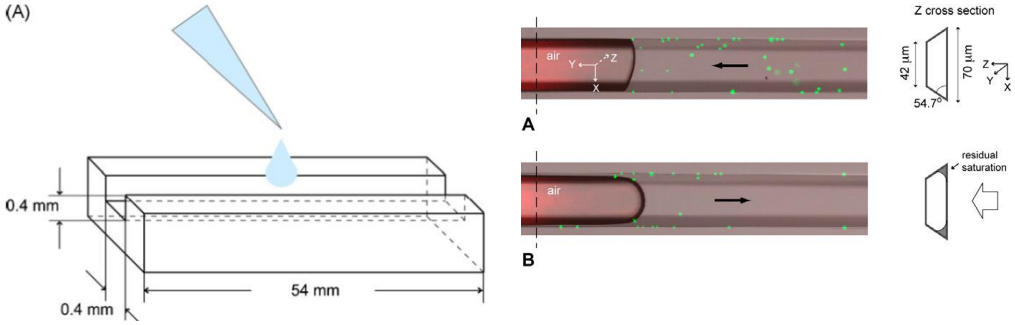

Fig. 2.7 *Schematic of an open glass channel (on the left) and closed micro-fluidic channel (on the right) under observation by a confocal microscope (Lazouskaya et al., 2008, 2011).*

An open triangular channel was employed by Zevi et al. (2011) to investigate how colloids are transported to the air-water-solid (AWS) contact line, and then retained, depending on the meniscus contact angle with the wall and the solution ionic strength. The micro-channel employed was made of borosilicate glass consisted of an isosceles triangular shape carved channel with a 90-degree angle, a length of 54mm and a wall height of 5mm (see Fig. 2.8). Colloids flow path, meniscus shape and meniscus-wall contact angle, and colloid retention at the AWS contact line were visualized and quantified with a confocal microscope.

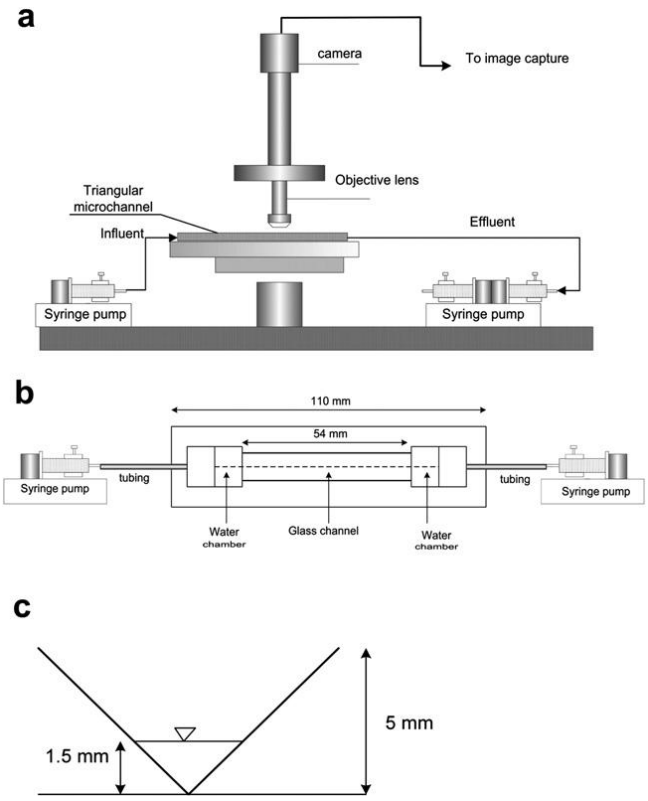

Fig. 2.8 *Schematic of the experimental set-up, detailed view of capillary channel, cross-section of the channel of Zevi et al. (2011).*

Flow cells

Crist et al. (2004, 2005) employed an open infiltration chamber filled with quartz sand (grain diameters ranged from 0.85mm to 1.70mm, and the porosity was around 0.36). The chamber was supported on a mounting assembly at an inclination varying between 15-45 degree from the horizontal and perpendicular to the camera. They could create unsaturated flow conditions. Fig. 2.9 shows a schematic of their experimental set-up. By using this system, they observed that colloids can accumulate close to the AWS contact line.

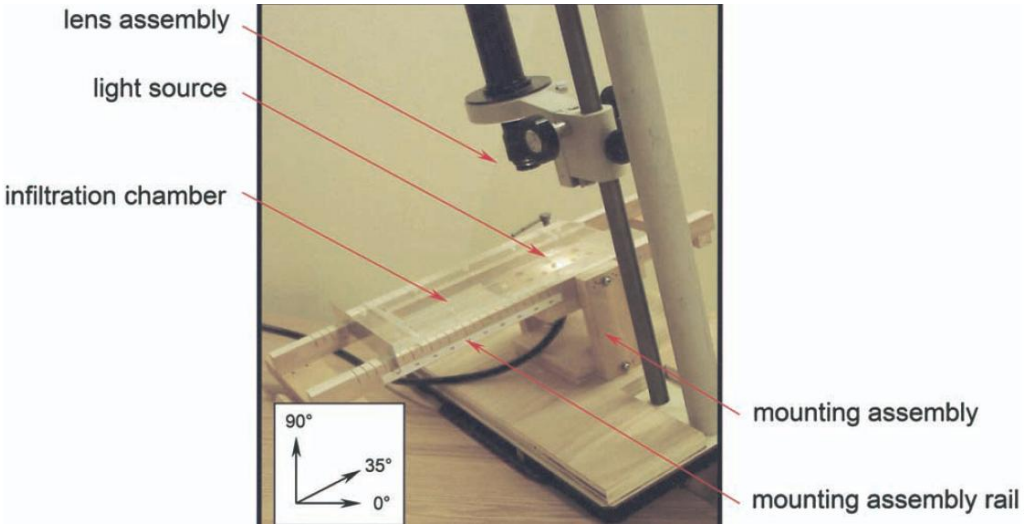

Fig. 2.9 *Experimental set-up of Crist et al. (2004, 2005).*

A similar system was employed by Zevi et al. (2005) to visualize collods through water film by confocal microscope. In order to allow enough light transmission, the sand layer was packed to 0.5cm in thickness. Later Zevi et al. (2009) used a chamber filled with 0.4-0.6mm diameter quartz sand, combined with a confocal microscope. They investigated the effect of ionic strength on the retention of colloids in unsaturated porous media.

Baumann and Werth (2005) investigated the effects of heterogeneous grain packing on colloid transport in a flow-through column using magnetic resonance imaging (MRI). The columns were packed with a core of fine-grained silica gel surrounded by a shell of coarse-grained silica gel. Apart from Baumaan and Werth, visualization systems based on MRI have been used by Potter et al. (1996) and Sherwood et al. (2003).

Gao et al. (2006) constructed a flow cell (as showen in Fig. 2.10) from transparent acrylic sheets. To enable the maintenance of a prescribed capillary pressure at the flow cell boundaries, two pieces of stainless steel membrane were sealed between rubber gaskets at the inlet and outlet ends of the flow cell. Employing this flow cell, they visualized retention and mobilization of 2μm carboxylate-modified polystyrene latex microspheres under various water contents through both steady-state and transient flow regimes.

Ochiai et al. (2005) developed a flow cell system filled with glass beads, quartz sand,

and forest soil. The flow cell they used was 0.1×1.0×50 mm capillaries with a wall thickness of 0.1 mm that approximates the thickness of a standard microscope slide cover slip (0.17 mm), allowing use of high-magnification objectives with standard working distances. They used this to investigate transport of Phytophthora spp. zoospores and cysts in saturated and unsaturated media.

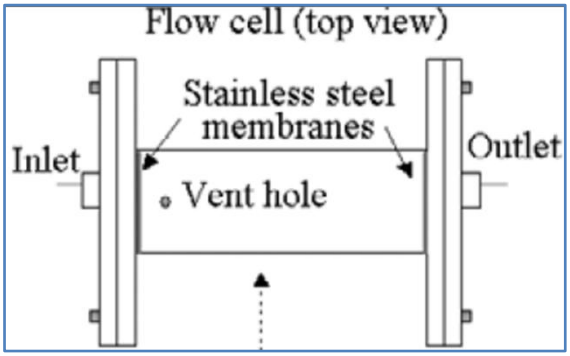

Fig. 2.10 *Schematic flow cell used by Gao et al. (2006).*

Micro-model

The micro-model is defined as an artificial representation of a porous medium, made of transparent material, containing a connected flow network.

The first micro-models were constructed by etching the flow network pattern on a glass plate, and using another glass plate to seal the model. Wan and Wilson (1994a) conducted pioneering visualization experiments in such a glass micro-model to investigate the role of air-water interface on the retention and transport of colloids. The pore structures of the glass micro-model they used are shown in Fig. 2.11 (left). The pore size was around 20μm to 250μm. Each network contained around 1250 pore bodies. They concluded that air-water interfaces are the main retention site for colloids. The glass micro-model they used were constructed by etching a pore network pattern and its mirror image on two glass plates, and then fused face to face at high temperature.

Bauman et al. (2004) constructed a silicon micro-model by photo-chemical etching of the pore network on a silicon wafer, and then bonded with a 0.5-mm-thick Pyrex plate (the pore structures are shown in Fig. 2.11). The silicon micro-model was mounted on an aluminum plate which could fit on the stage of fluorescence microscope. They used fluorescent microscopy to observe colloids transport inside the silicon micro-model.

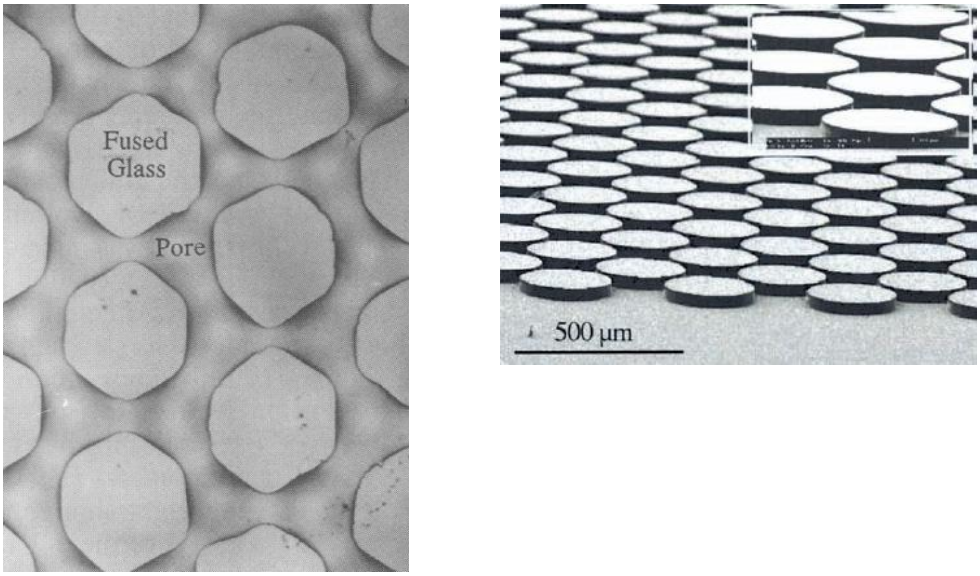

Fig. 2.11 *Pore structures of the micro-model. Left: glass micro-model employed by Wan and Wilson (1994a); Right: silicon micro-model employed by Baumann et al. (2004).*

As an elastomeric and cheap choice, PDMS became one of the most widely used materials for manufacturing micro-models, using soft photolithography. Details of the construction procedure for PDMS micro-models can be found in Quake and Schere (2000). Auset and Keller (2004) used PDMS micro-models (the pore structure are shown in Fig.12) to study the role of particle size on colloids dispersion.

Recently, a novel procedure was developed by Karadimitriou et al. (2012) in order to construct a stably hydrophobic and uniformly PDMS micro-models. Following that procedure, a PDMS micro-model with dimensions of 1mm×10mm was constructed, bearing roughly 90 pore bodies and 200 pore throats. One outlet channel and three inlet channels for the injection of the fluids and colloids were connected to the pore network. The pore-scale visualization of colloids movement was done with confocal microscopy.

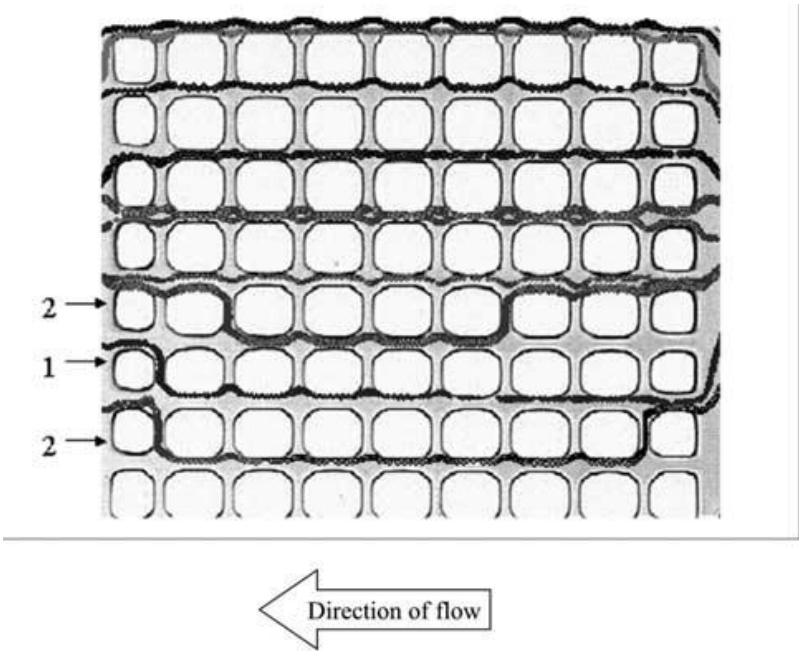

Fig. 2.12 *Homogeneous pore structure of the PDMS micro-model employed by Auset and Keller (2004).*

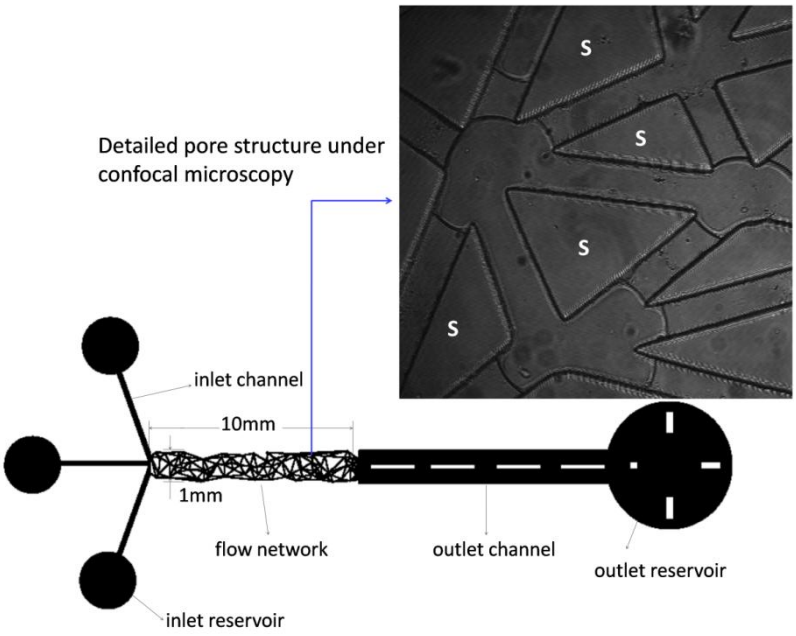

Fig. 2.13 *Schematic of the PDMS micro-model in Zhang et al. (2013).*

2.3.2 Retention of colloid in unsaturated porous media

In unsaturated porous media, due to the presence of air phase, colloids transport mechanisms become even more complicated. It is known that AWI can act as a major attachment site in addition to the SWI.

To better understand the mechanisms of attachment/detachment at the AWI, visualization experiments have contributed a lot. In most pore-scale imaging studies, the retention of colloids to the AWI has been studied during steady-state flow conditions. The main visualization experiments relevant and their findings were as the following:

Air was trapped as residual air bubbles in a glass micro-model of Wan and Wilson (1994a, b). Colloids were observed attached to the AWI, and they stated that the sorption of colloids to the AWI was irreversible because of capillary force. But these findings were disputed in later studies.

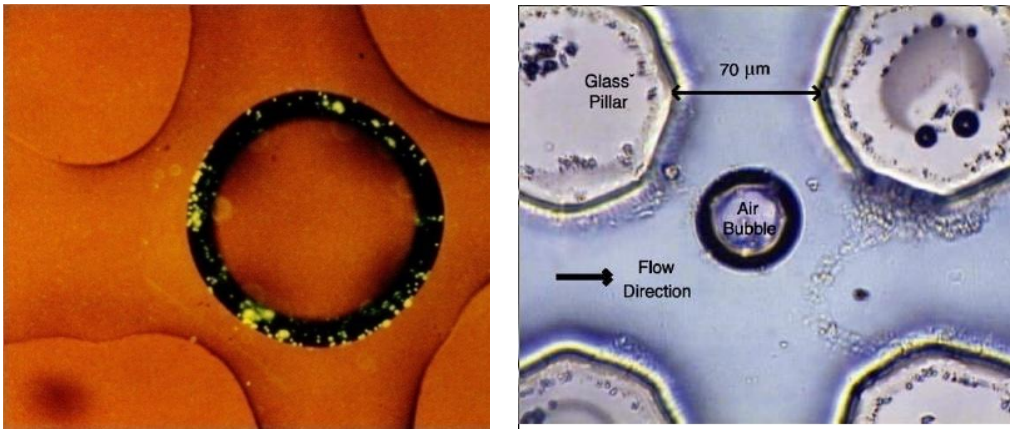

Fig. 2.14 *Visualization of colloids in an unsaturated porous medium. Left: Colloids retention at AWI (Wan and Wilson, 1994a); right: none of the colloids attached to the AWI (Chen and Flury, 2004).*

For example, Chen and Flury (2005) created a single air bubble centered between four glass pillars in a glass micro-model to observe colloid-gas bubble interactions. The size of the air bubble was controlled to be smaller than the width of the micro-model to make sure the air bubble was fully surrounded by the aqueous phase. Therefore, in their

experiment, there was no solid-liquid-air contact line. In contrast to the findings of Wan and Wilson, they reported that colloids moved with the flow and did not attach to the liquid-gas interface (as shown in Fig. 2.14).

Also, Crist et al. (2004) questioned whether the colloids attached irreversibly to the AWI. Visual evidences on colloids retention occur at AWS were provided (Crist et al., 2005; Zevi et al., 2005, 2006), one image taken by Zevi et al. (2006) is given in Fig. 2.15.

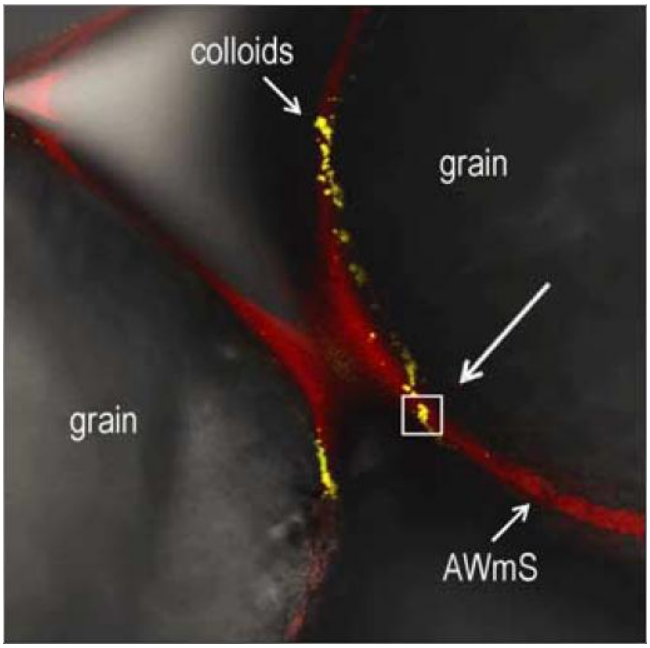

Fig. 2.15 *Confocal laser scanning image of colloids retention at AWS (Zevi et al., 2006).*

An additional mechanism of colloid attachment was introduced by Wan and Tokunaga (1997). They suggested that colloids can be retained by film straining, depending on the ratio of colloid size to film thickness. The film thickness was estimated to be in the range of 20-40nm (Wan and Tokunaga, 1997). Chu et al. in 2003 estimated a film thickness in the range of 15-21nm for different soils. The thickness of the water film presented in another medium was estimated to be 30-60nm (Keller et al., 2004).

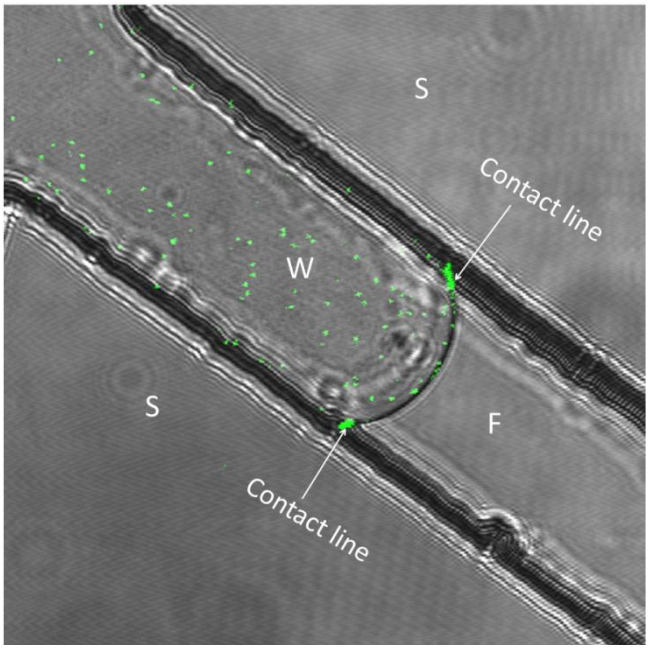

Fig. 2.16 *Confocal laser scanning image of colloids retention at FWSCs.*

Gao et al. (2006) observed colloids with a diameter of 2μm strained in water film in low-moisture content quartz sand. But, due to the small thickness of the film, the resolution of the visualization equipment made it very difficult to prove the absence or presence of film straining. As shown in Fig. 2.17, it is difficult to tell the colloids were retained at AWS or immobilized by film straining.

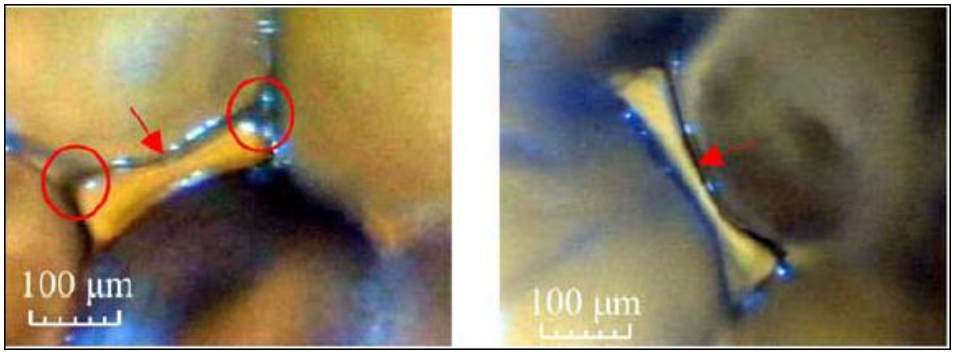

Fig. 2.17 *Colloids retention in thin water film in partially saturated pores (images of Gao et al. 2006).*

2.3.3 Remobilization with the moving AWI/AWS

In general, draining and re-saturating processes can result in significant remobilization of colloids from the SWI and the colloids that were regarded as irreversibly retained at the AWI. A few groups have addressed the mechanisms of colloids remobilization under transient hydraulic conditions by measuring concentration breakthrough curves of the effluent of column experiments (Saiers et al., 2003; Saiers and Lenhart, 2003; Zhuang et al., 2007, 2009; Shang et al., 2008; Cheng and Saiers, 2009). Visualization experiments of colloids release with the moving interfaces have been done by several groups (Gómez et al., 1999a, b; 2001a, b; Sharma et al., 2008; Aramrak et al., 2011; Zhang et al., 2013).

Visualization experiments have been conducted in order to provide evidence for the remobilization of colloids by the moving fronts. Using confocal microscopy, Sharma et al. (2008) observed the deposited colloids on the glass slide were released when the moving air-water interface passed over. Aramrak et al. (2011) conducted experiments in a set-up as shown in Fig. 2.6. Using confocal microscopy, they visualized and quantified the effects of air-water interface velocity on the detachment of polystyrene microspheres. They also reported that an advancing interface is more effective in detaching colloids.

During drainage process, big pores are emptied first; the reverse occurs during the imbibition process. The colloids that were remobilized by the drainage and imbibition fronts may re-deposit. Also, evaporation may exist in an open system and further result in transient conditions in the system. Thus, it is difficult to tell the occurring remobilization was due to drainage/imbibition or due to evaporation effect of the system. To overcome the shortcoming of open pores, Zhang et al. (2013) conducted colloids transport in a closed PDMS micro-model during two-phase flow under transient conditions. As can be seen from Fig. 2.18, the fluids distribution and re-deposition of colloids (highlighted in white circle) were clearly observed. Also, through video images, the release of colloids with the moving interfaces/contact lines was clearly observed.

2.4 Future research points

Through visualization, significant advances have been made in our understanding of transport, retention, and remobilization of colloids. But, there are still many questions

need to be answered.

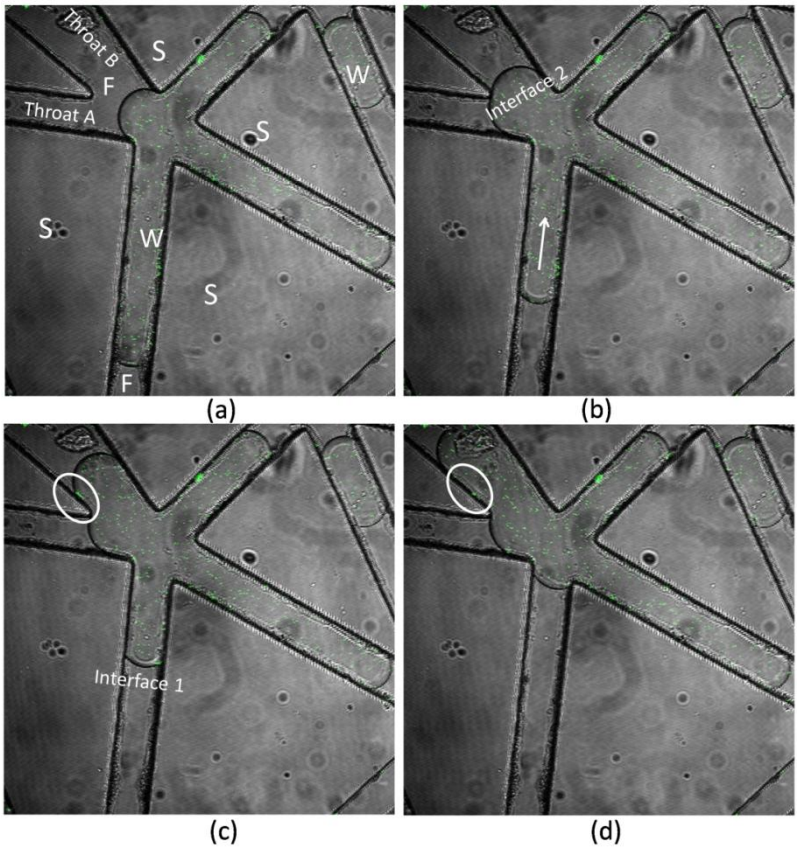

Fig. 2.18 *Detachment and re-deposit of colloids with the imbibition fronts in a micro-model (Zhang et al., 2013, Water Resources Research).*

We need to identify the attachment of colloids to the SWI or trapped in thin film by visualization experiments. Interactions of colloids with the AWI need to be quantified.

The shortcomings of the current visualization methods are that represent (ideal) porous medium were employed, such as single capillary channels or micro-models. Also the colloids are artificial colloids like microspheres. Therefore, the key challenge that remains is developing a set-up for visualization experiments to investigate transport of natural colloids in natural porous media.

References

(1) **Auset**, M., and A. A. Keller (2004), Pore-scale processes that control dispersion of colloids in saturated porous media, Water Resour. Res., 40, W03503, doi: 10.1029/2003WR002800.

(2) **Aramrak**, S., M. Flury, and J.B. Harsh (2011), Detachment of deposited colloids by advancing and receding air-water interfaces, Langmuir, 27, 9985-9993.

(3) **Baumann**, T., and C. J. Werth (2004), Visualization and modeling of polystyrol colloid transport in a silicon micro-model, Vadose Zone J., 3, 434– 443.

(4) **Baumann**, T., and C. J. Werth (2005), Visualization of colloid transport through heterogeneous porous media using magnetic resonance imaging, Colloids Surf. A, 265, 2– 10.

(5) **Boks**, N.P., W. Norde, H.C. van der Mei, H.J. Busscher. (2008), Forces involved in bacterial adhesion to hydrophilic and hydrophobic surfaces. Microbiology 154:3122-3133

(6) **Bradford**, S. A., and S. Torkzaban. (2008), Colloid Transport and Retention in Unsaturated Porous Media: A Review of Interface-, Collector-, and Pore-Scale Processes and Models, Vadose Zone J., 7, 667– 681.

(7) **Bradford**, S.A., S. Torkzaban, H. Kim, and J. Simunek (2012), Modelling colloid and microorganism transport and release with transients in solution ionic strength, Water Resour. Res., 48, doi: 10.1029/2012WR012468.

(8) **Burdick**, G.M., N.S. Berman, and S.P. Beaudoin. (2005), Hydrodynamic particle removal from surfaces, Thin Solid Films 488 ,116 – 123.

(9) **Bergendahl**, J., and D. Grasso. (1998), Colloid generation during batch leaching tests: Mechanics of disaggregation. Colloids Surf. A 135:193–205.

(10) **Bergendahl**, J., and D. Grasso. (1999), Prediction of colloid detachment in a model porous media: Thermodynamics. AIChE J. 45:475–484.

(11) **Bergendahl**, J., and D. Grasso. (2000), Prediction of colloid detachment in a model porous media: Hydrodynamics. Chem. Eng. Sci. 55:1523–1532.

(12) **Chen**, G., and M. Flury. (2005), Retention of mineral colloids in unsaturated porous media as related to their surface properties, Colloids and Surfaces A: Physicochem. Eng. Aspects, 256, 207-216.

(13) **Cheng** T., and J.E. Saiers. (2009), Mobilization and transport of in situ colloids during drainage and imbibition of partially saturated porous media. Water Resour. Res. 45, W08414, doi: 10.1029/2008WR007494.

(14) **Chu** Y., Jin Y, Baumann T, Yates MV. (2003), Effect of soil properties on saturated and unsaturated virus transport through columns. J Environ Qual, 32:2017–25.

(15) **Crist**, J.T., J.F. McCarthy, Y. Zevi, P. Baveye, J.A. Th roop, and T.S. Steenhuis. (2004), Pore-scale visualization of colloid transport and retention in partly saturated

porous media. Vadose Zone J. 3:444–450.

(16) **Crist**, J.T., Y. Zevi, J.F. McCarthy, J.A. Th roop, and T.S. Steenhuis. (2005), Transport and retention mechanisms of colloids in partially saturated porous media. Vadose Zone J. 4:184–195.

(17) **de Jonge**, L. W., C. Kjaergaard, and P. Moldrup. (2004a), Colloids and colloid-facilitated transport of contaminants in soils: An introduction, Vadose Zone J., 3, 321–325.

(18) **de Jonge**, L. W., P. Moldrup, G. H. Rubaek, K. Schelde, and J. Djurhuus. (2004b), Particle leaching and particle-facilitated transport of phosphorus at field scale, Vadose Zone J., 3, 462– 470.

(19) **Derjaguin**, B.V., and L.D. Landau. (1941), Th eory of the stability of strongly charged lyophobic sols and of the adhesion of strongly charged particles in solutions of electrolytes. Acta Physicochim. URSS 14:733–762.

(20) **Gao**, B., J. E. Saiers, and J. N. Ryan. (2006), Pore-scale mechanisms of colloid deposition and mobilization during steady and transient flow through unsaturated granular media, Water Resour. Res., 42, W01410, doi: 10.1029/2005WR004233.

(21) **Gao**, B., T. S. Steenhuis, Y. Zevi, V. L. Morales, J. L. Nieber, B. K. Richards, J. F. McCarthy, and J.-Y. Parlange. (2008), Capillary retention of colloids in unsaturated porous media, Water Resour. Res., 44, W04504, doi:10.1029/2006WR005332.

(22) **Geobel**, M., S. K. Woche, P.M. Abraham, G.E. Schaumann, and J. Bachmann. (2013), Water repellency enhances the deposition of negatively charged hydrophilic colloids in a water-saturated sand matrix, Colloids and Surfaces A: Physicochem. Eng. Aspects, 431, 150-160.

(23) **Gregory**, J. (1975), Interaction of unequal double layers at constant charge, J. Colloid Interface Sci., 51, 44– 51.

(24) **Gregory**, J. (1981), Approximate expression for retarded van der Waals interaction. J. Colloid Interface Sci. 83:138–145.

(25) **Gómez-Suárez**, C., J. Noordmans, H.C. van der Mei, and H.J. Busscher. (1999a), Detachment of colloidal particles from collector surfaces with different electrostatic charge and hydrophobicity by attachment to air bubbles in a parallel plate flow chamber. Phys. Chem. Phys., 1: 4423-4427.

(26) **Gómez-Suárez**, C., J. Noordmans, H.C. van der Mei, and H.J. Busscher. (1999b), Removal of colloidal particles from quartz collector surfaces as stimulated by the passage of liquid-air interfaces. Langmuir, 15: 5123-5127.

(27) **Gómez-Suárez**, C., H.J. Busscher, and H.C. van der Mei. (2001a), Analysis of bacterial detachment from substratum surfaces by the passage of air-liquid interfaces. Appl. Environ. Microbiol, 67(6): 2531-2537.

(28) **Gómez-Suárez** C., H.C. van der Mei, and H.J. Busscher. (2001b), Air bubble-induced detachment of polystyrene particles with different sizes from

collector surfaces in a parallel plate flow Chamber. Colloids and Surfaces A: Physicochemical and Engineering Aspects, 186(3): 211-219.

(29) **Goldman**, A.J., R.G. Cox, and H. Brenner. (1967), Slow viscous motion of a sphere parallel to a plane wall: I. Motion through a quiescent fl uid. Chem. Eng. Sci. 22:637–651.

(30) **Huang** CT, Peretti SW, Bryers JD. (1992), Use of flow cell reactors to quantify biofilm formation kinetics. Biotechnol Tech;6(3): 193–198.

(31) **Israelachvili**, J.N. (1992), Intermolecular and surface forces. 2nd ed. Academic Press, London.

(32) **Johnson**, K.L., K. Kendall, and A.D. Roberts. (1971), Surface energy and the contact of elastic solids. Proc. R. Soc. London Ser. A 11:301–313.

(33) **Keller** AA, Sirivithayapakorn S, Chrysikopoulos CV. (2004b), Early breakthrough of colloids and bacteriophage MS2 in a water-saturated sand column. Water Resour Res; 40(8). Art. No. W08304.

(34) **Keller**, A. A., and S. Sirivithayapakorn. (2004a), Transport of colloids in unsaturated porous media: Explaining large-scale behavior based on pore-scale mechanisms, Water Resour. Res., 40, W12403, doi:10.1029/ 2004WR003315.

(35) **Lanning** LM, Ford RM. (2002), Glass micromodel study of bacterial dispersion in spatially periodic porous networks. Biotechnol Bioeng;78:556–66.

(36) **Lazouskaya**, V., and Y. Jin. (2008), Colloid retention at air-water interface in a capillary channel, Colloids Surf. A, 325, 141– 151.

(37) **Lazouskaya**, V., L-P. Zhang, H.Gao, X. Shi, K. Czymmek, and Y. Jin. (2011), Pore-Scale Investigation of Colloid Retention and Mobilization in the Presence of a Moving Air–Water Interface ,Vadose Zone J., 10, 1250-1260.

(38) **Leenaars**, A. F. M. and S.B.G. O'Brien. (1989), Particle removal from silicon substrates using surface-tension forces. Philips J Res 44:183–209.

(39) **Lenhart**, J. J., and J. E. Saiers. (2002), Transport of silica colloids through unsaturated porous media: Experimental results and model comparisons, Environ. Sci. Technol., 36, 769-777, doi: 10.1021/es0109949.

(40) **Lenhart**, J. J., and J. E. Saiers. (2003), Colloid mobilization in water saturated porous media under transient chemical conditions, Environ. Sci. Technol., 37, 2780-2787, doi:10.1021/es025788v.

(41) **McCarthy**, J.F., and J.M. Zachara. (1989), Subsurface transport of contaminants. Environ. Sci. Technol. 23:496–502.

(42) **Ochiai**, N., E. L. Kraft, and J.S. Selker. (2006), Methods for colloid transport visualization in pore networks, Water Resour. Res., 42, doi: 10.1029/2006WR004961.

(43) **O'Neill**, M.N. (1968), A sphere in contact with a plane wall in a slow linear shear flow. Chem. Eng. Sci. 23:1293–1298

(44) **Potter**, K., R. L. Kleinberg, F. J. Brockman, and E. W. McFarland. (1996), Assay for bacteria in porous media by diffusion-weighted NMR, J. Magn. Reson., Ser. B, 113, 9– 15.

(45) **Quake**, S. R., and A. Scherer. (2000), Science, 290, 1536-1540.

(46) **Ryan**, J.N., andM.Elimelech. (1998), Colloid mobilization and transport in groundwater. Colloids Surf., A 107:1–56.

(47) **Saiers**, J. E. (2002), Laboratory observations and mathematical modeling of colloid-facilitated contaminant transport in chemically heterogeneous systems, Water Resour. Res., 38(4), 1032, doi: 10.1029/2001WR000320.

(48) **Saiers**, J. E., and G. M. Hornberger. (1996), The role of colloidal kaolinite in the transport of cesium through laboratory sand columns, Water Resour. Res., 32, 33–41.

(49) **Saiers**, J.E., G.M. Hornberger, D.B. Gower, and J.S. Herman. (2003), The role of moving air–water interfaces in colloid mobilization within the vadose zone. Geophys. Res. Lett . 30(21):2083. doi:10.1029/2003GL018418.

(50) **Saiers**, J.E., and J.J. Lenhart. (2003), Colloid mobilization and transport within unsaturated porous media under transient-flow conditions. Water Resour. Res. 39(1):1019. doi:10.1029/2002WR001370.

(51) **Sadeghi**, G., J.F. Schijven, T. Behrends, S.M. Hassanizadeh, J. Gerritse, and P.J. Kleingeld. (2011), Systematic study of effects of pH and ionic strength on attachment of phage PRD1, Ground Water 49:12–19. doi:10.1111/j.1745-6584.2010.00767.x.

(52) **Sadeghi**, G., T. Behrends, J.F. Schijven, and S.M. Hassanizadeh. (2013), Effect of dissolved calcium on the removal of bacteriophage PRD1 during soil passage: the role of double-layer interactions, J. Contam. Hydrol., 144(1):78-87. doi: 10.1016/j.jconhyd.2012.10.006.

(53) **Sang**, W., V.L. Morales, W. Zhang, C. R. Stoof, B. Gao, A. L. Schatz, Y. Zhang, and T.S. Steenhuis. (2013), Quantification of Colloid Retention and Release by Straining and Energy Minima in Variably Saturated Porous Media, Environ. Sci. Technol. doi: 10.1021/es400288c.

(54) **Shang**, J., M. Flury, G. Chen, and J. Zhuang. (2008), Impact of flow rate, water content, and capillary forces on in situ colloid mobilization during infiltration in unsaturated sediments. Water Resour. Res. 44, doi: 10.1029/2007WR006516.

(55) **Shang**, J., M. Flury, and Y. Deng. (2009), Force measurements between particles and the air-water interface: Implications for particle mobilization in unsaturated porous media. Water Resour. Res. 45, doi: 10.1029/2008WR007384.

(56) **Sharma** P., M. Flury, and J. Zhou. (2008), Detachment of colloids from a solid surface by a moving air-water interface, J. Colloid Interface Sci., 326, 143-150.

(57) **Sharma**, M. S., H. Chamoun, D. S. H. Sita Rama Sarama, and R. S. Schechter. (1992), Factors controlling the hydrodynamic detachment of particles from surfaces, J. Colloid Interface Sci., 149, 121– 134.

(58) **Sherwood**, J. L., J. C. Sung, R. M. Ford, E. J. Fernandez, J. E. Maneval, and J. A. Smith. (2003), Analysis of bacterial random motility in a porous medium using magnetic resonance imaging and immunomagnetic labeling, Environ. Sci. Technol., 37, 781–785.

(59) **Soltani**, M., and G. Ahmadi. (1994), On particle adhesion and removal mechanics in turbulent flows. J. Adhes. Sci. Technol. 8:763–785.

(60) **Stumm**, W. (1977), Chemical interaction in particle separation. Environ. Sci. Technol. 11:1066–1070.

(61) **Torkzaban**, S., S.M. Hassanizadeh, J.F. Schijven, A.M. de Bruin, and A.M. de Roda Husman. (2006a), Virus transport in saturated and unsaturated sand columns. Vadose Zone J. 5: 877-885.

(62) **Torkzaban**, S., S.M. Hassanizadeh, J.F. Schijven, and H.H.J.L. van den Berg. (2006b), Role of air-water interfaces on retention of viruses under unsaturated conditions. Water Resour. Res., 42, W12S14, doi: 10.1029/2006WR004904.

(63) **Wan**, J., and J.L. Wilson. (1994a), Visualization of the role of the gas–water interface on the fate and transport of colloids in porous media. Water Resour. Res. 30:11–23. doi:10.1029/93WR02403

(64) **Wan**, J., J.L. Wilson, and T.L. Kieft. (1994b), Influence of the gas–water interface on transport of microorganisms through unsaturated porous media. Appl. Environ. Microbiol. 60:509–516.

(65) **Wan**, J., and T.K. Tokunaga. (1997), Film straining of colloids in unsaturated porous media: Conceptual model and experimental testing. Environ. Sci. Technol. 31:2413–2420.

(66) **Zevi**, Y., A. Dathe, J.F. McCarthy, B.K. Richards, and T.S. Steenhuis. (2005), Distribution of colloid particles onto interfaces in partially saturated sand. Environ. Sci. Technol. 39:7055–7064.

(67) **Zevi**, Y., A. Dathe, B. Gao, B. K. Richards, and T. S. Steenhuis. (2006), Quantifying colloid retention in partially saturated porous media, Water Resour. Res., 42, W12S03, doi: 10.1029/2006WR004929.

(68) **Zevi**, Y., A. Dathe, B. Gao, W. Zhang, B.K. Richards, and T.S. Steenhuis. (2009), Transport and retention of colloidal particles in partially saturated porous media: Effect of ionic strength, Water Resour. Res., 45, doi: 10.1029/2008WR007322.

(69) **Zevi**,Y., B.Gao, W. Zhang, V.L. Morales, M.E. Cakmak, E.A. Medrano, W. Sang, and T.S. Steenhuis. (2011), Colloid retention at the meniscus-wall contact line in an open micro-channel, Water Research, 12, doi:10.1016/j.watres.2011.09.046.

(70) **Zhang**, L., L. Ren, and S. Hartland. (1996), More convenient and suitable methods for sphere tensiometry, J. Colloid Interface Sci., 180, 493–503.

(71) **Zhang**, Q.L., S.M. Hassanizadeh, A. Raoof, M.Th. van Genuchten, and S.M. Roels. (2012), Modeling virus transport and remobilization during partially saturated flow. Vadose Zone J. 11. doi:10.2136/vzj2011.0090.

(72) **Zhuang**, J., J.F. McCarthy, J.S. Tyner, E. Perfect, and M. Flury. (2007), In situ colloid mobilization in Hanford sediments under unsaturated transient flow conditions: Effect of irrigation pattern. Environ. Sci. Technol., 41: 3199- 3204, doi: 10.1021/es062757h.

(73) **Zhuang**, J., J.S. Tyner, E. Perfect. (2009), Colloid transport and remobilization in porous media during infiltration and drainage. J. Hydrol. 377:112-119.

(74) **Zhuang**, J., N. Goeppert, C. Tu, J. McCarthy, E. Perfect, and L. McKay (2010), Colloid transport with wetting fronts: Interactive effects of solution surface tension and ionic strength, Water Research, 44, 1270-1278. doi:10.1016/j.watres.2009.12.012.

Table 2.1 *Summary of the visualization experiments on colloid transport in unsaturated porous media*

Sites	Reference	Porous media	Dimensions	Pattern	Type of Microscopy	Particle information	Key role/findings
AWI	Wan and Wilson[1994a,b]	Etched glass micro-model	Pore network covered an area of about 3cm^2. Pore bodies and throats are sized 300μm and 20-100μm	Quadrilateral networks	Epifluorescence microscope	Fluorescent latex hydrophilic () and hydrophobic microspheres	AWI not only sorbed hydrophobic but also hydrophilic particles
	Chen and Flury [2005)	Glass micro-model	Cylindrical pillars of 100 μm diameter and pores formed by interstitial spaces	Rectangular structure	Optical light microscope	Colloids from Hanford sediments and pure clay minerals	No attachment of colloids to the AWI was observed.
	Lazouskaya et al. [2008]	An open capillary channel; PMMA micro-fluidic channel	0.4mm×0.4mm×54mm; depth and the length of the channels are 20μm and 85mm	trapezoid cross-section with bases of 42μm and 70μm	Confocal microscope	Sulfate and carboxylate-modified fluorescent colloids with diameter of 1.1μm	Colloid retention at AWS decreased with the increasing of Ionic strength
	Gao et al. [2006]	Transparent acrylic flow chamber packed quartz sand	6 cm in length, 1.6 cm in width, and 0.3 cm in depth	-	Epifluorescence microscope	Fluorescent polystyrene microspheres with diameter of 2μm	Colloids retention is dominated by adhesion to AWI at high moisture content and a combination of film straining and immobile water storage at low moisture content
AWS contact line	Crist et al. [2004] [2005]	Infiltration chamber filled with quartz sand of grain diameter between 0.43 and 0.6mm	26cm high, 4.8cm wide, and 0.5cm deep	Plate flow chamber, a stainless-steel wire mesh covered on the top	CCD camera	Fluorescent and non-fluorescent dyed polystyrene latex microspheres	Colloids retention occurred at the AWS contact line in sandy porous media Hydrophobic particles retained more in the narrow passages between grains; hydrophilic particles primarily retained at the AWS.
	Zevi et al. [2005]	Infiltration chamber filled with silica sand	limited to 2 cm width, and the sand layer thickness was 0.5 cm to allow sufficient light transmission.	-	Confocal microscope	Hydrophilic anionic carboxylated polystyrene microspheres colloids (0.8, 2.6, or 4.8μm	Colloids were retained at the AWS interface where the film thickness approximately equaled colloid diameter, more hydrophilic colloids were retained at AWS compared than

						diameters) and hydrophobic polystyrene microspheres (5.2μm)	SWI.
	Zevi et al. [2011]	an open channel	a 90-degree angle carved channel, 54mm in length, 5mm in wall height	triangular	Confocal microscope	Fluorescent yellow synthetic polystyrene microspheres (1μm in diameter)	Retention of colloids at the AWS contact line was observed, and it was due to
	Zevi et al. [2006]	acrylic glass flow chamber	10 mm ×30 mm × 3 mm	-	Confocal microscope	Fluorescent synthetic carboxylated latex and polystyrene microspheres	Retention of colloids at the AWS was quantified.
	Zevi et al. [2009]	Sand chamber (filled with quartz sand in diameter of 0.4-0.6mm)	40–60μm pore size	-	Confocal microscope	Synthetic polystyrene microspheres (1μm in diameter)	Colloids retained at AWS were observed and with the reduction of IS, the attachment reduces as well
Moving fluid-fluid front (interface and contact line)	Gómez-Suárez et al. [1999a][1999b][2001a] [2001b]	Quartz plates, Microscope glass slides	76×25×1.5 mm	parallel plate flow chamber	A phase-contrast with a 40× ultralong working distance, a charge-coupled CCD camera was connected to the microscope to get digital signals	Polystyrene microspheres	Air-bubble induced detachment of particles as a function of surface tension, flow velocity, and number of air-bubble passage
	Sharma et al. [2008]	An open Plexiglas flat channel: flow chamber	With a dimension of 16 cm× 2.7 cm×1 cm	rectangular	Confocal microscopy	Amidine-modified, carboxylate-modified, and sulfate-modified microspheres	Investigate the moving air-water interface on the removal of hydrophobic and hydrophilic colloids
	Sharma et al. [2005]	A parallel glass flow chamber	dimensions of 7.5 cm by 0.5 cm by 0.06 cm	With unidirectional inlet and flow cavity	MXR video camera mounted on a phase-contrast microscope with a	Bacterial strains	High flow rates can be effective in stimulating bacterial detachment, additional air-bubbles can detach more

				40× ultra long working distance		particles
Aramrak et al. [2011]	Glass channel	3.7 mm inner diameter and 7.5 cm length	Single cylinder channel	Confocal Microscopy	Hydrophilic carboxylate modified microspheres, 1μm diameter	Passage of air-water interface can detach particles deposited on the solid surface
Lazouskaya et al. [2011]	PMMA micro fluidic channels	widths of 42 and 70μm and height or depth of 20μm, the length of the channels was 85mm	trapezoidal cross-section	Confocal Microscopy	Carboxylate modified polystyrene microspheres, 500 nm diameter	A moving contact line can mobilize the attached particles and transfer to AWI
Zhang et al. [2013]	PMDS micro-model	Dimensions of 1mm ×10mm, average pore depth was 30μm	Rectangular cross-section	Confocal Microscopy	Carboxylated fluorescent polystyrene microspheres, with average diameter of 300nm	The moving contact line can remobilize the colloids originally deposited on the SWI

Chapter 3

Analysis of Remobilization of Viruses in Column Experiments

Abstract

Virus transport in porous media is affected by the water flow regime. During transient variably-saturated flow, fluctuating flow regimes can enhance virus detachment from both solid-water interfaces (SWIs) and air-water interfaces (AWIs). The objective of this study was to simulate the influence of drainage and imbibition events on the remobilization of attached viruses. Three different modelling approaches were examined. In the first approach, all attachment and detachment coefficients were assumed to be constant but the values of the detachment coefficients were increased drastically for the duration of transient unsaturated flow. The second and third modelling approaches involved extensions of the model of Cheng and Saiers, who assumed enhanced detachment of viruses to be proportional to the time rate of change in the water content. Their model was extended to include separate terms for virus attachment/detachment on SWIs and AWIs. In our second approach, we assumed kinetic sorption onto the AWI, with the desorption rate being described as a function of temporal changes in the air content.

Published as: Zhang, Q.L., S.M. Hassanizadeh, A. Raoof, M.Th. van Genuchten, and S.M. Roels, 2012, Modeling virus transport and remobilization during partially saturated flow, Vadose Zone Journal. 11. doi:10.2136/vzj2011.0090.

This approach did not explicitly account for the specific air-water interfacial area. Thus, in our third approach we explicitly included the presence and variation of air-water interfaces and assumed AWI attachment/detachment to be an equilibrium sorption process. The available air-water interfacial area was assumed to be a function of fluid saturation. The models were used to simulate a series of saturated-unsaturated virus transport experiments reported in the literature for conditions of both drainage and imbibition. The most promising results were obtained with the third approach, which explicitly accounts for adsorption to air-water interfaces and assumes equilibrium sorption on the available air-water interfacial area.

3.1 Introduction

Studies of virus and colloid transport during transient flow in variably-saturated porous media are important for devising optimal management and remediation practices of polluted water resources, especially for contaminants that may adsorb onto and migrate with colloids, including the transport of biological colloidal particles (Goyal et al., 1984; Ouyang et al., 1996). Transient flow regimes triggered by rainfall, irrigation, snowmelt or water table fluctuations predominate in the shallow vadose zone. Much evidence exists that fluctuating flows may remobilize deposited pathogenic microorganisms and can lead to very high peak concentrations in drinking water resources (DeNovio et al.2004; Zhuang et al., 2007). The presence of such peak events can be a major threat to public health.

Fate and transport processes of viruses and colloids in porous media are governed by advection, dispersion and inactivation, as well as by interactions with various interfaces (Keswick and Gerba, 1980; Yates et al., 1987; Schijven and Hassanizadeh, 2000). In unsaturated soils, the main removal processes are inactivation and attachment to solid surfaces and air-water interfaces (Powelson et al., 1990; Schijven and Hassanizadeh, 2000; Chu et al. 2001; Crist et al., 2005). These processes very much depend upon prevailing hydraulic and chemical conditions that are prone to spatial and temporal changes (e.g., see Sadeghi et al. (2011) for the effect of pH and ionic strength on virus removal). Of importance to virus and colloid transport in the unsaturated zone is also the air-water interfacial area (AWI) between the wetting (water) and non-wetting (air) phases, which is a function of the degree of saturation and the capillary pressure (Hassanizadeh and Gray, 1993). Much theoretical, experimental and modeling research has recently been carried out to understand and quantify the relationships between

air-water interfacial area, capillary pressure and fluid saturation (e.g., Pyrak-Nolte et al., 2008; Joekar-Niasar et al., 2010a).

Several studies of virus and colloid transport during variably-saturated flow have shown that attachment and release are enhanced at lower degrees of saturation (e.g., Torkzaban et al. 2006a; Chu and Yan Jin, 2000). However, most of these studies were carried out assuming steady-state flow with uniform degrees of saturation in time and space. Commonly, a steady-state flow regime is established first before the virus transport experiments are initiated. Results of such studies are valuable in that they show the dependence of sorption or attachment/detachment parameters on fluid saturation. However, natural systems usually involve transient flow conditions, which have been shown to often cause mobilization of attached viruses and colloids. Below, we give a brief overview of such investigations.

Gómez-Suárez et al. (1999a, 1999b, 2001b) studied the detachment of micro-sized particles from solid surfaces by passing air bubbles through a parallel plate flow chamber. They varied fluid properties and hydraulic conditions to study their effect on colloid detachment. Detachment was found to decrease linearly with increasing air bubble velocity and decreasing air-water interfacial tension. The percentages of detachment by passing air bubbles also varied greatly depending upon the characteristics of the bacterial strain and the solid surface (Gómez-Suárez et al., 2001a; Sharma et al., 2005; Boks et al., 2008). Results indicated that at low air bubble velocities, the hydrophobicity of the substratum had no influence on detachment. However, at high air bubble velocities, all bacterial strains were more efficiently detached from hydrophilic glass substrata. Particle shape (Gómez-Suárez et al., 2001a) and size (Gómez-Suárez et al., 2001b) were also found to be an important factor in air bubble-induced detachment. Sharma et al. (2008a, b) performed similar experiments as Gómez-Suárez et al. (1999a). They observed that an infiltrating or draining water front removed colloids that were deposited on the solid surfaces whenever the colloids came into contact with the moving AWI.

Several pore-scale visualization studies on the role of moving AWIs on colloid transport have been performed. For example, Sirivithayapakorn and Keller (2003) conducted pore-scale imbibition experiments in an unsaturated physical micro-model. They found that colloids strongly attached to the AWI. In subsequent studies, Keller and Auset (2007) showed how imbibition events thicken the water films where colloids were originally trapped and mobilize colloids attached to the AWI. They found that resaturation eventually remobilized all colloids attached to the AWI or trapped within

thin water films. Crist et al. (2004, 2005) performed three-dimensional micro-model visualization experiments using a packed-sand infiltration chamber. They found that colloids not only attached to the AWI but also were trapped in thin regions where the AWI and the solid surface meet, often referred to as the air-water-solid contact line (AWS). Other pore-scale experiments on colloid transport, including retention and mobilization in unsaturated media during imbibition, were carried out by Gao et al. (2006). As the water content increased and immobile water was converted to mobile water, particles were found to be released from the immobile water zones.

Several drainage and imbibition column experiments have been carried out to study the remobilization of colloids/viruses as a result of transient unsaturated flow. Results showed that the concentration of viruses at the outlet increased when a wetting front arrived (Ryan et al., 1998; Powelson and Mills, 2001; Saiers et al., 2003; Torkzaban et al., 2006a, b; Shang et al., 2008; Zhuang et al., 2009; Cheng and Saiers, 2009). These studies suggest that temporal changes in saturation, whether drainage or imbibition, promote the remobilization of attached viruses/colloids.

In order to account for colloid remobilization during transient flow, Cheng and Saiers (2009) proposed a semi-empirical model in which the detachment coefficient is assumed to be a function of the temporal change in fluid saturation. They used the model to simulate results of their colloid remobilization experiments. Unfortunately, the model has two shortcomings: (1) the dependency of the attachment and detachment coefficients on fluid saturation was not taken into account, and (2) attachment/detachment to/from air-water interfaces was not specifically included in the model.

The objective of this study was to investigate the utility of the Cheng and Saiers model, and several modifications and extensions thereof, to describe experimental data reported by Torkzaban et al. (2006a, b). We modified the model of Cheng and Saiers (2009) in attempts to remove the two shortcomings mentioned above. Below, we first briefly summarize the experiments of Torkzaban et al. (2006a, b), and then describe in detail the models used for analyzing their data.

3.2 Description of Column Experiments

The virus transport experiments of Torkzaban et al. (2006a, b) were designed to determine the effect of water content on the attachment of viruses in soil during steady-state unsaturated flow. They focused especially on the interaction of viruses with the solid-water and air-water interfaces. In their studies, Torkzaban et al. used cylindrical

PVC columns with an internal diameter of 10 cm and length of 23 cm. Sand with a median grain size (d_{50}) of 140 μm and uniformity coefficient (d_{60}/d_{10}) of 1.6 was packed into the columns following procedures of Robinson and Friedman (2001) to produce a as homogeneous packing as possible. Both saturated and unsaturated flow experiments at constant flow rates and constant saturations were carried out. The pH and ionic strength were also varied among the experiments. Table 3.1 lists relevant parameters of the experiments. The experiments were designed such that constant saturation levels and capillary pressures existed along the column and versus time. This was done by establishing zero pressure gradients in the column such that gravity was the only driving force for water flow.

Table 3.1. *Experimental condition of the column experiments and modeling parameters (average ± standard deviations) as reported by Torkzaban et al. (2006a, b).*

Parameter	Unit	Experiment LpHi100	Experiment HpLi65	Imbibition-drainage
Ph	-	7	9	6.2
Ionic Strength	Mm	19	0.6	19
Initial Saturation	%	100	65	50
Pore water velocity	cm min^{-1}	0.68	0.56	0.46
Measured dispersivity	cm	0.06	0.44	0.56
Seeding duration	Pore volumes	4.2	8.0	10.4
Column length	cm	23	23	23
Porosity, θ_s	-	0.41	0.41	0.41
Saturated hydraulic conductivity	cm min^{-1}	1.13	1.13	1.13
Soil dry bulk density, ρ_b	kg cm^{-3}	1650	1650	1650
Residual water content, θ_r	-	0.055	0.055	0.055
SWI attachment coefficient, k_{att}^{s}	min^{-1}	8.2 (±1.7) x 10^{-3}	0.82 (±0.34)x 10^{-3}	0.2 (±0.06)x 10^{-3}
SWI detachment coefficient, $k_{\det}^{s}$	min^{-1}	1.4 (±0.2) x 10^{-3}	7.0 (±1.4)x10^{-3}	9.5 (±1.6)x 10^{-3}
AWI attachment coefficient, k_{att}^{a}	min^{-1}	-	8.5 (±1.4)x 10^{-3}	1.5 (±0.06)x 10^{-3}
AWI detachment coefficient, $k_{\det}^{a}$	min^{-1}	-	0.0052 (±0.001)x 10^{-3}	0.0063 (±0.001)x 10^{-3}
Inactivation rate (Fix174), μ_s, μ_w, μ_a	min^{-1}	1.3 x 10^{-5}	1.3 x 10^{-5}	1.5 x 10^{-5}
Transient condition	-	Drained	Drained	Resaturated, then drained

Once steady-state flow was established, a virus suspension was added to the inlet solution. Effluent samples were taken from the outlet of the column at regular intervals and analyzed for virus concentrations. The virus seeding was continued until almost steady-state breakthrough curves were obtained. At the end of the seeding period, the flow of clean water and measurement of the breakthrough curve continued. Some of the steady-state experiments were followed by a transient drainage or imbibition flow phase. For transient drainage, the inflow of water at the top of the columns was terminated and the columns were allowed to drain by gravity to nearly residual water saturation. The unsaturated columns in several other transient experiments were gradually resaturated to almost full saturation by flooding them from below, after which they were drained to the residual water content. Both types of transient experiments caused steep increases in the breakthrough concentrations of the viruses, as shown by typical breakthrough curves in Figs. 3.1 and 3.4. Torkzaban et al. (2006a, b) used the Hydrus-1D code (Simunek et al., 1998) to model the virus experimental data during steady-state flow. They did not try to simulate the transient part of their experiments.

3.3 Mathematical Formulations

3.3.1 Flow in Unsaturated Porous Media

Transient flow of water through the unsaturated columns was modeled using the standard Richards equation as follows:

$$\frac{\partial \theta}{\partial t} = \frac{\partial}{\partial x}\left[K(h)\left(\frac{\partial h}{\partial x} + 1 \right) \right] \tag{3.1}$$

where h [L] is the water pressure head, θ [-] is the volumetric water content, K [LT^{-1}] is the hydraulic conductivity, t [T] is time, and x [L] is the vertical coordinate, taken positive in the upward direction. We employed the expressions of van Genuchten (1980) to describe the nonlinear relationships between θ and h and between K and h:

$$h = -\frac{1}{\alpha}\left[S_e^{-1/m} - 1 \right]^{1/n} \tag{3.2a}$$

$$K(h) = K_s S_e^{\frac{1}{2}} \left[1 - (1 - S_e^{1/m})^m \right]^2 \tag{3.2b}$$

$$S_e = \frac{\theta - \theta_r}{\theta_s - \theta_r} \tag{3.3}$$

where θ_s [-] and θ_r [-] are saturated and residual water contents respectively, S_e [-] is effective saturation, and α [L^{-1}], n [-], and m [-] are empirical parameters, with m=1-1/n.

3.3.2 Virus Transport during Transient Unsaturated Flow

In this section, we describe three alternative models of virus transport during transient variably-saturated flow. We first provide the general equations governing virus transport in variably-saturated media, including terms accounting for sorption onto SWIs and AWIs, as stated by Torkzaban et al. (2006b), among others:

$$\frac{\partial \theta C_w}{\partial t} = \frac{\partial}{\partial x}(\theta D \frac{\partial C_w}{\partial x}) - \frac{\partial q C_w}{\partial x} - \mu_w \theta C_w - \gamma_s - \gamma_a \tag{3.4a}$$

$$\frac{\partial \rho_b C_s}{\partial t} = \gamma_s - \mu_s \rho_b C_s = \theta k_{att}^s C_w - k_{\det}^s \rho_b C_s - \mu_s \rho_b C_s \tag{3.4b}$$

$$\frac{\partial \theta_a C_a}{\partial t} = \gamma_a - \mu_a \theta_a C_a = \theta k_{att}^a C_w - k_{\det}^a \theta_a C_a - \mu_a \theta_a C_a \tag{3.4c}$$

where C_w [pfu L^{-3}] is the number concentration of viruses in water (number of plaque-forming units per volume of water); C_s [pfu M^{-1}] is the number of viruses adsorbed to the SWI per unit mass of dry soil; C_a [pfu L^{-3}] is the concentration of viruses adsorbed to the AWI in terms of number of viruses per unit volume of air; ρ_b [ML^{-3}] is the soil bulk density; θ_a [-] is air content (volume of air per unit volume of the soil); D [L^2T^{-1}] is the dispersion coefficient, q [LT^{-1}] is the Darcy-Buckingham flow rate; γ_s and γ_a [pfu $L^{-3}T^{-1}$] are rates of adsorption to SWIs and AWIs, respectively; μ_w, μ_s and μ_a [T^{-1}] are inactivation rate coefficients associated with the water, solid and air phases, respectively; k_{att}^s and k_{det}^s [T^{-1}] are attachment and detachment rate coefficients of viruses to and from the solid-water interface, respectively; and k_{att}^a and k_{det}^a [T^{-1}] are similar attachment and detachment rate coefficients associated with the air-water interface, respectively. According to Schijven and Hassanizadeh (2000), the ratio of μ_l and μ_s is generally close to unity.

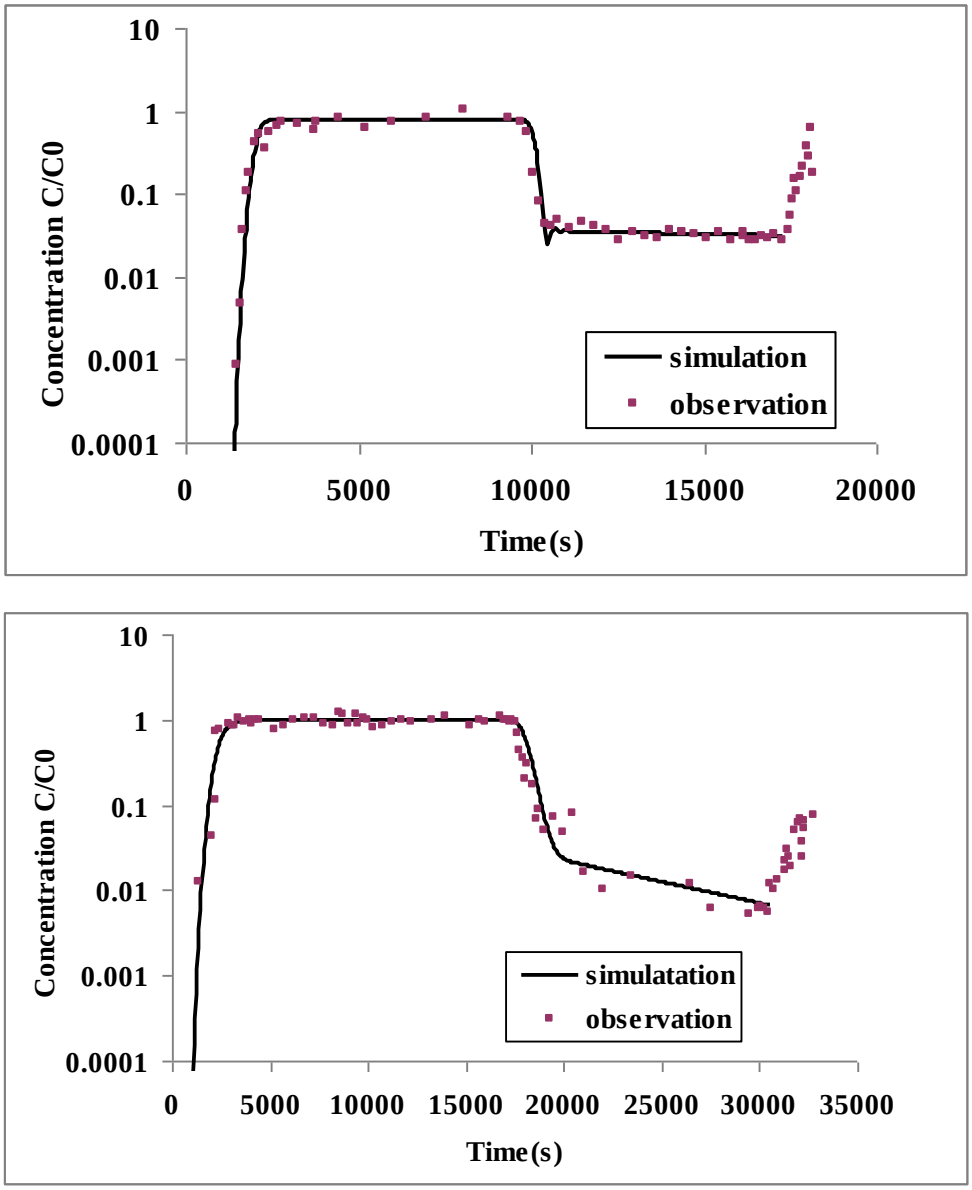

Fig. 3.1. *Normalized virus concentration breakthrough curves. Top plot: pH=7, fluid saturation=100%. Bottom plot: pH=9, fluid saturation=65%. Figures constructed based on data and parameter values reported by Torkzaban et al. (2006a).*

Torkzaban et al. (2006a, b) determined values of the attachment and detachment coefficients at different constant saturation values. However, those data cannot be used

to provide a dependence of the attachment/detachment coefficients on saturation during transient flow. As explained in the Introduction, various authors have reported that during both drainage and imbibition a remobilization of attached viruses may occur. One way to model this remobilization using Eqs. (3.4a, b, c), is to assign a much larger, yet constant, value to k_{det} for the duration of a drainage or imbibition process. We shall refer to this as the *constant-detachment model*. A more physically-based model was proposed by Cheng and Saiers (2009), further referred to it as the *Cheng-and-Saiers model*, which is described in the following section. This model was extended in two different ways to include the effect of AWIs.

3.3.3 The Cheng-and-Saiers Model

Cheng and Saiers hypothesized that mobilization of adsorbed colloids occurs only in pores that are being emptied during drainage or are filled during imbibition. During drainage, air enters the larger pores first. As the capillary pressure increases (or water pressure decreases) smaller pores subsequently undergo drainage. The variability in pore sizes leads to a distribution of compartments (pores) that empty at a distribution of entry pressures, referred to as the snap-off pressures by Cheng and Saiers (2009). Once a compartment empties as its entry pressure is being reached, adsorbed particles are removed from the pore walls of that compartment and enter the water phase.

If the concentration of viruses that are adsorbed within a compartment i is denoted by C_{si} (number of adsorbed viruses per unit mass of dry soil), then the total adsorbed concentration to SWI at any given time and position is given by:

$$C_s = \sum_{i=1}^{Nc} C_{si} \tag{3.5}$$

where N_c is the number of compartments. Cheng and Saiers (2009) assumed that the desorption of viruses occurs as a consequence of two separate processes: a steady-state part, modeled by the standard desorption coefficient k_{det}^s, and an additional part accounting for mobilization of viruses from a drained compartment, modeled as $k_{det}^i(t)C_{si}$. Thus, under transient conditions, equation (3.4b) is extended to the following form:

$$\frac{\partial \rho_b C_s}{\partial t} = \theta k_{att}^s C_w - \rho_b k_{det}^s C_s - \rho_b \mu_s C_s - \rho_b \sum_{i=1}^{N_c} k_{det}^i(t) C_{si} \tag{3.6}$$

where k_{det}^i [T^{-1}] is the transient detachment coefficient, standing for detachment from the solid grains induced by a passing AWI. This coefficient is nonzero only if the corresponding compartment is being drained. Thus, Cheng and Saiers (2009) proposed the following dependency for k_{det}^i:

$$k_{det}^i = \begin{cases} 0 & for \quad h > h_{si} \\ N_{dr} \left| \dfrac{\partial \theta}{\partial t} \right| & for \quad h \le h_{si} \end{cases} \tag{3.7}$$

where N_{dr} [-] is an empirical coefficient that quantifies the kinetics of virus mobilization during a drainage event and h_{si} is the entry pressure head for compartment *i*. According to Eq. (3.7), detachment of viruses within a given compartment takes place only when the water pressure head is less than the critical water pressure head h_{si} of that compartment. Once air enters a pore, detachment occurs as long as flow is locally unsteady (i.e., $\partial\theta/\partial t \neq 0$).

The same formula is applied during imbibition, but with different restrictions since a pore fills with water when the water pressure head exceeds the critical entry (snap off) pressure head:

$$k_{det}^i = \begin{cases} 0 & for \quad h < h_{si} \\ N_{imb} \left| \dfrac{\partial \theta}{\partial t} \right| & for \quad h \ge h_{si} \end{cases} \tag{3.8}$$

where N_{imb} [-] is an empirical coefficient that quantifies the kinetics of virus mobilization during an imbibition event. The coefficients N_{dr} and N_{imb} are assumed to be the same for all compartments.

The entry pressure head distribution h_{si} for different compartments can be obtained from capillary pressure head-water content curves such as those given by Eq. (3.2a). Our choice was to divide the water content range between [θ_r, θ_{ini}] evenly into N_C compartments, with each compartment *i* then providing a corresponding value of the critical water pressure head, h_{si}. The approach assumes that viruses attach uniformly throughout the entire pore size distribution range.

3.3.4 Model Two: Kinetic Detachment from AWI as a Function of Changes in the Air Content

The model of Cheng and Saiers (2009) does not specifically account for attachment/detachment to air-water interfaces. During imbibition, AWIs are destroyed and viruses adsorbed onto the AWI enter the water phase. This desorption from the air phase to the water phase may be accounted for by redefining the sorption rate γ_a in Eqs. (3.4a, c) by:

$$\gamma_a = \begin{cases} 0 & for \quad h < h_{si} \\ C_a^0 \left| \frac{\partial \theta_a}{\partial t} \right| & for \quad h \geq h_{si} \end{cases} \tag{3.9}$$

where C_a^0 is the last known concentration of AWI-adsorbed viruses before imbibition starts. Note that C_a^0 is constant in time but varies in space.

3.3.5 Model Three: Equilibrium AWI Attachment/Detachment as a Function of Air-water Interfacial Area

An alternative and somewhat simpler formulation may be obtained by assuming that attachment/detachment at the air-water occurs as a function of available air-water interfacial area. The governing equation for virus transport in the liquid phase, including adsorption to SWIs and AWIs, is then obtained by adding Eqs. (3.4a) and (3.4c) to eliminate γ_a, resulting in:

$$\frac{\partial \theta C_w}{\partial t} + \frac{\partial a C_{aw}}{\partial t} = \frac{\partial}{\partial x}(\theta D \frac{\partial C_w}{\partial x}) - \frac{\partial q C_w}{\partial x} - \theta k_{att}^s C_w + \rho_b k_{det}^s C_s - \mu_w \theta C_w - \mu_a a C_{aw} \tag{3.10}$$

This equation should be solved in conjunction with Eq. (3.6) for sorption onto the solid phase. In Eq. (3.10), C_{aw} [pfu L^{-2}] is the concentration of viruses adsorbed to the AWI in terms of number of viruses per unit air-water interfacial area; and a [L^2/L^3] is the air-water interfacial area per unit volume of porous medium. Next we assume linear equilibrium partitioning of viruses between the water and air-water interface:

$$C_{aw} = K_D^a C_w \tag{3.11}$$

where K_D^a [L] is the equilibrium distribution coefficient for sorption onto the AWI, expressed as $K_D^a = \frac{\theta k_{att}^a}{a k_{det}^a}$. Eq. (3.10) then reduces to:

$$\frac{\partial \theta R C_w}{\partial t} = \frac{\partial}{\partial x}(\theta D \frac{\partial C_w}{\partial x}) - \frac{\partial q C_w}{\partial x} - \theta k_{att}^s C_w + \rho_b k_{det}^s C_s - \mu_t \theta C_w \tag{3.12}$$

where

$$R = 1 + \frac{a K_D^a}{\theta} \qquad \mu_t = \mu_w + \frac{\mu_a a K_D^a}{\theta} \tag{3.13a,b}$$

Eq. (3.12), in conjunction with (3.6), is applicable to both transient and steady-state saturated and unsaturated flow.

The specific air-water interfacial area (a) in the above equations is very much a transient parameter. Its value may depend not only on saturation but also on capillary pressure (Hassanizadeh and Gray, 1993; Marle, 1981; Joekar-Niasar and Hassanizadeh, 2010b). For the purpose of this study, we assumed that a depends on water saturation, being zero when the medium is fully saturated or completely dry. We considered several specific relationships between interfacial area, a, and the degree of fluid saturation, $S_w=\theta/\theta_s$. The best results were obtained using the following equation:

$$a = a_0 (1 - S_w)^3 S_w \tag{3.14}$$

where a_0 [L^2/L^3] is the specific interfacial area corresponding to residual saturation of the medium.

Equation (3.14) assumes that the effective AW interfacial area for virus sorption increases when the medium saturation decreases, except at very low fluid saturations when the liquid water films around particles may become too thin to allow unrestricted movement of viruses in the liquid phase to/from AWIs. The latter effect is accounted for by multiplication with S_w in Equation (3.14). This equation, without the last term (S_w), is consistent with both theoretical (e.g., Bradford and Leij, 1999; Oostrom et al, 2001) and experimental (e.g., Kim et al., 1999) analyses of air-water interfacial areas as a function of fluid saturation. The data of Kim et al. (1999) for a coarse-textured sand, similarly to the one used in this study, indicate values of approximately 3 for the exponent in (3.14). The value of 400 cm^{-1} for a_0, which we used in our study was determined by using simple power function $a=400(1-S_w)^3$ which is physically realistic to match the data of Kim et al. (1999).

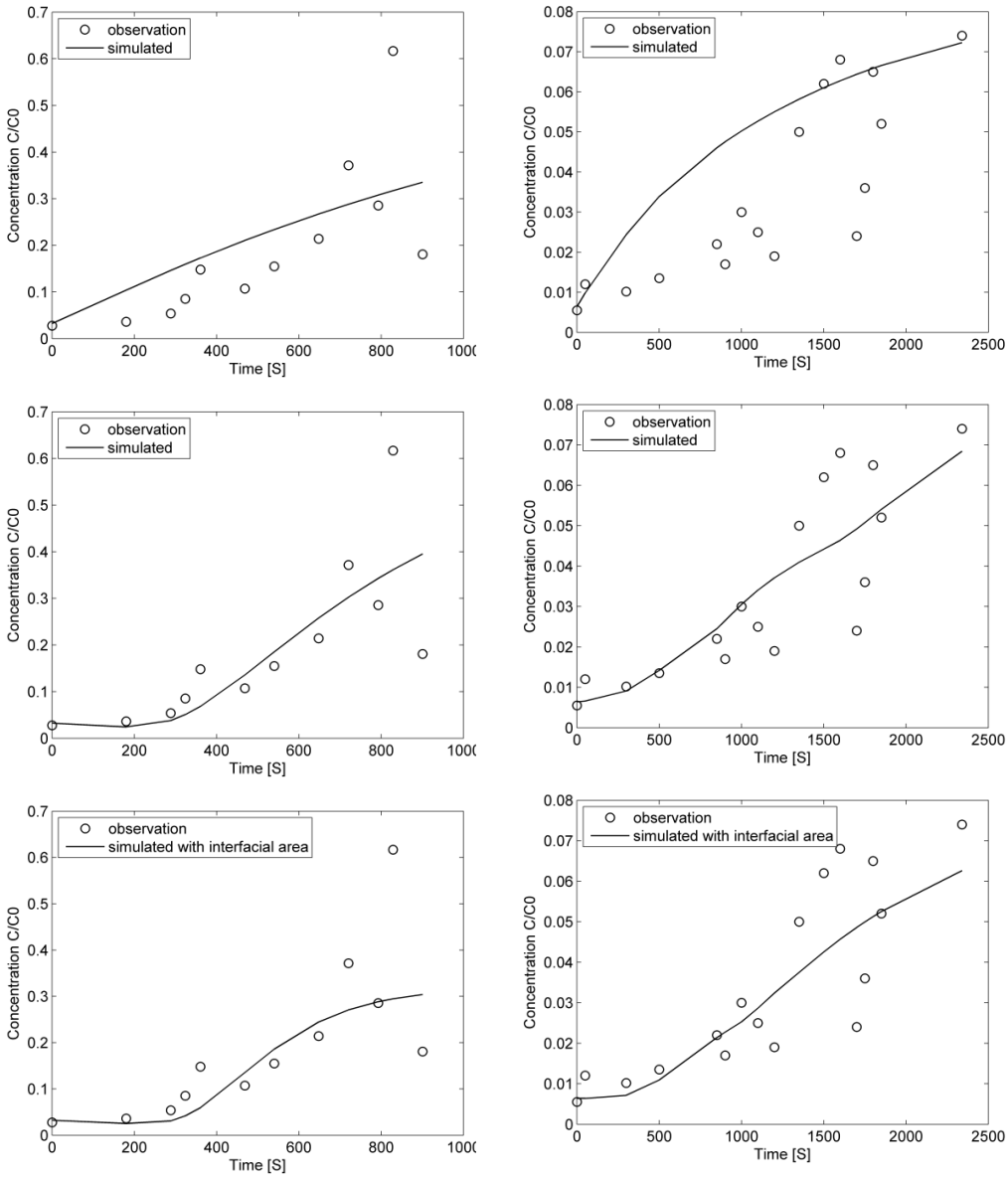

Fig. 3.2. *Observed (open circles) and fitted (lines) virus remobilization breakthrough curves for two drainage experiments: Left: Experiment LpHi100 (low pH, high ionic strength, 100% fluid saturation) and Right: HpLi65 (high pH, low ionic strength, 65% fluid saturation). Plots from top to bottom represent simulations assuming constant k_{det} values, variable k_{det} values, and equilibrium partitioning on the air-water interface.*

3.4 Results

3.4.1 Parameter Optimization

The three different transport models presented above were solved by means of COMSOL Multiphysics 3.5a (Comsol, 2009). Model parameters were estimated by fitting calculated concentration breakthrough curves to the experimental data of Torkzaban et al. (2006a, b). To do so, the sum of squared of residuals between calculated and measured effluent concentrations was used as the objective (or fitness) function (Raoof and Hassanizadeh, 2010). The objective function was minimized using a genetic algorithm (GA) to allow for both constrained and unconstrained optimization problems (Houck et al. 1995). Genetic algorithms differ from more traditional search algorithms in that they work with a number of candidate solutions (a population) rather than only one solution. The algorithm begins by creating a random initial population. Then at each step individuals are selected at random from the current population and used to produce the next generation. Over successive generations, the population "evolves" toward an optimal solution (for details of the method, readers are referred to Houck et al., 1995). We used in our study the Genetic Algorithm Toolbox included in Matlab (Mathworks, Natick, MA, USA).

Our main objective was to estimate values of detachment model parameters that would fit the measurements satisfactorily. Steady-state model parameter values, such as D, k_{att}^{s}, k_{det}^{s}, k_{att}^{a}, k_{det}^{a}, μ_w, μ_s, μ_a, obtained by fitting the virus breakthrough curves with the two-site kinetic attachment/detachment model are presented in Table 1. The parameter N_c was assigned a fixed value of 5 following a sensitivity analysis (larger values did not materially change the optimization results). The hydraulic parameters α and n had be estimated also since no water retention data were available. For this reason we estimated these parameters as well as N_{dr} from the virus concentrations of the drainage experiment.

The van Genuchten hydraulic parameters in Eq. (3.2a) and (3.2b) for a very coarse-textured soil, in our case a medium sand with a median grain size of 140 μm and a uniformity coefficient of 1.6, are generally between 2 and 15 for n and between 14 m^{-1} and 35 m^{-1} for α (e.g., Schaap et al., 2001). These values were specified as limiting values in the optimization process to ensure that the parameter values remained physically realistic. The genetic algorithm repeatedly modified a population of

individual solutions. In our case, each individual solution consisted of three parameters values. We used a population size of 20 individual solutions and a repetition of 10 generations.

Table 3.2. *Best-fit soil hydraulic parameter values[a] for different experiments*

Experiment		Retention curve parameters		Cheng-Saiers extended model				
		α [m^{-1}]	n [-]	N_{imb} [-]	N_{dr} [-]	a_0 [cm^{-1}]	K_D[a] [m]	SSQ
LpHi100, drainage		14.29	12.6	-	152.5 (±8.54)	-	-	0.0137
HpLi65, drainage		14.29	12.6	-	171.5 (±7.72)	400 (±5)	0.04 (±0.01)	0.0632
Imbibition-drainage	Imbibition*	28.5	12.6	0.15 (±0.008)	-	400 (±5)	0.02 (±0.01)	0.0478
	Drainage	14.29	12.6	-	25.59 (±1.41)	400 (±5)	0.02 (±0.003)	

**estimated from drainage curve*

[a] Values are plus or minus the standard error of the fitted parameter estimate.

SSQ is sum of squared residuals.

Optimized values of the hydraulic parameters α and n and the drainage detachment constant N_{dr} are listed in Table 3.2. For imbibitions, we used the same value of n as for drainage, but shifted the drainage curve by increasing the value of α by a factor of 2 (e.g., Luckner et al., 1989). With known unsaturated soil hydraulic parameters, only the transient imbibition detachment constant N_{imb} had to be optimized. The estimated value for N_{imb} is included in Table 3.2.

3.4.2 Simulations of the Virus Transport Experiments

3.4.2.1 Simulations of the Drainage Experiments

Figure 1 presents normalized virus concentration breakthrough curves for the column experiments conducted by Torkzaban et al. (2006a) at two different fluid saturations. The solid line is the simulated breakthrough curve obtained with Eqs. (3.4a, b) as fitted to the steady-state flow part of the curve. Corresponding parameters for the simulation are

presented in Table 3.1. The two figures show significant increases in the virus concentration due to the drainage of the column at the end of the experiments.

As discussed in the theoretical sections, virus remobilization can be modeled in several ways: (1) increasing the otherwise constant value of detachment coefficient by some constant factor as soon as drainage or imbibition starts; (2) changing the value the detachment coefficient, k_{det}, as a function of changes in fluid saturation and/or air content, or (3) changing attachment/detachment as a function of the available air-water interfacial area. Results of three modeling approaches are compared with the experimental virus drainage data in Fig. 3.2. Notice that only data for the transient flow period (and the ensuing remobilization) are shown, starting from the time when transient flow is initiated. Parameter values for the three models are listed in Tables 3.1 and 3.2. For the constant-coefficient model, the value of k_{det} was increased from 1.38 x 10^{-3} min^{-1} to 3.9 x 10^{-2} min^{-1} in case of 100% fluid saturation (experiment LpHi100) and from 7.02 x 10^{-3} min^{-1} to 6 x 10^{-2} min^{-1} in case of 65% saturation (experiment HpLi65) as determined from the optimizations. The results are shown in the tops graphs of Fig. 3.2. It is clear that the fits are poor; even the trends in the data are not properly simulated with this model.

Results for the variable-coefficient model of Cheng and Saiers (2009) are shown in the middle graphs of Fig. 3.2. This model fitted the data much better as compared to the constant-coefficient formulation. The variations in the detachment coefficient k_{det}^{i} with time at a position 10 cm below the column inlet are shown in Fig. 3.3. The maximum value occurred when the drainage front reached this position. It is evident that this maximum value will be reached at later times at positions farther down to the column.

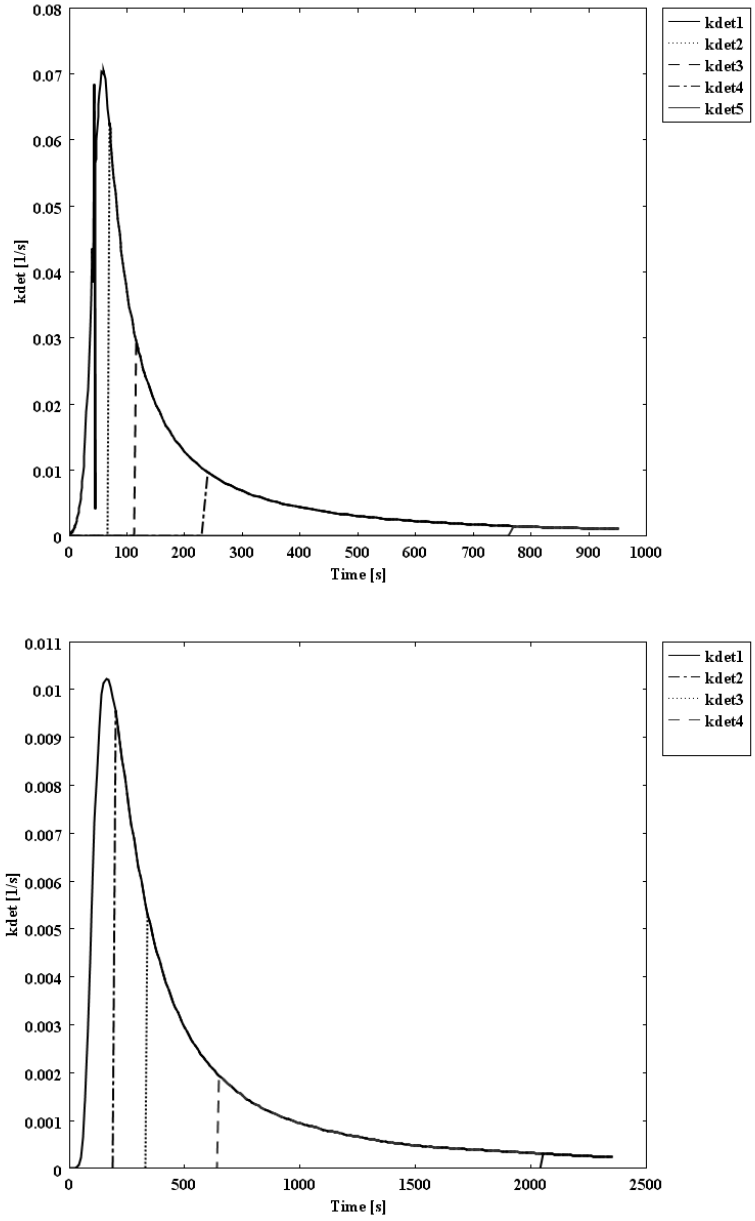

Fig. 3.3. *Variable detachment rates during drainage at 10cm below the column inlet. Top plot: drainage starting from a saturated column; bottom plot: drainage starting from a fluid saturation of 65%. Vertical bars indicate the value of* k_{det} *where the compartments defined in Cheng and Saiers model are drained.*

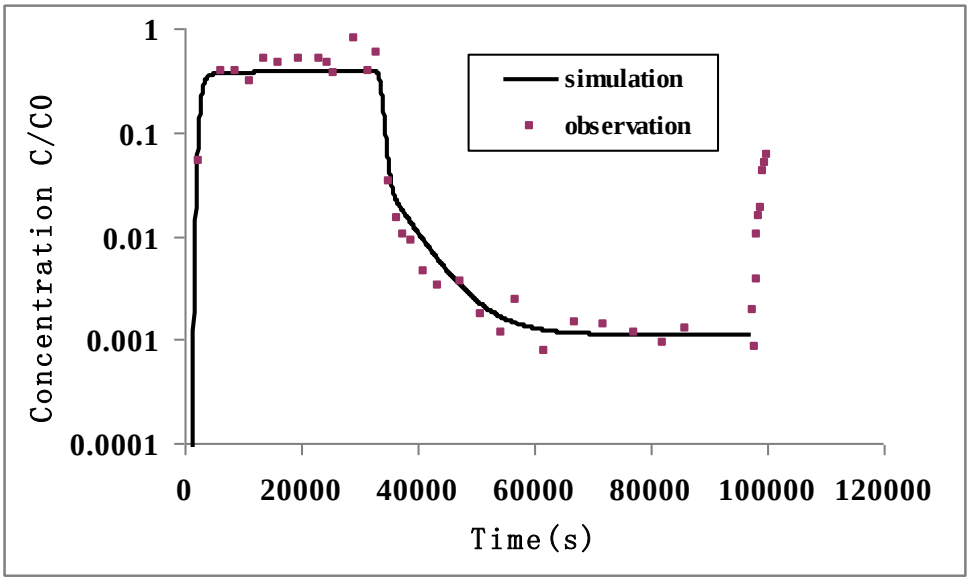

Fig. 3.4. *Measured and fitted φx174 normalized virus concentration breakthrough curve for the steady-state part of the imbibition-drainage experiment (at saturation of 50%) of Torkzaban et al. (2006a, b).*

Results of the modeling approach assuming linear equilibrium virus partitioning between the water phase and the available (transient) air-water interfacial area are shown in the bottom graphs of Fig. 3.2. Simulations using this approach provided somewhat better fits with the data than the variable detachment model of Cheng and Saiers as reflected by lower values of the sum of squared residuals (SSQs) between measured and calculated virus concentrations in the optimization process. Fitted parameters using this approach are listed in Table 3.2. The equilibrium distribution coefficients (2-4 cm) in our study were found to be several orders of magnitude larger than values (about 0.015 cm) reported by Wan and Tokunaga (1998). We do not have a good explanation for these differences, except perhaps the different experimental protocols used in the two studies (transient imbibition-drainage experiments in our study and a steady-state bubble column method by Wan and Tokunaga). Further studies about these differences are required.

3.4.2.2 Simulations of the Imbibition-Drainage Experiment

The measured breakthrough curve, including remobilization, of the imbibition-drainage experiment of Torkzaban et al. (2006a, b) is shown in Fig. 3.4. The solid line is again the simulated breakthrough curve using the conventional virus attachment/detachment model based on Eqs. (3.4a, b, c) fitted to the steady-state flow period. The column in this case was resaturated to nearly full saturation by raising the hanging water tube, and then was drained to residual water saturation.

The transient part of this experiment was simulated with the variable-detachment model as well as the formulation based on equilibrium partitioning between the water phase and air-water interfacial area during both resaturation and drainage. Optimized values of the detachment parameters N_{imb} and N_{dr}, as well as other parameters, are listed in Table 3.2. Figure 3.5 shows the measured and fitted breakthrough curves for two approaches. The time is again presented from the start of resaturation.

As can be seen from Fig. 3.5, the simulations assuming equilibrium sorption onto the air-water interfacial area agree very well with the observed data. It is encouraging to see that the simpler equilibrium sorption models works as well, or better, that the numerically more intricate variable detachment formulation. We note here that the formulation based on sorption onto the air-water interfacial area requires an expression relating the specific interfacial area to the degree of fluid saturation, or alternatively the air content. In this study we used Eq. (3.14) for this purpose, which performed better than several other expressions we investigated for a, including simple power functions of relative fluid saturating such as $a=a_0(1-S_w)^p$. Equation (3.14) suggests that, as expected, the effective AWI for virus sorption increases when the medium desaturates, except in very dry systems. Alternative expressions for Eq. (3.14) may need to be investigated in future work, especially for medium- and fine-textured sand.

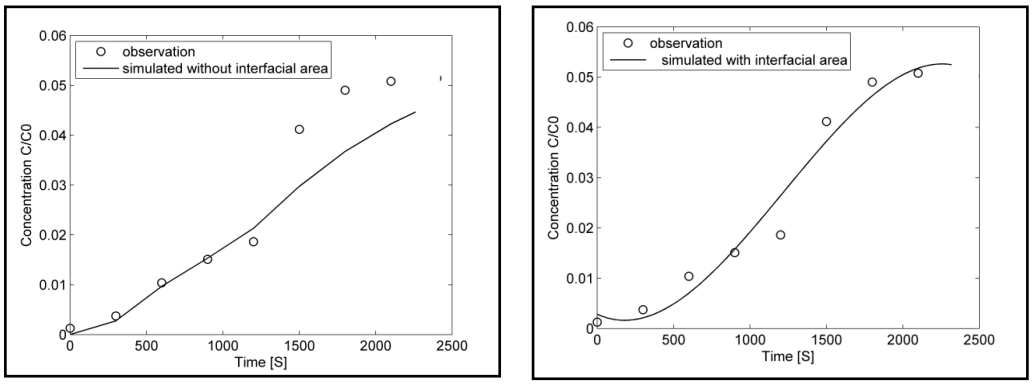

Fig. 3.5. *Observed (open circles) and fitted (lines) virus remobilization breakthrough curves for the imbibition-drainage experiment of Torkzaban et al. (2006a, b). Left plot: Breakthrough results using the model that AWI virus attachment/detachment as a function of air content; Right plot: Breakthrough results of the model that AWI attachment/detachment as a function of air-water interfacial area.*

3.5 Concluding Remarks

Virus remobilization during draining column experiments and during the processes of resaturation conducted by Torkzaban et al. (2006a, b) was modeled. First we employed the *constant-detachment coefficient* model, which just increased the detachment coefficient by a constant factor. Then we modified the model of Cheng and Saiers (2009) by including the effect of virus attachment on air-water interfaces. Two alternative formulations were considered; one was virus attachment/detachment on the AWI modeled as a function of transient changes in the air content, and one was for virus sorption on the air-water interface modeled as an apparent linear equilibrium partitioning process subject to the available (transient) air-water interfacial area (being zero at full saturation). The latter model formulation was found to fit the observed data satisfactorily. Separate SWI and AWI virus mass balances (see Fig. 3.6 and Fig. 3.7) showed that, in total, more viruses accumulated at, and released from, the solid water interface as compared to the air-water interface.

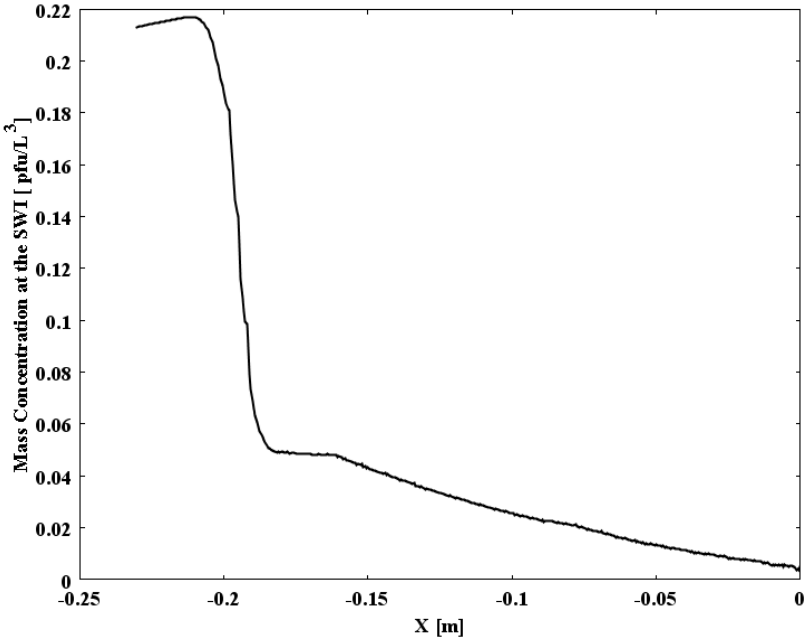
Mass Concentration at the SWI [pfu/L 3]
0.22
0.2
0.18
0.16
0.14
0.12
0.1
0.08
0.06
0.04
0.02
0
-0.25
-0.2
-0.15
-0.1
-0.05
0
X [m]

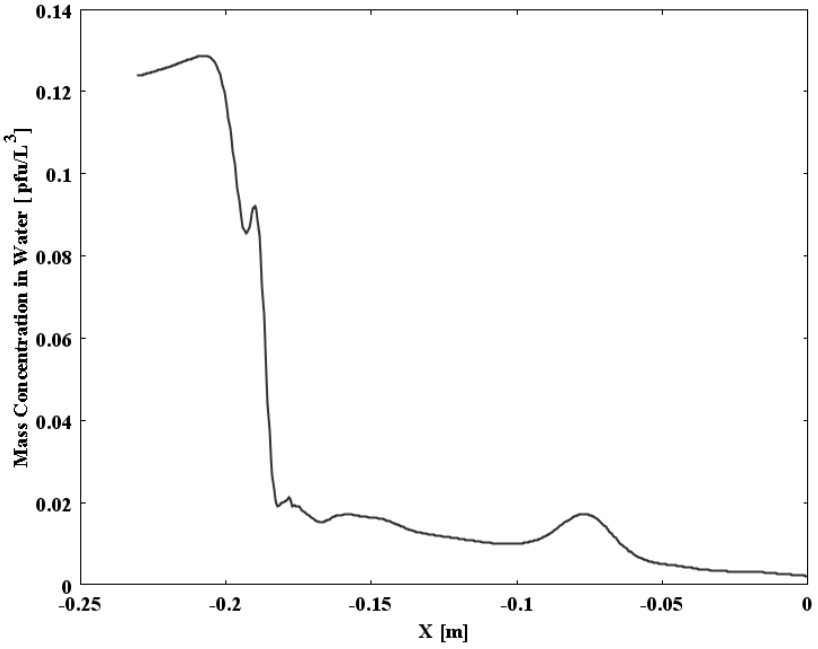
Mass Concentration in Water [pfu/L 3]
0.14
0.12
0.1
0.08
0.06
0.04
0.02
0
-0.25
-0.2
-0.15
-0.1
-0.05
0
X [m]

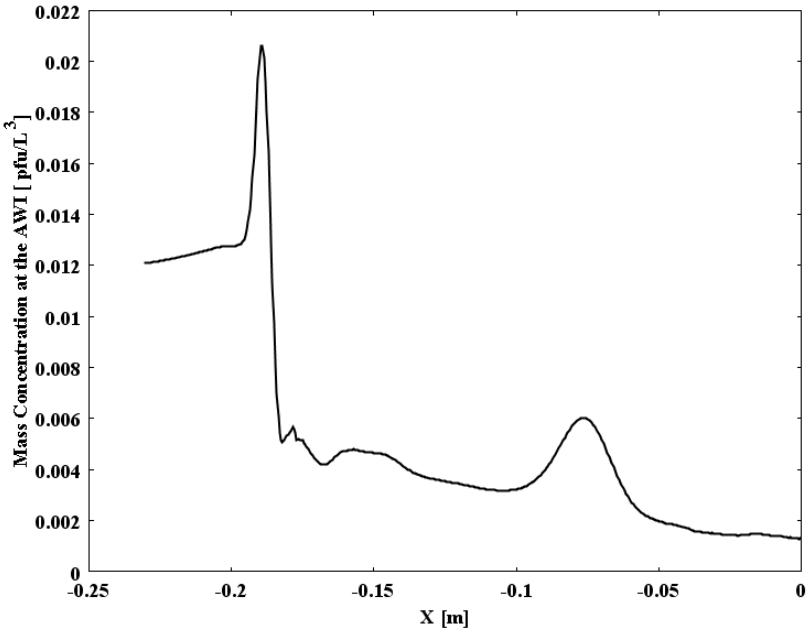

Fig. 3.6. *Profiles of amount of viruses being retained at the SWI ($\rho_b C_s$), in water (θC_w), and at the AWI (aC_{aw}).*

One point needing emphasis is that the experiments of Torkzaban et al. (2006a, b) showed that steady-state attachment coefficients obtained from experiments carried out at different fluid saturations are different (see Table 3.1). This means that in drainage/imbibition experiments, the steady-state attachment coefficients k_{att}^{s} and k_{att}^{a} should be some function of fluid saturation. As such we included in our transient simulations a linear dependence of the attachment coefficient on saturation. However, comparison of results with the constant-attachment model simulations showed very little difference. This may have been due to the large values of the transient detachment coefficients, which may have obscured any variations in the attachment coefficients (causing them to have little effect on the results).

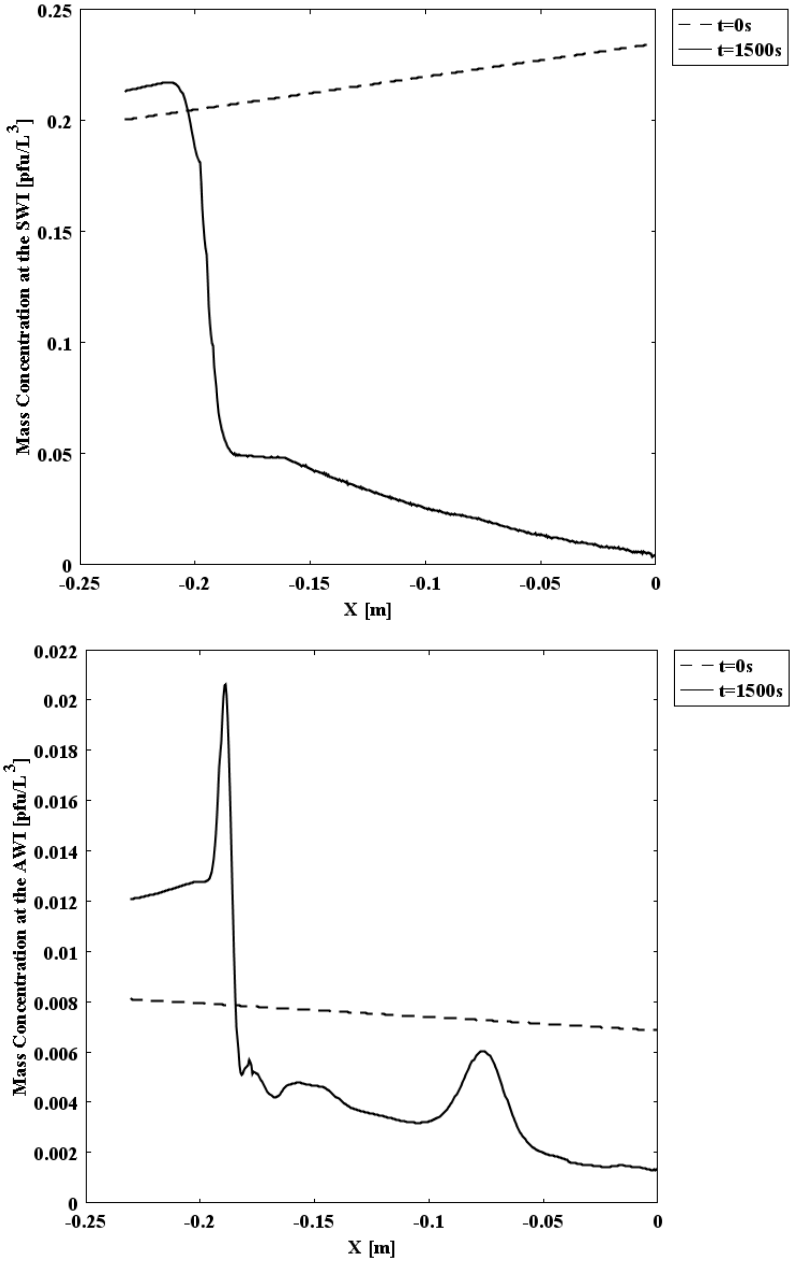

Fig. 3.7. *Concentration profiles of viruses at the SWI and AWI. Dashed lines represent concentration profiles at the very beginning of the remobilization simulation. Solid lines represent concentration profiles at the end of the remobilization simulation.*

In this paper we studied the effect of fluid saturation changes on colloid remobilization at the column scale. As noted by Bradford et al. (2009), among others, column scale analysis, especially if limited to breakthrough curves, provide only limited information about the exact processes involved. While important, such column scale studies may need to be augmented with more intricate pore-scale theoretical and experimental studies to more precisely identify the underlying processes responsible for colloid remobilization during transient imbibition and drainage events. Additional research is also needed to investigate the applicability of the model of Cheng and Saiers (2009), or the formulations developed in this paper, for virus transport in structured field soils, as well as for two- or three- dimensional flow conditions. It is further worth noting that recent studies by Sadeghi et al. (2011) have shown that transient changes in water chemistry also result in the remobilization of adsorbed viruses. It would be important to investigate which other transient effects may have similar consequences for virus transport in soil systems.

Acknowledgements

Saeed Torkzaban（CSIRO, Adelaide, Australia）is gratefully acknowledged for providing the experimental data. We are thankful to Jack Schijven (National Institute of Public Health and the Environment, the Netherlands) and Vahid Joekar-Niasar (Utrecht University, Netherlands) for very helpful discussions. Financial help for the first author by the China Scholarship Council is greatly appreciated. We are thankful to Sabine Goldberg (VZJ associate editor) and three anonymous reviewers for their critical comments and valuable recommendations that helped to improve our manuscript. The first three authors are members of the International Research Training Group NUPUS, financed by the German Research Foundation (DFG) and Netherlands Organization for Scientific Research (NWO).

References

(1) **Boks**, N.P., W. Norde, H.C. van der Mei, and H.J. Busscher. 2008. Forces involved in bacterial adhesion to hydrophilic and hydrophobic surfaces. Microbiol. 154:3122-3133.

(2) **Bradford**, S.A., and F. J. Leij. 1997. Estimating interfacial areas for multi-fluid soil systems. J. Contam. Hydrol. 27:83-105.

(3) **Bradford**, S.A., S. Torkzaban, F.J. Leij, J. Šimůnek, and M.Th. van Genuchten.

2009. Modeling the coupled effects of pore space geometry and velocity on colloid transport and retention. Water Resour. Res. 45, W02414, doi: 10.1029/2008WR007096.

(4) **Cheng** T., and J.E. Saiers. 2009. Mobilization and transport of in situ colloids during drainage and imbibition of partially saturated porous media. Water Resour. Res. 45, W08414, doi: 10.1029/2008WR007494.

(5) **Chu**, Y., Y. Jin, M. Flury, and M.V. Yates. 2001. Mechanisms of virus removal during transport in unsaturated porous media. Water Resour. Res. 37 (2): 253-263, doi: 0043-1397/01/2000WR900308.

(6) **COMSOL**. 2006. COMSOL Multiphysics 3.5a. COMSOL Inc., Burlington, MA, USA.

(7) **Crist**, J.T., J.F. McCarthy, Y. Zevi, P. Baveye, J.A. Throop, and T.S. Steenhuis. 2004. Pore-scale visualization of colloid transport and retention in partly saturated porous media. Available at www.vadosezonejournal.org. Vadose Zone J. 3:444-450.

(8) **Crist**, J.T., Y. Zevi, J.F. McCarthy, J.A. Troop, and T.S. Steenhuis. 2005. Transport and retention mechanisms of colloids in partially saturated porous media. Vadose Zone J, 4:184-195.

(9) **DeNovio**, N.M., J.E. Saiers, and J.N. Ryan. 2004. Colloid movement in unsaturated porous media: Recent advances and future directions. Vadose Zone J., 3:338-351.

(10) **Gao**, B., J.E. Saiers, and J. N. Ryan. 2006. Pore-scale mechanisms of colloid deposition and mobilization during steady and transient flow through unsaturated granular media, Water Resour. Res. 42, W01410, doi: 10.1029/ 2005WR004233.

(11) **Gómez-Suárez**, C., J. Noordmans, H.C. van der Mei, and H.J. Busscher. 1999a. Detachment of colloidal particles from collector surfaces with different electrostatic charge and hydrophobicity by attachment to air bubbles in a parallel plate flow chamber. Phys. Chem. Phys., 1: 4423-4427.

(12) **Gómez-Suárez**, C., J. Noordmans, H.C. van der Mei, and H.J. Busscher. 1999b. Removal of colloidal particles from quartz collector surfaces as stimulated by the passage of liquid-air interfaces. Langmuir, 15: 5123-5127.

(13) **Gómez-Suárez**, C., H.J. Busscher, and H.C. van der Mei. 2001a. Analysis of bacterial detachment from substratum surfaces by the passage of air-liquid interfaces. Appl. Environ. Microbiol, 67(6): 2531-2537.

(14) **Gómez-Suárez** C., H.C. van der Mei, and H.J. Busscher. 2001b. Air bubble-induced detachment of polystyrene particles with different sizes from collector surfaces in a parallel plate flow Chamber. Colloids and Surfaces A: Physicochemical and Engineering Aspects, 186(3): 211-219.

(15) **Goyal**, S.M., B.H. Keswick, and C.P. Gerba. 1984. Viruses in groundwater beneath sewage irrigated cropland. Water Res. 18: 299-302

(16) **Hassanizadeh**, S.M., and W.G. Gray. 1993. Thermodynamic basis of capillary pressure in porous media, Water Resour. Res., 29: 3389-3405 doi: 0043-1397/93/93WR-01495

(17) **Houck**, C.R., J.A. Joines, and M.G. Kay. 1995. A genetic algorithm for function optimization: A Matlab implementation. Technical Report NCSU-IE-TR-95-09, North Carolina State University, Raleigh, NC.

(18) **Joekar-Niasar**, V., M. Prodanovic, D. Wildenschild, and S.M. Hassanizadeh. 2010a. Network model investigation of interfacial area, capillary pressure and saturation relationships in granular porous media. Water Resour. Res., 46, doi: 10.1029/2009WR008585.

(19) **Joekar-Niasar**, V., S.M. Hassanizadeh, and H.K. Dahle. 2010b. Non-equilibrium effects in capillarity and interfacial area in two-phase flow: Dynamic pore-network modelling, J. Fluid Mech., doi: 10.1017/S0022112010000704.

(20) **Keller**, A.A., and M. Auset. 2007. A review of visualization techniques of biocolloid transport processes at the pore scale under saturated and unsaturated conditions. Adv. Water Resour. 30:1392-1407.

(21) **Keswick**, B.H., and C.P. Gerba. 1980. Viruses in ground water. Environ. Sci. Technol. 14:1290-1297.

(22) **Kim**, H., P.S.C. Rao, and M.D. Annable. 1999. Gaseous tracer technique for estimating air-water interfacial areas and interface mobility. Soil Sci. Soc. Am. J. 63:1554–1560.

(23) **Leenaars**, A.F.M., and S.B.G. O'Brien. 1989. Particle removal from silicon substrates using surface-tension forces. Philips J. Res., 44:183-209.

(24) **Luckner**, L., M.Th. van Genuchten, and D.R. Nielsen. 1989. A consistent set of parametric models for the two-phase flow of immiscible fluids in the subsurface. Water Resour. Res., 25 (10): 2187-2193, doi: 0043-1397/89/89WR-01269.

(25) **Marle**, C.M., 1981. From the pore scale to the macroscopic scale: Equations governing multiphase fluid flow through porous media, in Proceedings of Euromech 143, edited by A. Verruijt and F.B.J Barends, pp. 57-61, A. A Balkema, Rotterdam, the Netherlands.

(26) **Oostrom**, M., M.D. White, and M.L. Brusseau. 2001. Theoretical estimation of free and entrapped nonwetting-wetting fluid interfacial areas in porous media. Adv. Water Resour. 24:887-898.

(27) **Ouyang**, Y., D. Shinde, R.S. Mansell, and W. Harris. 1996. Colloid enhanced transport of chemicals in subsurface environments: A review, Crit. Rev. Environ. Sci. Technol., 26: 189-204, doi: 10.1080/10643389609388490.

(28) **Pyrak-Nolte**, L.J., D.D. Nolte, D. Chen, and N.J. Giordano. 2008. Relating capillary pressure to interfacial areas, Water Resour. Res., 44, W06408, doi: 10.1029/2007WR006434.

(29) **Powelson**, D.K., J.R. Simpson, and C.P. Gerba. 1990. Virus transport and survival in saturated and unsaturated flow through soil columns. J. Environ. Qual. 19: 396–401.

(30) **Powelson**, D.K., and A.L. Mills. 2001. Transport of Escherichia in sand columns with constant and changing water contents. J. Environ. Qual. 30: 238-245.

(31) **Raoof**, A., and S.M. Hassanizadeh. 2010. A new method for generating pore-network models of porous media. Transp. Porous Media. 81: 391-407.

(32) **Robinson**, D.A., and S.P. Friedman. 2001. The effect of particle size distribution on the effective dielectric permittivity of saturated granular media. Water Resour. Res., 37: 33-40, doi: 10.1029/2000WR900227.

(33) **Ryan** J.N., T.H. Illangasekare, M.I. Litaor, and R. Shannon. 1998. Particle and plutonium mobilization in macroporous soil during rainfall simulations. Environ. Sci. Technol., 32: 476-482.

(34) **Saiers**, J.E., and J.J. Lenhart. 2003. Colloid mobilization and transport within unsaturated porous media under transient-flow conditions, Water Resour. Res., 39(1): 10-19, doi: 10.1029/2002WR001370.

(35) **Sadeghi** G., J.F. Schijven, T. Behrends, S.M. Hassanizadeh, J. Gerritse, and P.J. Kleingeld. 2011. Systematic study of effects of Ph and ionic strength on attachment of phage PRD1. Ground Water, 49, doi: 10.1111/j.1745-6584.2010.00767.x.

(36) **Schaap**, M.G., F.J. Leij and M.Th. van Genuchten. 2001. Rosetta: A computer program for estimating soil hydraulic parameters with hierarchical pedotransfer functions. J. Hydrol. 251: 163-176.

(37) **Schijven** J.F., and S.M. Hassanizadeh. 2000. Removal of viruses by soil passage: Overview of modeling, processes, and parameters. Crit. Rev. Environ. Sci. Technol, 30:49-127.

(38) **Simunek** J., M. Sejna, and M.Th. van Genuchten. 1998. The Hydrus-1D software package for simulating the one-dimensional movement of water, heat, and multiple solutes in variably-saturated media, Version 2.0., USDA-ARS, U.S. Salinity Laboratory, Riverside, CA.

(39) **Shang**, J., M. Flury, G. Chen, and J. Zhuang. 2008. Impact of flow rate, water content, and capillary forces on in situ colloid mobilization during infiltration in unsaturated sediments. Water Resour. Res. 44, doi: 10.1029/2007WR006516.

(40) **Sharma**, P., M. Flury, and J. Zhou. 2008a. Detachment of colloids from a solid surface by a moving air-water interface. J. Colloid and Interface Sci. 326: 143-150.

(41) **Sharma**, P., H.M. Abdou, and M. Flury. 2008b. Effect of the lower boundary condition and flotation on colloid mobilization in unsaturated sandy sediments, Vadose Zone J. 7:930-940.

(42) **Sharma**, P.K., M.J. Gibcus, H.C. van der Mei, and H.J. Busscher. 2005. Influence of

fluid shear and micro bubbles on bacterial detachment from a surface. Applied and Environ. Microbiol. 71(7): 3668-3673.

(43) **Sirivithayapakorn**, S., and A.A. Keller. 2003. Transport of colloids in unsaturated porous media: A pore-scale observation of processes during the dissolution of air-water interface. Water Resour. Res. 39(12), 1346, doi: 10.1029/2003WR002487

(44) **Torkzaban**, S., S.M. Hassanizadeh, J.F. Schijven, A.M. de Bruin, and A.M. de Roda Husman. 2006a. Virus transport in saturated and unsaturated sand columns. Vadose Zone J. 5: 877-885.

(45) **Torkzaban**, S., S.M. Hassanizadeh, J.F. Schijven, and H.H.J.L. van den Berg. 2006b. Role of air-water interfaces on retention of viruses under unsaturated conditions. Water Resour. Res., 42, W12S14, doi: 10.1029/2006WR004904.

(46) **van Genuchten**, M.Th. 1980. A closed-form equation for predicting the hydraulic conductivity of unsaturated soils. Soil Sci. Soc. Am. J, 44:892-898.

(47) **Wan** J., and T.K. Tokunaga. 1998. Measuring partition coefficients of colloids at air-water interfaces. Environ. Sci. Technol, 32:3293-3298.

(48) **Yates**, M.V., S.R. Yates, J. Wagner, and C.P. Gerba. 1987. Modeling virus survival and transport in the subsurface. J. Contam. Hydrol. 1:329-345.

(49) **Zhuang**, J., J.F. McCarthy, J.S. Tyner, E. Perfect, and M. Flury. 2007. In situ colloid mobilization in Hanford sediments under unsaturated transient flow conditions: Effect of irrigation pattern. Environ. Sci. Technol., 41: 3199- 3204, doi: 10.1021/es062757h.

(50) **Zhuang**, J., J.S. Tyner, E. Perfect. 2009. Colloid transport and remobilization in porous media during infiltration and drainage. J. Hydrol. 377:112-119.

Chapter 4

Visualization of Colloid Transport in a Micro-Model; Methods and Materials

Abstract

As a representation of a porous medium, a closed micro-fluidic device made of polydimethylsiloxane (PDMS), with uniform wettability and stable hydrophobic properties, was designed and fabricated. A flow network, with a mean pore size of 40 microns, was formed in a PDMS slab, covering an area of $1mm \times 10mm$. The PDMS slab was covered and bonded with a 120-micron-thick glass plate to seal the model. The glass plate was first spin-coated with a thin layer, roughly 10 microns, of PDMS. The micro-model was treated with silane in order to make it uniformly and stably hydrophobic. Fluorescent particles of 300nm in diameter were used as colloids.

It is known that more removal of colloids occurs under unsaturated conditions, compared to saturated flow in soil. At the same time, the change of saturation has been observed to cause remobilization of attached colloids. The mechanisms for these phenomena are not well understood. This is the first time that a closed micro-model, made of PDMS with uniform and stable wettability, has been used in combination with confocal microscopy to study colloid transport under transient two-phase flow

Published as: Zhang, Q.L., N.K. Karadimitriou, S.M. Hassanizadeh, P. J. Kleingeld, and A. Imhof, 2013, Study of Colloids Transport during Two-Phase Flow using a Novel Polydimethylsiloxane Micro-model, J. Colloid Interface. Sci.:10.1016/j.jcis.2013.02.04.

conditions. With confocal microscopy, the movement of fluorescent particles and flow of two liquids within the pores can be studied. One can focus at different depths within the pores and thus determine where the particles exactly are. Thus, remobilization of attached colloids by moving fluid-fluid interfaces was visualized. In order to allow for the deposition and subsequent remobilization of colloids during two-phase flow, three micro-channels for the injection of liquids with and without colloids were constructed. An outlet channel was designed where effluent concentration breakthrough curves can be quantified by measuring the fluorescence intensity. A peak concentration also indicated in the breakthrough curve with the drainage event. The acquired images and breakthrough curve successfully confirmed the utility of the combination of such a PDMS micro-model and confocal microscopy for the visualization of colloid transport in a flow network filled with two fluids, and in particular, the colloids retention, mobilization, and transport under transient flow conditions.

4.1 Introduction

As a representation of a porous medium, micro-models are commonly employed to study and visualize physical, chemical, and biological processes at the pore scale. During the last few decades, micro-models have proven to be a valuable tool for the study and observation of flow of fluids and transport of solutes within the pore space. They have been increasingly used to study diverse applications, such as energy-related multiphase transport in porous media [1], reservoir engineering [2], and two-phase flow experiments [3-11]. An extensive review of micro-models and their use in two-phase flow research can be found in Karadimitriou and Hassanizadeh [12], including fabrication methods, materials used, and visualization techniques.

The use of micro-chips in colloids transport is a relatively recent development. So far, mostly, an open micro-channel combined with microscopy has been used to study colloids transport [13], [14], [15], [16] and [17], where visualization is relatively simple. But, micro-channels are too simple and in particular, various two-phase phenomena occurring in a porous medium will not occur there. One needs to have a network containing a large number of pores. Pioneering visualization experiments on colloid retention in unsaturated media were performed by Wan and Wilson [18] and [19] in glass micro-models under optical microscopy with fluorescent lighting system. In their system,

the air phase was stagnant and water phase flowed at steady state. Later on, etched glass micro-models were used by other research groups [20] and [21] to study colloids movement at pore scale with optical microscopy, the interaction of colloids and air bubble under steady-state was visualized. Also, silicon micro-models have been used to study colloids hydrodynamic behaviors in saturated medium [22]. PDMS micro-fluidics has been used in biochemical engineering applications [23], blood micro-particles distribution [24], and multiphase/two phase flow in porous media. Compared to glass and silicon, a soft material like PDMS is more suitable for making inexpensive micro-models by rapid prototyping [25].

One of the open questions in the transport of colloids in unsaturated porous media and/or in two-phase flow is the role of fluid-fluid interfaces, as well as fluids-solid contact line, in the attachment and remobilization of colloids. Optical microscopy provides a lumped image of the whole channel depth. But, in order to investigate the interactions between colloids and fluid-fluid interfaces and/or contact lines in a two-fluid system, one needs to focus and get images at various depths within the pore space. This can be achieved with a confocal microscope. Confocal microscopy is a point-by-point visualization method. One of the fluids should either be dyed with fluorescent dyes or contain some fluorescent particles. With confocal microscopy, the sample can be tracked spatially in three dimensions by superposing two dimensional images taken at sequential z stacks [26] (z being the coordinate in the depth). Furthermore, it allows real-time information about the complex mechanisms under dynamic conditions. However, confocal microscopes have a limited depth of view. Generally, they give good results for a depth of view up to 250 microns [27]. That is the reason that mostly open micro-channels have been used in studies involving confocal microscopy; a cover plate takes up much of the depth of view and thus a very limited depth of the channel can be visualized.

In this work, we describe the design and fabrication of a closed PDMS micro-model, following a procedure described by Xia and Whitesides [28]. PDMS micro-models are very cheap to produce, and can be made under normal laboratory conditions (so, for example, a clean room is not needed). Moreover, the PDMS micro-model that we designed and manufactured had some important properties that are usually lacking in other PDMS models. First, the micro-model was made uniformly and stably hydrophobic. Second, the model was sealed with a very thin glass plate, coated with a film of PDMS. This made it possible to focus at locations throughout the whole depth of the model (30 microns). Third, the system of injection of fluids, with and without

colloids, was constructed such as to avoid mixing of fluid phases at the entrance. Fourth, the inner surfaces of the pores were all PDMS. This made sure that the fluids would experience the same wetting properties everywhere; there was no mixed wettability.

To the best of our knowledge, this is the first application of PDMS micro-model combined with confocal laser scan microscopy to study the movement of fluorescent particles in a flow network. It is also the first study of colloids transport in a porous network with transient flow two immiscible liquids. Acquired images were used to analyze colloids interaction with liquid phases, fluid-fluid and fluid-solid interfaces, as well as with the fluids-solid contact lines.

4.2 Experimental Setup, Materials, and Methods

4.2.1 Liquids and particles

As mentioned above, we were interested in generic studies of the fate of adsorbing colloidal particles under transient two-phase flow conditions. So, it is not crucial which phase is the wetting phase and which one is the nonwetting. As the two immiscible fluids, we selected deionized water and Fluorinert FC-43(3M). Given the fact that our PDMS micro-model was hydrophobic, water was the non-wetting phase and fluorinert was the wetting phase. The fluorinert liquid type was chosen such that it had nearly the same index of refraction as water (1.291 and 1.332, respectively, at 20℃). Carboxylated fluorescent microspheres (Polysciences Inc. GmbH), with an average diameter of 300nm were used as model colloids. They were hydrophilic and weakly negatively charged at neutral pH and were labeled with fluorescein. We were interested in colloid transport and mobilization under transient hydraulic conditions.

4.2.2 The flow network

A two-dimensional pore network was designed using Delaunay triangulation. Delaunay triangulation is considered to be a good representation of a natural porous medium [29]. The network comprised an assembly of pore bodies (large pores) connected to each other by smaller pores, called pore throats. In Delaunay triangulation, points are connected to their neighbors by non-intersecting bonds. Connected points form triangles that are as equilateral as possible. The coordinates of the triangulation points were

generated in MatLab. These points were considered to be the centers of the pore bodies. The network was then exported to AutoCAD sketch for further processing. An outlet channel, along with three inlet channels for the introduction of the fluids and the colloids, was added to the same sketch and connected to the end of the network.

As can be seen in Fig. 4.1., the final design of the micro-model had five parts: (1) three inlet reservoirs (each 0.5mL in volume); (2) three inlet channels (6*mm* in length, 0.5*mm* in width and 30μm in depth) for the wetting phase, the non-wetting phase, and the colloid suspensions in non-wetting phase; (3) the flow network; (4) the outlet channel; (5) the outlet reservoir. The overall network dimensions were 1 mm by 10 mm, with 90 pore bodies and roughly 200 pore throats. The mean diameter of pore bodies was 40 μm. This was also the depth of all parts of the network, which was measured and found to be constant within a margin of 0.5% throughout the micro-model. The diameter of pore throats was between 25 μm to 30 μm. The outlet channel, as well as the outlet reservoir had some pillars (white strips) added for structural strength. Given the aspect ratio between the width and the depth of the channel and the reservoir, without the pillars the top surface would collapse [30].

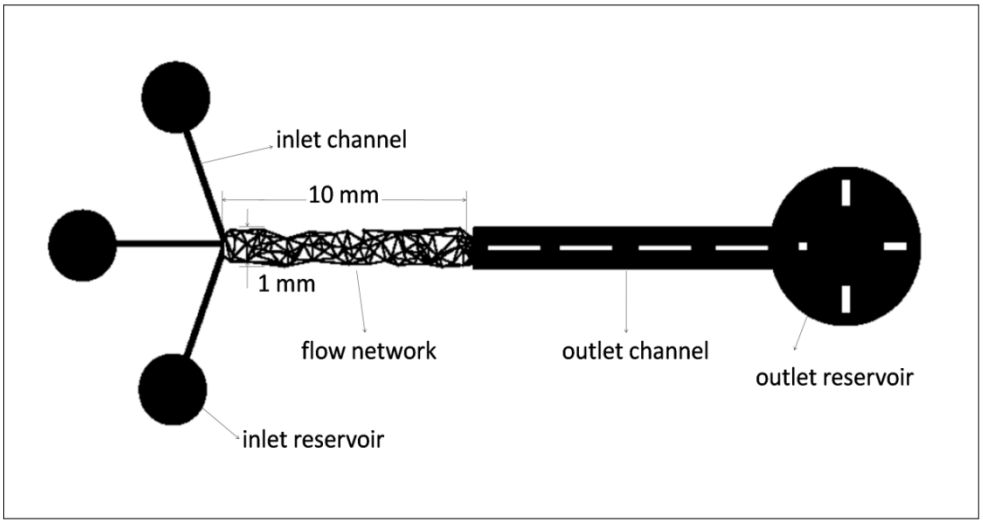

Fig. 4.1. *Schematic representation of the micro-model (not to scale).*

4.2.3 Fabrication of the micro-model

Here, the fabrication of the micro-model is briefly explained. A detailed description of

the procedure is given by Karadimitriou et al. (2012) [10]. The pore network pattern was printed on a high-resolution mask (made by CAD/Art Services, Oregon, USA). The resolution of the mask was 20,000 dpi. The mask was used to etch the flow network on a silicon wafer. This was done in a class-10,000 clean room (Kavli Institute of Nanoscience, Delft). Using the wafer, a soft-lithographic procedure was employed and the flow network with the reservoirs was formed in a PDMS slab. A 120-microns-thick glass plate from Menzel-Glaeser was then used to seal the model. The glass plate was pre-coated with a very thin layer of PDMS (less than 10 microns) with the use of a spin coater (Laurell Technologies). In this way, the phases involved in the experiments would experience the same wetting properties of the solid phase throughout the whole network. The sum of PDMS-coated glass plate thickness and the flow channel depth was kept below 250 microns. Thus, the whole channel depth was fully within the working distance of the confocal microscope. The bonding of the PDMS slide and the sealing glass slide was achieved following a corona treatment procedure. Thereafter, the model was left in an oven overnight at 68℃ to enforce bonding. The constructed micro-model was shown in Fig. 4.2.

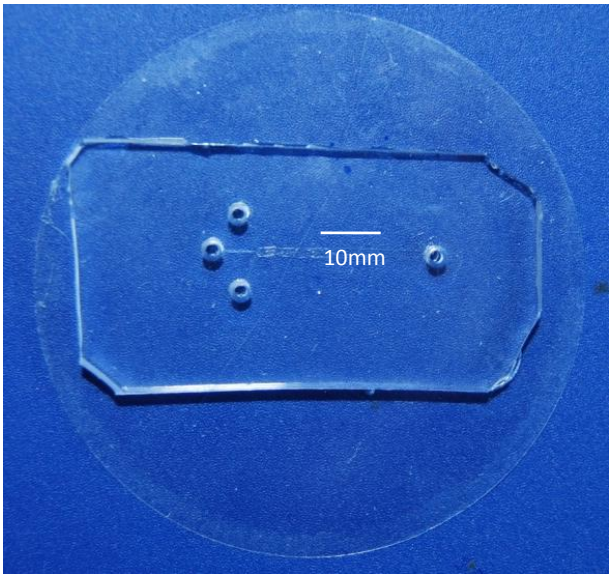

Fig. 4.2. *Picture of the micro-model. The three inlet reservoirs, the outlet reservoir, and the flow network are visible.*

4.2.4 Silanization of the micro-model

Since PDMS is a polymeric material, its wetting properties may change with time. However, after bonding, the treated PDMS becomes hydrophilic but not stably; it degrades with time and eventually recovers its hydrophobicity. This effect starts almost immediately after exposure, and it continues until reaching the initial condition [31, 32]. In order to make the wettability of the model uniform and stable, the micro-model was silanized with the use of a solution of Trichloro-perfluoro-octyl-silane and 96% pure ethanol. The solution was prepared in a small air-proof beaker, and thoroughly stirred with a stirring machine. One milliliter of the solution was taken out of the beaker with a 1-ml Terumo syringe. The syringe was then put in a syringe pump, and the solution was injected into the flow network at the flow rate of 3μl/min. We let the solution flow through the flow network for half an hour. Then, the model was put in an oven at 68℃ and was left overnight to dry out. This silanization process ensured that the micro-model became permanently and uniformly hydrophobic; even after months of use, the PDMS surface remained unchanged with time. Given that the model was hydrophobic, water was the non-wetting phase, while fluorinert was the wetting one. Using the software *ImageJ*, the contact angle between FWI and PDMS solid surface was measured to be between 0 °and 4 °[33].

4.3 Experimental Setup

The experimental setup for the visualization of colloids movement (shown in Fig. 4.3) consisted of the following components.

1) Injection system: It comprised a dual-direction syringe pump (Harvard Apparatus GmbH), two syringes, a three-way valve, three flow-regulated reservoirs (volume of 0.5 mL each), and supply tubing (inner diameter of 0.15 mm). The dual-direction syringe pump could be used for both injection and withdrawal of fluids at highly-controlled small flow rates. The two syringes had volumes of 25 μL and 1 μL. The 1-μL syringe allowed us to control the flow rate in the range of 1 pL/min to 1 μL/min for displacement experiments. The bigger syringe was used for initial filling of the system with high flow rates.

The syringes, the three-way valve, and the lines up to the three flow-regulated reservoirs, as well as the flow-regulated fluorinert reservoir were filled with fluorinert at all times. The “fluorinert supply reservoir” ensured that the lines were always filled with

fluorinert. The lower parts of flow-regulated water reservoir and colloid-suspension reservoir were also filled with fluorinert, and the rest was filled with water and colloid-suspension, respectively. Using the three-way valve, we could select the desired liquid to be injected into or withdrawn from the micro-model. The fact that the pump was always operated with the same liquid meant that it needed one calibration curve only. The supply reservoirs ensured that the flow-regulated reservoirs always remained filled with their corresponding liquid.

2) The imaging system: It consisted of an inverted confocal laser scan microscope with oil immersion objective lens of 63× magnification (Leica TCS SP2, Heidelberg GmbH), with a numerical aperture of 1.4. We also used an oil immersion lens of 40× magnification with a numerical aperture of 1.25 during dynamic experiments. We used a 488-nm line of argon laser for excitation of fluorescent particles.

3) The PDMS micro-model: The model, described in previous section, was fixed on a support to prevent its movement under the fluid injection pressure. This assembly was placed horizontally on the stage of the microscope.

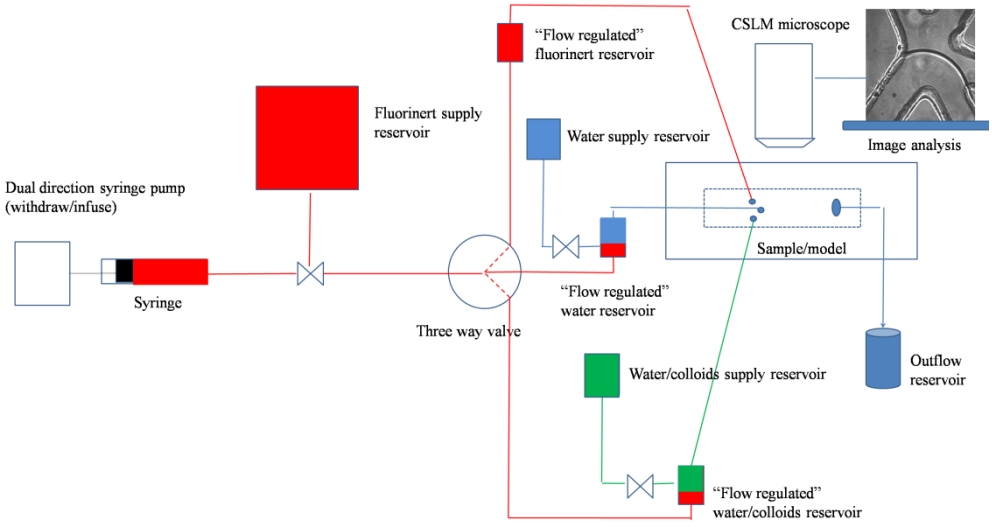

Fig. 4.3. *Schematic of the experimental set-up.*

4.4 Experimental procedure

At the beginning of the experiment, the micro-model contained air only. Using the syringe pump, fluorinert was introduced into the micro-model at a constant injection rate for an extended period to expel the air and saturate the model with fluorinert. Then,

de-ionized water containing colloids was injected at a constant flow rate until the model got to steady-state. Before injection, the colloids-water suspension was immersed in an ultrasound bath for 30 minutes to prevent coagulation. In this process, colloids-DI water suspension partly displaced the fluorinert phase to create the FWIs.
During transient experiments, following the steps described above, either water without colloids or fluorinert was injected into the micro-model to cause drainage or imbibition, respectively. The flow rate of the invading fluid was set to 50nL/min, which means the flow velocity of the FWI was around 25μm/s. Average duration of the experiments was approximately three hours.

4.5 Results and Discussion

4.5.1 Visualization of Colloid Retention under Quasi-static Conditions

Once fluorinert-water interfaces were created, images were taken focusing at various depths of the model. A set of still images taken at one location are shown in Figure 4.4. Image 4.4A was obtained by confocal microscopy in fluorescence mode, where only fluorescent particles were visualized. Then, in order to locate the particles relative to the flow network and the FWI, the same part of the flow network was also imaged by confocal microscopy in transmission mode (as shown in image 4.4B). Finally, image 4.4C was produced by the superposition of images 4.4A and 4.4B.

In images 4.4B and 4.4C, parts of three pore throats and one pore body are visible. The FWI can be clearly seen. Particles were found dispersed in the water, attached to the SWI, and retained at both FWI and FWSC. No particles were found in the fluorinert, since the particles are hydrophilic. This still image only represents the behavior of the colloids at the time when the picture was taken.

Colloids did not attach to the SWIs uniformly but in the form of clusters. This is in agreement with Zevi et al., [34] who observed that particles clustered on the sand grain surfaces. This is due to the roughness of the solid surface, where micro depressions provide favorable sites for colloids deposition [35] and [36].

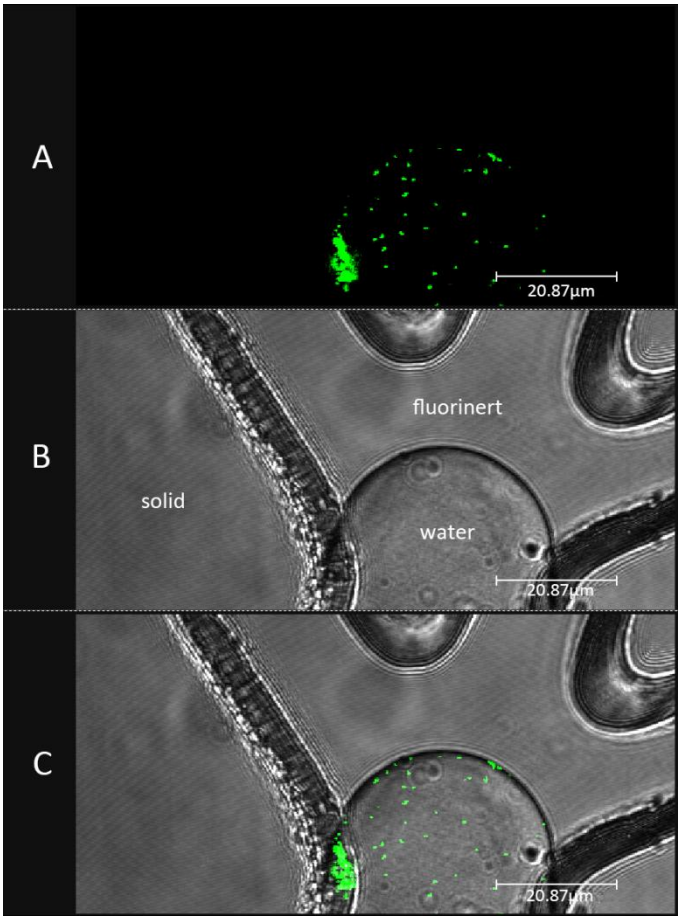

Fig. 4.4. *Colloid retention in fluorinert and water system (images with resolution of 512×256 pixels). Snapshots were taken in the middle section of the micro-model. Image C is the overlaid images of A and B. Green dots are fluorescent particles.*

In figure 4.5, we have focused on colloids accumulating at the FWSC. The two images are from exactly the same domain but taken 30 minutes apart. The accumulation is probably due to strong capillary forces at the FWI-PDMS contact line; the contact angle was measured to be less than 4°. Support for this explanation can be found in the force analysis by Shang and Flury [37]. Some of the colloids relocated and some were mobilized after 30 minutes. We measured the fluorescent intensities of the particles by using *ImageJ*; the results indicated that after 30 minutes around 20% of the particles were mobilized. According to the forces investigation by Shang et al. in 2008, we

speculated due to the local water film thickness changed, the filling angle of some particles vanished, then the capillary force exerting on varied as well. When the capillary force became repulsive force, the colloids were released and relocated accordingly.

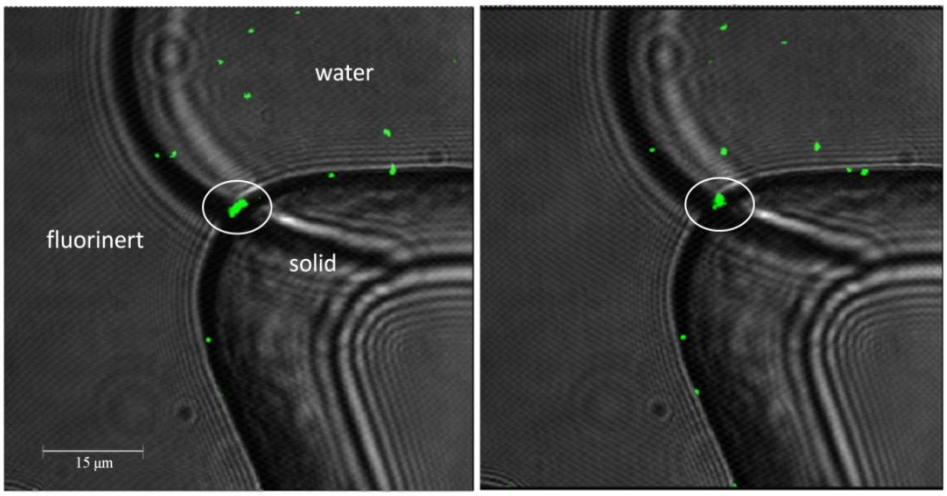

Fig. 4.5. *Retention of colloids at FWSC. The two images are from the same location, but 30 minutes apart, under no-flow conditions.*

The experiments were repeated, and similar behaviors of particles were observed. Images obtained showed that the micro-model can provide clear visualization of particles retention at fluid-fluid and fluid-solid interfaces, as well as fluids-solid contact lines in quasi-static two-phase system.

4.5.2 Visualization of Colloid Mobilization under Transient Conditions

After the deposition of colloids, the micro-model was drained; i.e. DI water (without colloids) was injected.

Real-time images were continuously captured while the moving FWI passed through our target area; see sequence of images shown in Fig. 4.6. Co-currently, we quantified the effluent colloids concentration breakthrough curve (as shown in Fig. 4.7.) by measuring the fluorescent intensities at the outlet channel. These images were captured at a speed of 2 frames per second, with a resolution of 512 by 512 pixels per inch. The non-wetting phase (DI water) entered the imaged domain from the upper left corner. The larger pore throat A (shown in figure 4.6a) was drained first, and then the smaller pore throat B.

Image 4.6a shows the initial distribution of the colloids just before the micro-model was drained. As can be seen, a significant number of particles had been deposited on the solid surface. Image 4.6b was taken 8 seconds later, as pore A was being invaded. Image 4.6c shows the micro-model after 20 seconds of interface moving, and image 4.6d is after pore A was completely drained. Images 4.6e through 4.6f were taken while pore throat B was being drained. Comparison of images 4.6a and 4.6h (especially at the position highlighted by the red circle) shows that that a large fraction of colloids were detached from the solid surface. Video images of these events, Movie 4.1 and Movie 4.2, are provided in the Auxiliary Materials. Agreed with the visualization results, quantitative breakthrough analyses showed that effluent concentration climbed rapidly and peaked shortly after the passage of drying fronts.

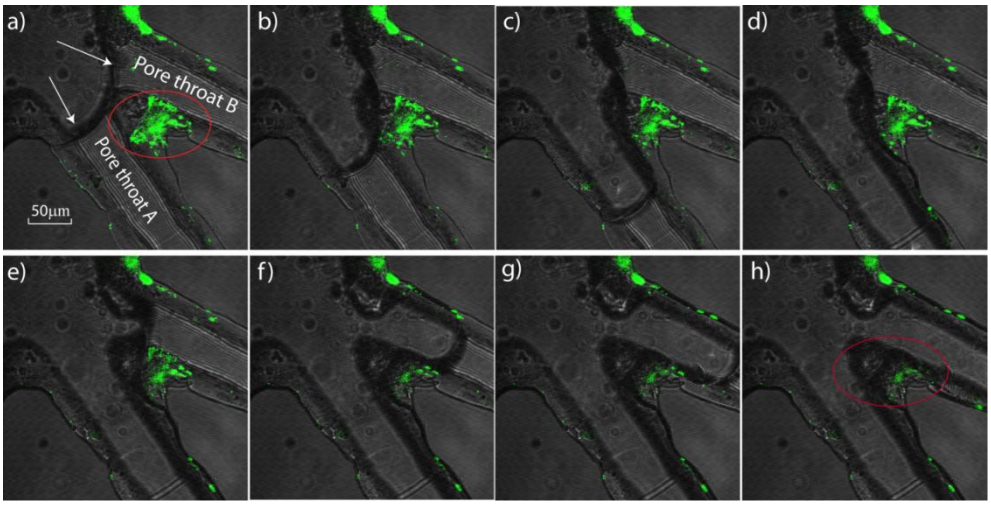

Fig. 4.6. *Transport of colloids with the moving FWI in the micro-model. Arrows stand for the flow direction.*

During dynamic processes, the particles were detached, and then transported either with FWIs and the FWSC. Gomez-Suarez et al. in 1999 [38] reported that the lower the velocity, the more contact time we have. Also in the work of Sharma et al. [39], the lower velocity was presented to create enough time for the particles to contact with the moving interface/contact line. Only when the contact time overcomes the induction time can attachment occur. The flow rate in our experiment had in the same order of

magnitude as in Sharma et al., so the contact time was enough as well, the capillary force exerting on the colloids exceeds the DLVO force, then mobilization occurs. But from the movies, one can also observe some colloids strained along the pore walls where probably there is a thin water film, which is agreement with the observation of Auset et al [40]. Besides, the surface roughness also has a significant effect on colloids attachment; since it can provide preferential sites for the deposition of the colloids [41]. According to findings of Auset and Keller in 2006 [42], surface roughness may also alter the streamlines. That's could be the reason that the particles on the top wall of pore throat B were not clearly detached. Force balance and torque balance computations will be performed in order to explain these processes.

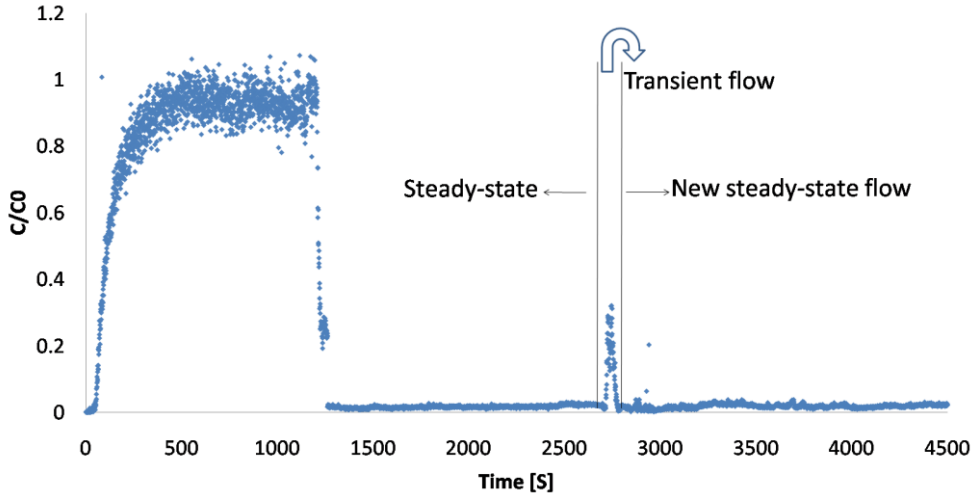

Fig.4.7. *Measured effluent colloid concentration breakthrough curve of the micro-model.*

4.6 Summary

In this work, a closed micro-fluidic device made of PDMS, with uniform wettability and stable hydrophobic properties was designed and constructed. The use of this micro-model, in combination with confocal microscopy was demonstrated; for the study of colloids transport during two-phase flow in a porous medium.

Water and 3M fluorinert^{TM} FC-43 were used as two immiscible phases with nearly the same index of refraction. Colloids transport in the micro-model under both quasi-static and transient conditions were studied. The behavior of colloids in the

micro-model was monitored with a confocal microscope. The use of transparent PDMS micro-models and confocal microscopy provides clear images at the pore scale.

The setup made it possible to perform both quasi-static and dynamic experiments and attachment/detachment of particles in partially-saturated porous media. Three separate inlet channels allowed the injection of fluids without mixing them. Colloids retention at the fluorinert-water interfaces (FWIs), water-solid interfaces (WSIs) and fluorinert-water-solid contact lines (FWSCs) were clearly visible. It was observed that FWSCs act as the major retention sites for colloids. Under transient conditions, mobilization of deposited colloids from the solid surface was clearly visualized. Co-currently a concentration peak was indicated in the effluent breakthrough curve. The images and breakthrough curve confirm the utility of such PDMS micro-model and confocal microscopy for the study of colloids transport in porous media.

Acknowledgements

We would like to acknowledge Dr. Bing Liu and Bo Peng (both from Debye Institute, Utrecht University) for training the first author on the confocal microscope. Financial support was provided by the China Scholarship Council (CSC) to the first author. The first three authors are members of the International Research Training Group NUPUS, financed by the German Research Foundation (DFG) and Netherlands Organization for Scientific Research (NWO). We are grateful to the two anonymous reviewers for their thoughtful suggestions and comments for revision that improved the presentation of our work.

References

(1) **Berejnov**, V., Djilali, N., and Sinton, D, Lab on a Chip, 2008, 8, 689-693.
(2) **Naga Siva**, G., Bera, B., Karadimitriou, N. K., Mitra, S. K., and Hassanizadeh, S.M., Lab on a Chip, 2011, doi: 10.1039/C1LC20556K.
(3) **Chatenever**, A. and Calhoun Jr., J.C. (1952), Petroleum Transactions, 1952, AIME 195, pp. 149–156.
(4) **Chen**, J.-D., and Wilkinson D, Phys. Rev. Lett., 1985, 55, pp. 1892-1895.
(5) **Wan**, J., Togunaga, T.K., Tsang, C.F. and Bodvarsson, G.S., Water Resources Research, 1996, 32, pp. 1964–1995.
(6) **Tóth**, T., D. Horváth, and Á. Tóth, J. Chem. Phys., 2007, 127, 234506.
(7) **Chang**, L.-C., J.-P. Tsai, H.-Y. Shan, H.-H. Chen, Environ Earth Sci, 2009, 59:901-911, doi: 10.1007/s12665-009-0085-6.

(8) **Dawe**, R.A., Caruana, A., Grattoni, C.A., Transp. Porous Media. 2010, doi: 10.1007/s11242-010-9642-4.
(9) **Karadimitriou**, N. K., V. Joekar-Niasar, S.M. Hassanizadeh, P. J. Kleingeld, and L.J. Pyrak-Nolte, Lab on a Chip, 2012, doi: 10.1039/C2LC40530J.
(10) **Wu**, M., Xiao, F., Johnson-Paben R.M., Retterer S.T., Yin X., and Neeves K.B., Lab on a Chip, 2012, 12, 253-261.
(11) **Karadimitriou**, N. K., and S.M. Hassanizadeh, A review of micro-models and their use in two-phase flow studies, Vadose Zone J., 2012, doi:10.2136/vzj2011.0072.
(12) **Lazouskaya**, V., Y. Jin, and D. Or, J. Colloid Interface Sci., 2006, 303, 171-184.
(13) **Lazouskaya**, V., and Y. Jin, Colloids Surf. A, 2008, 325, 141-151.
(14) **Lazouskaya**, V., L-P. Zhang, H.Gao, X. Shi, K. Czymmek, and Y. Jin, Vadose Zone J., 2011, 10, 1250-1260.
(15) **Wang**, F., C. H. Chon, and D. Li, J. Colloid Interface Sci., 2010, 352, 580-584.
(16) **Aramrak**, S., M. Flury, and J.B. Harsh, Langmuir, 2011, 27, 9985-9993.
(17) **Wan**, J., and J. L. Wilson, Water Resour. Res., 1994a, 30, 857-864.
(18) **Wan**, J., and J. L. Wilson, Water Resour. Res., 1994b, 30, 11-23.
(19) **Lanning**, L. M., and R. M. Ford, Biotechnol. Bioeng., 2002, 78, 556-566.
(20) **Chen**, G., and M. Flury, Colloids and Surfaces A: Physicochem. Eng. Aspects, 2005, 256, 207-216.
(21) **Baumann** T, Werth CJ, Vadose Zone J., 2004, 3, 434-443.
(22) **Fujii** T., Microelectronic Engineering, 2002, 907-914.
(23) **Ashcroft** B. A., J. de Sonneville, Y. Yuana, S. Osanto, R. Bertina, M. E. Kuil, and T. H. Oosterkamp, Biomed Microdevices, 2012, 14, 641-649.
(24) **Quake**, S. R., and A. Scherer, Science, 2000, 290, 1536-1540.
(25) **Prasad**, V., D Semwogerere, and Eric R Weeks, J. Phys.: Condense. Matter, 2007, 19, doi: 10.1088/0953-8984/19/11/113102.
(26) **Ekman** J. and D. Zhang, Introductions for Leica SP2 Confococal Microscope, 2011.
(27) **Xia**, Y. and Whitesides, G. M., Soft Lithography, Angewandte Chemie International Edition, 1998, 37: 550–575.
(28) **Heiba**, A., Sahimi, M., Scriven, L., and Davis, H., SPE Reserv. Eng., 1992, 7, 123-132.
(29) **Bietsc**h, A. and Michel, B, J. Appl. Phys, 2000, 88, 4310-4318.
(30) **Friz**, J. L., and M. J. Owen, Journal of Adhesion, 1995, 54, 33-45.
(31) **Murakami**, S. I., T. Kuroda, and Z. Osawa, J. Colloid Interface Sci., 1998, 202, 37-44.
(32) **Karadimitriou**, N. K., I. Xiarchos, and S. M. Hassanizadeh, 2012, Surface treatment

of PDMS to enhance natural hydrophobicity, submitted to Appl. Surf. Sci.

(33) **Zevi**, Y., A. Dathe, B. Gao, W. Zhang, B.K. Richards, and T.S. Steenhuis, Water Resour. Res., 2009, 45, doi: 10.1029/2008WR007322.

(34) **Bradford**, S.A., J. Simunek, M. Bettahar, M. T. van Genuchten, and S. R. Yates, Water Resour. Res., 2006, 42, doi: 10.1029/2005WR004791.

(35) **Morales**, V.L., B. Gao, and T.S., Steenhuis, Vadose Zone J., 2009, 8, 11-20.

(36) **Shang** J, M. Flury, G. Chen, and J. Zhuang, Water Resour. Res., 2008, 44, doi: 10.1029/2007WR006516.

(37) **Gomez-Suarez** C., J. Noordmans, H. C. van der Mei, H. J. Busscher, Phys. Chem. Chem. Phys, 1999.

(38) **Sharma** P., M. Flury, and J. Zhou, J. Colloid Interface Sci., 2008, 326, 143-150.

(39) **Auset** M, Keller AA, Brissaud F, Lazarova V, Water Resour. Res., 2005, 9, doi: 10.1029/2004WR003611.

(40) **Shen** C, V. Lazouskaya, H. Zhang, F. Wang, B. Li, Y. Jin, and Y. Huang, Colloids and Surfaces A: Physicochem. Eng. Aspects, 2012, 98-110.

(41) **Auset** M. and AA. Keller, Water Resour. Res., 2006, 42, doi: 10.1029/2005WR004639.

Chapter 5

Pore-scale Study of Flow Rate on Colloid Transport in Single-Phase Flow

Abstract

Colloid straining is considered to be an important retention mechanism under unfavorable conditions during single-phase flow. It is influenced by colloid size, pore size, flow rate, etc. Precise quantitative information on how these various factors affect colloid attachment/detachment is still largely lacking. There exist theoretical studies but they were based on the assumption that the surface of the grains is perfectly smooth.

In this work, we experimentally studied the effect of flow rate on colloid retention and remobilization in saturated porous media under unfavorable conditions, considering the effect of surface roughness. Colloid transport experiments under saturated conditions with different flow rates were conducted in a micro-model. The micro-model was made of Polydimethylsiloxane (PDMS), and colloids were hydrophilic fluorescent carboxylate-modified polystyrene latex microspheres, with a mean diameter of 300nm. We directly observed the movement of colloids within the pores using a confocal microscope. We also obtained concentration breakthrough curves by measuring the fluorescence intensity in the outlet of the micro-model. In addition, our experiments

Zhang, Q.L., A. Raoof, S.M. Hassanizadeh, and N.K. Karadimitriou, "Pore-scale study of flow rate on colloid retention and remobilization in single phase flow", prepared for submission to Transport in Porous Media.

were reproduced by a pore-network model (PNM) which was based on the pore structure of the micro-model Local colloid concentration was calculated by solving local mass balance equations in all network elements and then averaged over the whole micro-model.

The study of breakthrough curves showed that with the increase of flow rate, the colloid attachment rate decreased. Colloid remobilization was observed when the flow rate was increased by a factor ten. The measured breakthrough curves were successfully simulated by the PNM.

5.1 Introduction

In saturated porous media, colloid deposition is commonly described by the colloid filtration theory (CFT) developed by Yao et al. (1971). It assumes that colloid attachment rate coefficient is controlled by three mechanisms: Brownian diffusion, interception, and sedimentation. CFT successfully predicts colloids deposition under favorable chemical conditions (where DLVO energy barriers are absent). A major assumption of CFT was that surfaces of both colloids and collector are perfectly smooth. However, the surface of natural colloids and collectors always contain some roughness (Suresh and Walz, 1996). Indeed, the discrepancies of colloid attachment/detachment between theoretical predications and experimental results are believed to be mainly due to the presence of surface roughness, surface charge heterogeneity, and secondary minimum, which may reduce the DLVO energy barrier (Suresh et al., 1996; Ryan and Elimelech, 1996; Hoek et al., 2003, 2006; Shen et al., 2008, 2012). Johnson et al. (2011) also argued that surface charge heterogeneity and surface roughness may result in enhanced colloid attachment under unfavorable conditions. Indeed, colloid deposition has been found to increase on rough surfaces in studies using atomic force microscopy (Shellenberger et al., 2002; Morales et al., 2009; Chen et al., 2010).

Colloid attachment-detachment depends on forces and torques that acting on colloids (Cushing and Lawler, 1998; Torkzaban et al., 2007). Under favorable conditions, the adhesive force due to DLVO interactions dominates and therefore results in colloid retention (Torkzaban et al., 2007, Bradford et al., 2009). But, under unfavorable conditions, hydrodynamic shear may be the dominant process (O'neill, 1968; Kaplan et al. 1993; Weisbrod et al., 2002). The induced shear force is opposed by the adhesive force due to DLVO interactions (Cushing and Lawler, 1998; Bergendahl and Grasso, 2000; Torkzaban et al., 2007; Bradford and Torkzaban, 2008).

Some researchers have studied the combined effect of DLVO force and hydrodynamic force on colloid attachment to and detachment from a collector surface (Cleaver and Yaters, 1973; Sharma et al., 1992; Bergendahl and Grasso, 2000; Burdick et al., 2005). Bergendahl and Grasso (2000) illustrated how attached polystyrene microspheres to glass beads in a packed column could be detached by hydrodynamic shear force, depending on the flow velocity and the magnitude of the DLVO interaction forces. Johnson et al. (2007) demonstrated large colloids may experience larger hydrodynamic shear force at a given flow rate and solution chemistry.

Another mechanism for colloid retention is reported to be straining. During the last decade, a number of studies have focused on colloid retention in saturated porous media. Straining was regarded as the dominant retention mechanism under unfavorable attachment conditions; e.g. when Derjaguin-Landau-Verwey-Overbeek [DLVO] energy barriers are present (Li et al., 2005, 2006; Xu et al., 2006, 2008; Johnson et al., 2007; Bradford et al., 2002, 2003, 2005; Shen et al., 2008; Du et al., 2013). Colloid retention was reported to be affected by flow velocity in saturated porous media (Bradford et al., 2007, 2011; Johnson et al., 2007; Du et al., 2013). They found that increasing flow velocity causes a decrease of colloid straining in porous media under unfavorable chemical conditions. There are some shortcomings in the literature, which is straining was considered as the dominant mechanism of colloid retention under unfavorable chemical conditions by assuming that the solid surfaces perfectly smooth. Also the flow rate and surface roughness on colloid detachment is a very complex issue.

Pore-scale models can provide detailed information on transport processes at the microscopic pore-scale. Using pore-scale modeling, it is possible to develop relationships for attachment/detachment rates at the macro-scale. One of the widely-employed approaches is the use of a pore-network model (PNM). Compared to other pore-scale modeling approaches, PNMs allow simulation of transport processes over larger domain sizes, and make it possible to be upscale from pore scale to macro scale (*cf.* Raoof and Hassanizadeh, 2000). As a surrogate for experimental work, pore-network modeling has been extensively employed to obtain pore scale information (Nsir and Schäfer, 2010; Bodla et al., 2010; Varloteaux et al., 2012; Raoof and Hassanizadeh, 2012). For example, PNM approach has been used in the upscaling of reactive/adsorptive transport (Acharya et al., 2005; Raoof et al., 2010; Kohne et al., 2011).

The aim of this study was to examine the effect of flow rate on colloid retention and remobilization in saturated porous media at the pore scale, considering surface

roughness. Pore-scale visualization experiments and breakthrough measurement were conducted at various flow velocities in a PDMS micro-model. Also, we employed the pore network modeling to get more quantitative pore-scale information on the dependence of attachment/detachment coefficient on flow rate. We then provided comparisons of pore-network simulation results to experimental data.

5.2 Micro-model experiments

The PDMS micro-model used in our experiments contained 98 pore bodies (large pores) connected by 217 pore throats (smaller pores). The flow network of the micro-model, shown in Fig. 5.1, covered an area of 1mm×10mm, with a mean pore size of 30μm. The micro-model was treated by a silanization process (see Chapter 5 in Karadimitriou, 2013) to make it uniformly and stably hydrophobic. Fluorescent carboxylate-modified polystyrene microspheres with a mean diameter of 300nm (Polysciences Inc. GmbH) and a particle density of 1.055g/cm^3 (reported by the manufacturer) were used as model colloids. The particles were hydrophilic and had negatively charged surfaces. The colloid suspensions were prepared by dispersing the microspheres in de-ionized (DI) water to reach a final concentration of around 5.8×10^{10} particles per liter. The pH of the suspension was monitored and kept between 6.8 and 7.0 during the experiments. Also, the value of ionic strength was kept constant at 1.2×10^{-3}mM. Details of the experimental set-up can be found in Zhang et al. [2013].

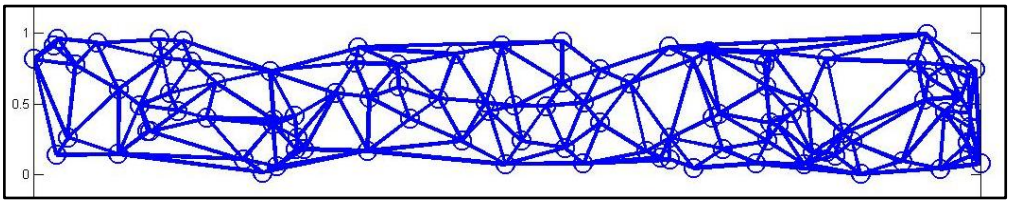

Fig. 5.1. *Representative domain of the flow network.*

The experiments were conducted in two stages. The ***first stage*** was designed in order to create a fully saturated steady-state flow of water with no colloids. To do this, the model was put vertically and then flushed with carbon dioxide for few minutes to expel the air. After that, the micro-model was put horizontally on the stage of the confocal microscope and connected to the injection tubes. Then, DI water was introduced into the

micro-model at specified constant flow rate in order to displace and dissolve the carbon dioxide, leading to a fully saturated micro-model. We performed three sets of experiments at three flow rates: 50nL/min, 250nL/min, and 500nL/min. These are denoted by ***q***, ***5q***, and ***10q***, respectively.

The ***second stage*** involved colloids transport under steady-state flow conditions. In all experiments, the flow rate was the same as during steady-state flow and the particle suspension was injected for 20 minutes. This was followed by the injection of colloids-free DI water for 25 minutes, again without changing the flow rate. So, the second stage of each experiment, i.e. colloid transport under steady-state flow, lasted for 45 minutes.

We also performed transient flow experiments. In these experiments, a third stage was added to the above-mentioned procedure, we dramatically increased the flow rate by a factor of ten to 5μL/min. This experiment was aimed to investigate the effect of flow rate changes on the transport of colloid.

5.3 Theoretical calculation of interaction energies/forces

The interaction energy among colloids and between a colloid and the PDMS surface was estimated by the classic DLVO theory. The van der Waals attraction was calculated based on the expression by Gregory (1981); the calculated electrical double layer interaction for a sphere with a surface was based on the equation described by Norde and Lyklema (1989). The total interaction energy can be expressed as (Gregory, 1981):

$$\Delta G_{tot} = 64\pi\varepsilon R(\frac{kT}{ve})^2\gamma_1\gamma_2 exp(-\kappa h) - \frac{AR}{6h}[1-\frac{5.32h}{\lambda_0}\ln(1+\frac{\lambda_0}{5.32h})] \quad (5.1)$$

where R is the radius of the particle; ε is the dielectric permittivity of the liquid (in our case, 80.1 for DI water); k is the Boltzmann constant; T is the absolute temperature; v is the ion valence; e is the electron charge; $\gamma_i = tanh[ve\psi_{0,i}/(4kT)]$; κ is the Debye-Hückel reciprocal length; h is the separation distance; A_{123} is the Hamaker constant; and λ_0 is a characteristic length of 100 nm. The two terms in this equation are due to electrostatic and van der Waals interaction energies, respectively.

The calculated DLVO interaction energy profile between the colloid (in DI water) and PDMS surface is shown in Fig.2. In these calculations, the zeta potential of polystyrene microspheres was taken to be -36.6mV (measured using a Zetasizer, Malvern Instruments, UK); the zeta potential of the PDMS surface was taken to be -80 mV (Sze

et al., 2003). A value of 3.9×10^{-21}J was used for the Hamaker constant for the polystyrene-water-PDMS system, as calculated in other studies (Israelachvili, 1992; Bradford et al., 2008). As can be seen from Fig. 5.2, there is a significant energy barrier between colloid and PDMS surface, also there is absent of secondary minima, which means colloid attachment to the PDMS surface is highly improbable in DI water. But one should note that, we didn't consider surface charge heterogeneity and surface roughness in our calculations.

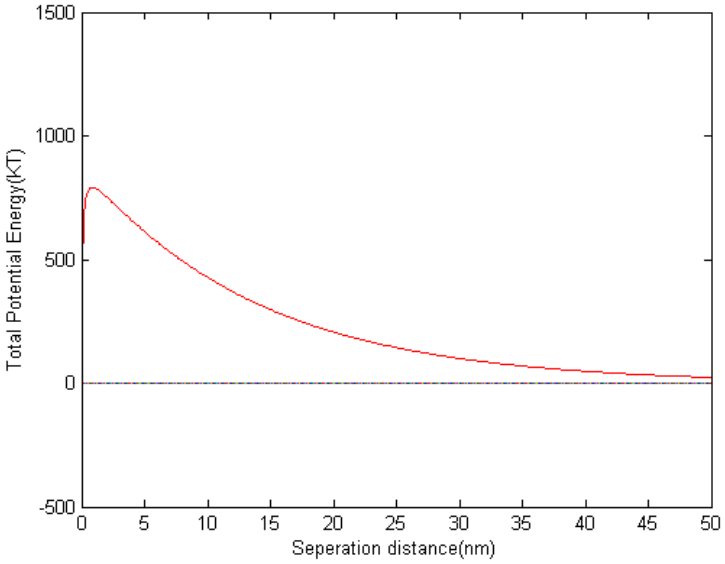

Fig. 5.2 *Calculated DLVO interaction energy profile for the colloid (diameter of 300nm) with PDMS surface.*

On a rough surface, a colloid may experience a friction force against movement. A schematic of forces acting on a colloid, with radius of *R*, attaching to a rough PDMS solid surface in moving water is shown in Fig.3. The forces showing in the figure are Van der Waals force (F_{vdw}), electrostatic force (F_{el}), drag force (F_D), friction force (F_{fric}), hydrodynamic torque (T_{hydro}) and resisting torque (T_{resist}).

The total DLVO force is

$$F_{DLVO} = \frac{d}{dh}(\Delta G_{tot}) \tag{5.2}$$

The drag force can be calculated as (Goldman et al., 1967; O'Neill, 1968):

$$F_D = 10.205\pi\mu(\frac{\partial V}{\partial r})R^2 \tag{5.3}$$

where μ is the water dynamic viscosity, $\mu\partial V / \partial R$ is the shear rate to be calculated at a distance of R from the surface.

The friction force is given by:

$$F_{fric} = \mu_f F_{DLVO} \tag{5.4}$$

where μ_f is the static friction coefficient.

These forces also may exert nonzero torque on the colloid even if their own re sultant is zero.The adhesive torque for colloids is expressed as:

$$T_{resist} = F_{DLVO}\, l_x \tag{5.5}$$

The hydrodynamic torque caused by drag force is given as (Goldman et al., 1967; O'Neill, 1968):

$$T_{hydro} = F_D l_y \tag{5.6}$$

where l_x and l_y is the lever arm for DLVO force and drag force, respectively, and are given in terms of roughness height by:

$$l_y = R - r$$

$$l_x = \sqrt{R^2 - l_y^{\,2}} = \sqrt{2rR - r^2}$$

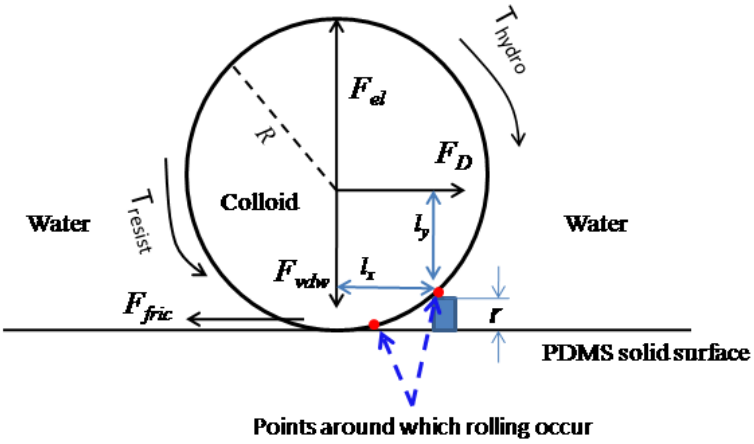

Fig. 5.3 *Schematic of forces acting on an adhering colloid in moving water.*

5.4 Pore-network modeling

Pore-network modeling is a valuable tool for the study of transport phenomena at the pore scale. We have constructed a pore-network model on the basis of actual pore geometry our micro-model, which means the porous medium, was simulated by pore bodies and pore throats of different sizes connecting to each other.

5.4.1 Configuration of the pore network model

A two-dimensional pore network model was constructed based on the pore network geometry and topology of the micro-model. Both pore body radii and pore throat size were taken from the map of the PDMS micro-model. Thus, the pore network model was exactly the same as the micro-model structure that was employed in our experiments. The distribution of pore body and pore throat sizes is shown in Fig. 5.4. Properties of the pore network are given in Table 5.1.

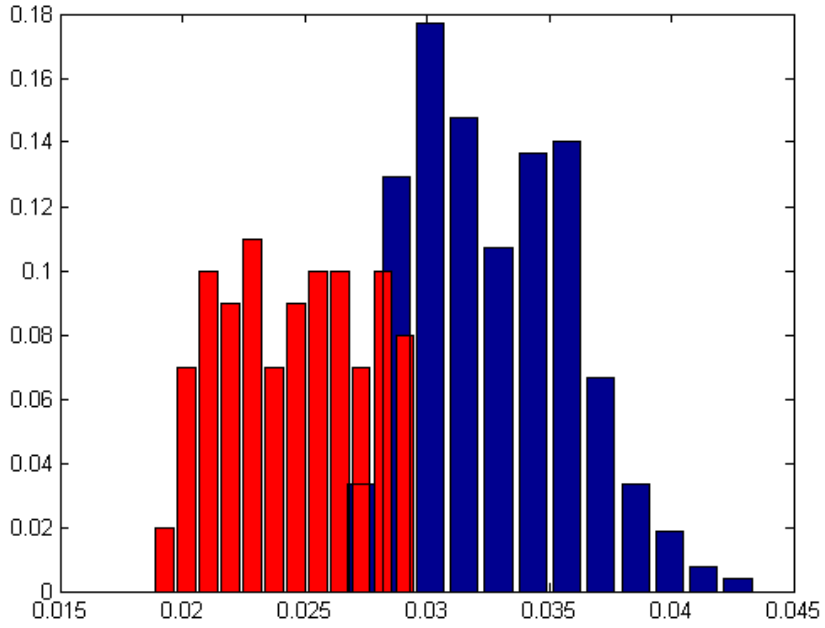

Fig. 5.4 *Distribution of pore body radius (blue box) together with pore throat width (red box).*

5.4.2 Flow simulation

In this work, we considered saturated flow through the network. The flow field across the pore network was established by applying a pressure gradient between the two opposing vertical boundaries of the network. All other boundaries of the network parallel to the overall flow direction were treated as no-flow boundaries. The discharge through a given pore throat, *ij*, (as shown in Fig. 5.3) can be expressed as (Acharya et al., 2004):

$$q_{ij} = g_{ij}(P_j - P_i) \tag{5.7}$$

where q_{ij} is the total volumetric flow rate through pore throat *ij*, g_{ij} is conductance of pore throat *ij*, and p_i and p_j are the fluid pressures in pore bodies *i* and *j*, respectively.
The conductance, g_{ij}, for a pore throat with rectangular cross section is:

$$g_{ij} = \frac{[0.0351*(0.6109*16*g_{sh}) + 0.0630*(16*g_{sh})^2 + 0.3214*(16*g_{sh})^3]*(0.03*R_{ij})^2}{\mu l_{ij}} \tag{5.8}$$

where R_{ij} is pore throat radius, μ is the fluid dynamic viscosity, l_{ij} is length of the pore throat, and g_{sh} is the shape factor for a rectangular cross section, expressed as

$$g_{sh} = \frac{R_{ij}*0.03}{4*(0.03+R_{ij})^2} \tag{5.9}$$

For incompressible, steady-state flow, the sum of discharges of pore throats connected to a pore body must be zero:

$$\sum_{j=1}^{z_i} q_{ij} = 0 \qquad j = 1,2,...,z_i \tag{5.10}$$

where z_i is the coordination number of pore body *i*. Equation (10) is applied to all pore bodies except those on the inflow and outflow boundaries where pressures are specified.
Considering the network as an REV, the average pore water velocity can be determined as:

$$\overline{V} = \frac{QL}{V_f} \tag{5.11}$$

where *Q* is the total discharge through the network (the sum of fluxes through all pore throats at the inlet or outlet boundary of the network), *L* is the network length in the flow direction, and V_f is the total fluid volume present in the network. Because we are modeling single-phase flow condition, the fluid volume is the sum of volumes of all pore

bodies and pore throats.

5.4.3 Pore scale transport formulations

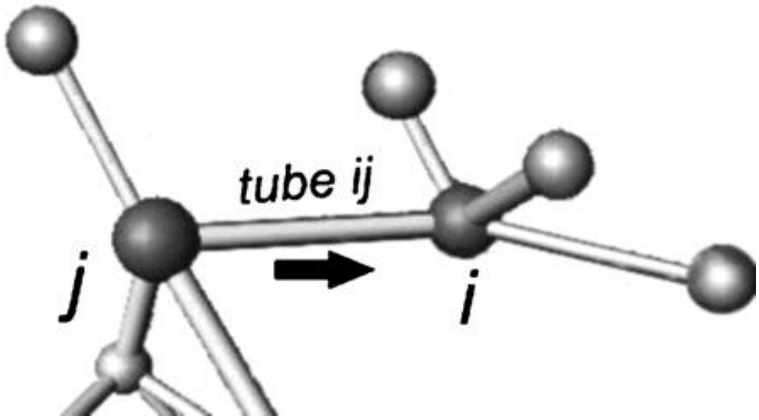

Fig. 5.5 *An example of interconnected pore bodies and pore throats. Flow direction is from pore body j, the upstream node, into pore body i, through pore throat ij.*

An example of interconnected pore bodies and pore throats is shown in Fig. 5.5. Pore body *j* is the upstream node, assuming flow from pore body *j* towards pore body *i*, through pore throat *ij*.

Colloid transport within a saturated pore throat can be written as

$$V_{ij}\frac{dc_{ij}}{dt} = \left|q_{ij}\right|c_i - \left|q_{ij}\right|c_{ij} - V_{ij}k_{att,ij}c_{ij} + V_{ij}k_{det,ij}s_{ij} \tag{5.12}$$

The kinetic attachment rate of colloids within a pore throat can be written as

$$\frac{ds_{ij}}{dt} = k_{att,ij}c_{ij} - k_{det,ij}s_{ij} \tag{5.13}$$

where c_{ij} is the pore throat average mass concentration, s_{ij} is the average adsorbed concentration, and $k_{att,ij}$ and $k_{det,ij}$ are attachment and detachment rate coefficients of throat *ij*, respectively.

discretization of equation (5.12) in fully implicit scheme gives

$$V_{ij}\frac{(\overline{c_{ij}}^{t+\Delta t} - \overline{c_{ij}}^{t+\Delta t})}{\Delta t} = q_{ij}(\overline{c_j}^{t+\Delta t} - \overline{c_{ij}}^{t+\Delta t}) - V_{ij}\alpha_{ij}(K_{d,ij}\overline{c_{ij}}^{t+\Delta t} - \overline{s_{ij}}^{t+\Delta t}) \tag{5.14}$$

where $\alpha_{ij}=k_{det,ij}$ and $K_{d,ij}=k_{att,ij}/k_{det,ij}$.

discretization of equation (5.13) giv

$$\frac{(\overline{s_{ij}}^{t+\Delta t} - \overline{s_{ij}}^{t})}{\Delta t} = \alpha_{ij}(K_{d,ij}\overline{c_{ij}}^{t+\Delta t} - \overline{s_{ij}}^{t+\Delta t}) \tag{5.15}$$

Substituting $\overline{s_{ij}}^{t+\Delta t}$ from equation (5.15) into equation (5.14) gives

$$\overline{c_{ij}}^{t+\Delta t} = \frac{1}{B}\overline{c_{ij}}^{t} + \frac{\Delta t\alpha_{ij}}{B(1+\alpha_{ij}\Delta t)}\overline{s_{ij}}^{t} + \frac{1}{B}\frac{q_{ij}\Delta t}{V_{ij}}\overline{c_{ij}}^{t+\Delta t} \tag{5.16}$$

where

$$B = 1 + \frac{q_{ij}\Delta t}{V_{ij}} + \Delta t\alpha_{ij}K_{d,ij} - \frac{\Delta t^2\alpha_{ij}^2K_{d,ij}}{(1+\alpha_{ij}\Delta t)} \tag{5.17}$$

Mass balance equation for a saturated pore body can be written as

$$V_i\frac{dc_i}{dt} = \sum_{j=1}^{N_{in}} q_{ij}c_{ij} - Q_ic_i \tag{5.18}$$

Discretization of equation (5.18) using a fully implicit scheme results in

$$V_i\frac{\overline{c_i}^{t+\Delta t} - \overline{c_i}^{t}}{\Delta t} = \sum_{j=1}^{N_{in}} q_{ij}\overline{c_{ij}}^{t+\Delta t} - Q_i\overline{c_i}^{t+\Delta t} \tag{5.20}$$

We use equation (5.16) to substitute for $\overline{c_{ij}}^{t+\Delta t}$ in equation (5.20), and collect unknown terms on the 1.h.s. and known terms on r.h.s. to get:

$$E\overline{c_i}^{t+\Delta t} - I\sum_{j=1}^{N_{in}} F\overline{c_j}^{t+\Delta t} = \overline{c_i}^{t} + I\sum_{j=1}^{N_{in}}(G\overline{c_{ij}}^{t} + H\overline{s_{ij}}^{t}) \tag{5.21}$$

where:

$$E(N_{node}) = 1 + \frac{\Delta tQ_i}{V_i}; \qquad I(N_{node}) = \frac{\Delta t}{V_i}; \qquad F(N_{tube}) = \frac{1}{B}\frac{q_{ij}^2\Delta t}{V_{ij}}; \qquad G(N_{tube}) = \frac{q_{ij}}{B};$$

$$H(N_{tube}) = \frac{q_{ij}\Delta t\alpha_{ij}}{B(1+\Delta t\alpha_{ij})}$$

Equation (5.21) constitute a set of N_{node} linear equations to be solved for concentrations of colloids at all pore bodies (i.e., $\overline{c_i}^{t+\Delta t}$ and $\overline{c_j}^{t+\Delta t}$). After each time step, the concentration of colloids in pore throats and attached colloid concentrations can be calculated using equation (5.16).

We used the pore-network model described above to simulate our experimental results at macro-scale.

Table 5.1. *Properties of the pore network (the micro-model)*

Parameters	Values
Number of pore bodies	98
Number of pore throats	217
Mean pore body size (diameter)	30μm
Porosity	0.39
Area of the flow network	1mm×10mm

5.5 Results and discussion

5.5.1 Effect of flow rate on colloid attachment

Fig. 5.6 presents the colloid concentration breakthrough curves measured at the outlet reservoir of the PDMS micro-model at three different flow rates. As can be seen, when flow rate was *q*, the normalized effluent concentration was approximately 0.68. When the flow rate was increased to *5q*, the maximum concentration went up to about 0.8. Under the flow rate of *10q*, even less attachment was observed; a maximum concentration of around 0.95 was reached. It is clear that the colloid attachment decreases with the increase of flow rate. This is probably because, as can be seen from equations (5.3 and 5.4), the drag force increases with the flow rate, whereas the adhesive force remains constant. This means that the potential for colloid attachment reduces with an increase of the flow rate.

As mentioned earlier, the profile of the interaction energy between colloid and PDMS surface (see Fig. 5.2) shows a repulsive energy barrier. Thus, no attachment of colloids should have occurred. But in our DLVO calculations, we did not consider surface roughness. In our case, the surface roughness of the PDMS micro-model was around 50nm, which was still significant correspond to the colloids employed, with diameter of 300nm. The surface roughness may result in forces coming into action that resists the sliding or rolling of the colloids on the PDMS surface. These forces oppose the hydrodynamic forces.

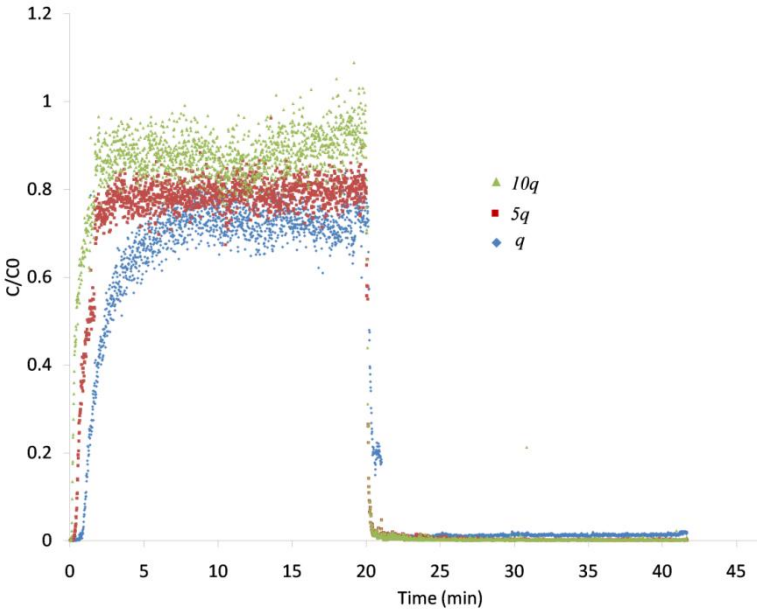

Fig. 5.6 *Measured effluent concentration breakthrough curves of colloid transported through the PDMS micro-model at different flow rates (q, 5q, and 10q).*

Another mechanism that may cause the retention of colloids is straining at very small pore openings. Du et al. (2013) demonstrated that retention of colloids in DI water is mainly due to colloids straining at stagnant zone where grain-grain contacts exist. Also, other studies (Bradford et al., 2006, 2009; Torkzaban et al., 2010) have shown that the retained colloids at lower ionic strength (< 0.001M) were mainly strained at grain-grain junctions, which indicated that the main retention mechanism at low IS is straining. However, in our micro-model, there were no grain-grain contact zones. This is because the pore throats in our micro-model have parallel walls (as it can be seen in the Movie 1 in the Ancillary material). So, straining could not occur in our micro-model. Our explanation is similar to Johnson et al. (2006, 2010, 2011), that the main attachment mechanism in the micro-model was mainly due to surface roughness.

5.5.2 Effect of rapid flow rate change on colloid remobilization

Results of breakthrough concentration measurements in experiments under transient flow rate are shown in Fig. 5.7. At the start of stage 3, the flow rate was increased by a factor of ten (from 50nL/min to 500nL/min). The rapid increase of flow rate caused the

remobilization of colloids that were remained in the micro-model at the end of stage 2. This is seen as a spike in the breakthrough curve in Fig. 5.7. Based on the mass balance calculations, around 11.5% of the remaining colloids were remobilized.

Real-time images of colloid remobilization during the rapid increase of flow rate can be found in the Ancillary Material (see Movie 1). The video showed that some of the colloids attached to the PDMS surface were released, but during their transport, some of them re-deposited downstream.

For colloids to be released from the solid surface, there are three mechanisms: sliding, lifting, and rolling. Previous studies have shown that rolling is the main mechanism for colloid detachment [Sharma et al., 1992; Burdick et al., 2001]. Now, the colloid behavior is determined by force balance and torque balance (see Fig. 5.3). Only when the hydrodynamic torque overcomes the resisting torque, rolling can occur. From equations (5.1)-(5.6), we can find that the increase in flow rate can result in the increase of drag force and hydrodynamic torque. Thus, an initially stable colloid can be released. This has been also confirmed in other studies (see e.g., Ryan et al., 1998; Shang et al., 2008; Bradford et al., 2008).

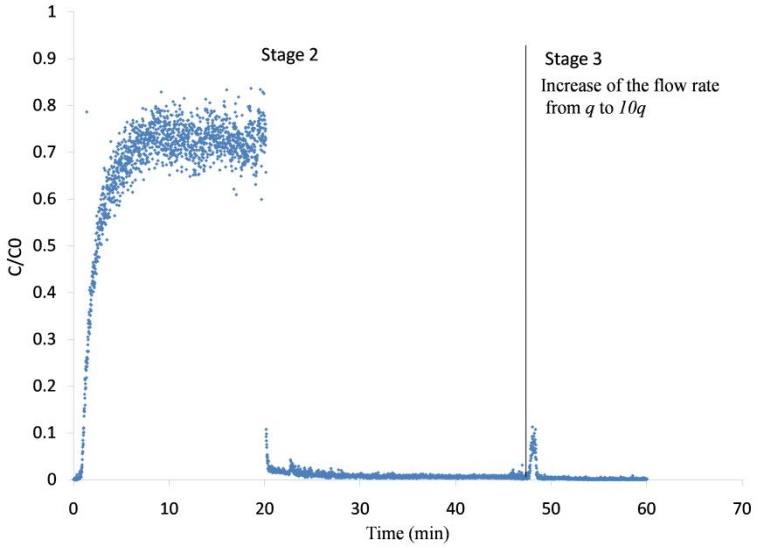

Fig. 5.7 *Measured concentration breakthrough curves at the outlet reservoir of the micro-model, when the flow rate changed from q to 10q.*

Our findings disagreed with Shen et al. (2012), who reported that the rough asperity

(which is ubiquitous) on collector surfaces provides tangential attraction force, which can prevent colloids from being swept away by hydrodynamic shear. But one should notice that, in their case, the solution ionic strength was larger than 0.01M.

(A)

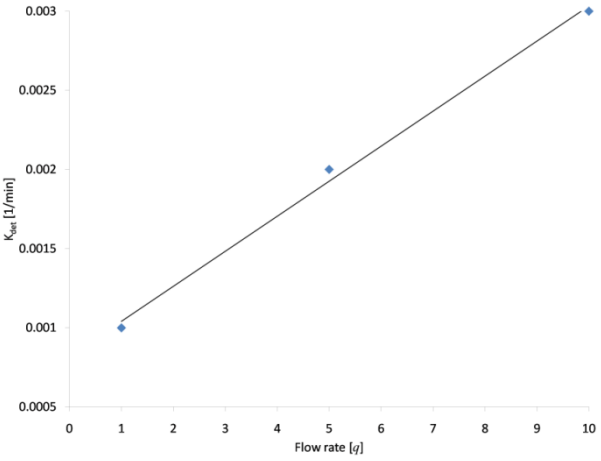

(B)

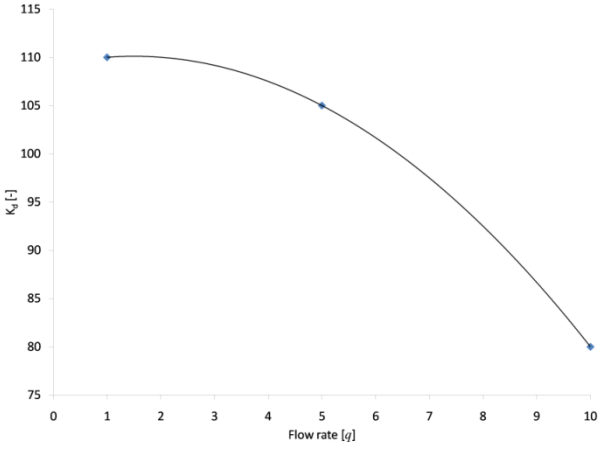

Fig. 5.8 *(A) Detachment rate coefficient and (B) distribution coefficient showed as a function of flow rate.*

Pore-network model described above was used to simulate breakthrough curves. In doing so, we chose values of pore-scale detachment coefficients, $k_{det,ij}$, and distribution

coefficient, $K_{d,ij}$, in order to fit the breakthrough curves as closely as possible. We found different values of $k_{det,ij}$ and $K_{d,ij}$ for different flow rates. Results are plotted in Fig. 5.8A and 5.8B. The measured and simulated breakthrough curves are shown in Fig. 5.9. Fig. 5.10 presents one example of the colloids concentration distribution inside the flow network.

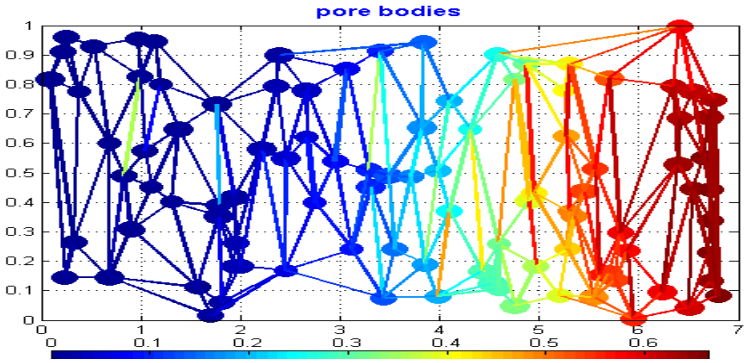

Fig. 5.9 *Colloid concentration distribution during the transport process simulated by pore network modeling. In the figure, the left side is the inlet, right side is the outlet.*

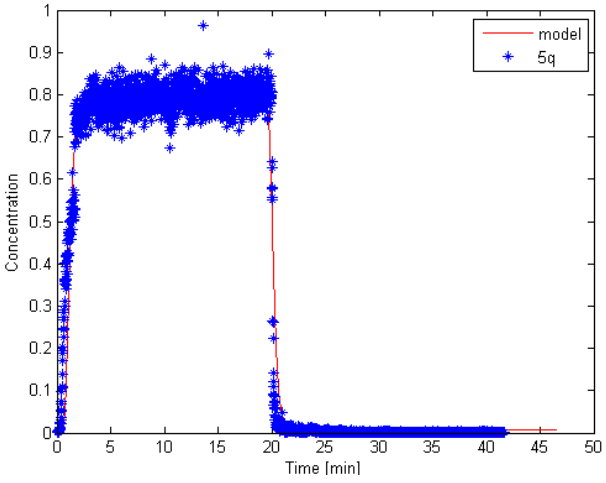

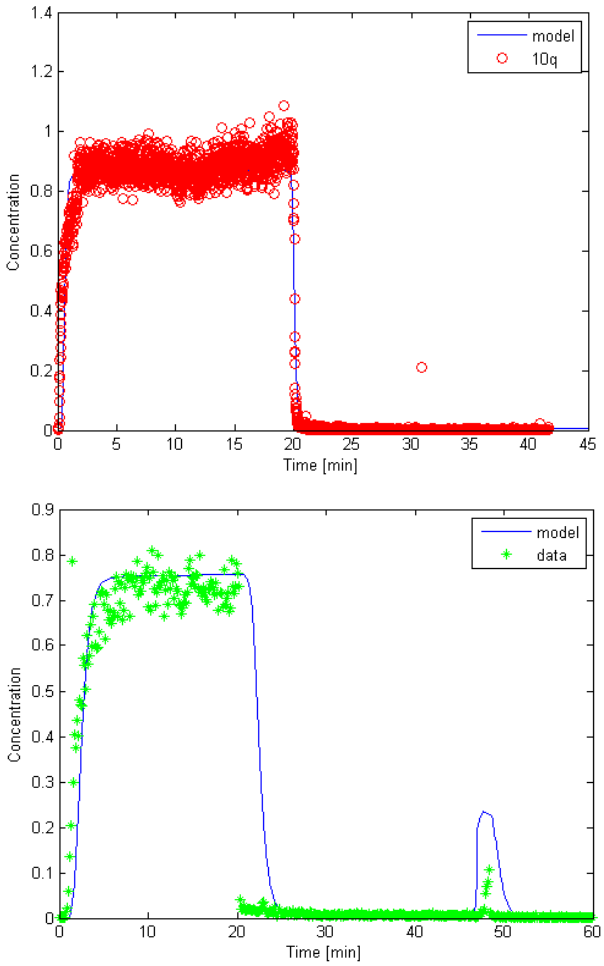

Fig. 5.10 *Simulated (lines) and measured (symbols) breakthrough curves of colloids transport at different flow rates.*

Generally good agreements were obtained between the measurement and simulation. This provides confidence that our pore-network modeling can be applied to model the flow rate effect on colloid transport and remobilization. The pore-network model provides detailed information on concentration distribution at the pore scale. This is illustrated in Fig. 5.9.

5.6 Summary

We investigated effect of the flow rate on colloid transport in saturated porous media at the pore scale. Direct visual observation combined with measured breakthrough curves showed that, increasing the flow rates reduced the retention of colloids in saturated porous media. Colloid remobilization occurs during transient flow (rapid flow rate change). Pore-scale model was used and successfully simulated these experimental measurements.

Further work, like developing relationships for macro-scale attachment and detachment rate coefficients as a function of flow rate, is needed.

References

(1) **Acharya**, R., S. van der Zee, A. Leijinse (2005), Transport modeling of nonlinearly adsorbing solutes in physically heterogeneous pore networks, Water Resour. Res. 41 (2), W02020.

(2) **Bergendahl**, J., and D. Grasso (1998), Colloid generation during batch leaching tests: Mechanics of disaggregation, Colloids Surf. A, 135, 193-205, doi:10.1016/S0927-7757(97)00248-3.

(3) **Bradford**, S.A., S.R. Yates, M. Bettahar, J. Simunek (2002), Physical factors affecting the transport and fate of colloids in saturated porous media. Water Resour. Res. 38(12), doi: 10.2029/2002WR001340.

(4) **Bradford**, S.A., J. Simunek, M. Bettahar, M.T. van Genuchten, S.R. Yates (2003), Modeling colloid attachment, straining, and exclusion in saturated porous media. Environ. Sci. Technol., 37:2242-2250.

(5) **Bradford**, S.A., J. Simunek, M. Bettahar, Y.F. Tadassa, M.T. van Genuchten, S.R. Yates (2005), Straining of colloids at textural interfaces. Water Resour. Res. 41, doi: 10.2029/2004WR003675.

(6) **Bradford**, S. A., and S. Torkzaban (2008), Colloid Transport and Retention in Unsaturated Porous Media: A Review of Interface-, Collector-, and Pore-Scale Processes and Models, Vadose Zone J., 7, 667-681.

(7) **Bradford**, S. A., S. Torkzaban, S.L. Walker (2007), Coupling of physical and chemical mechanisms of colloid straining in saturated porous media. Water Res. 41, 3012-3024.

(8) **Bradford**, S. A., S. Torkzaban, J. Simunek (2011), Modeling colloid transport and

retention in saturated porous media under unfavorable attachment conditions. Water Resour. Res. 47, doi: 10.1029/2011WR010812.

(9) **G. Burdick**, N. Berman, S. Beaudoin, (2001), Describing Hydrodynamic Particle Removal from Surfaces using the Particle Reynolds Number, J. Nanopart. Res. 3:455-467.

(10) **Chen**, G., Bedi, R. S., Yan, Y. S., and Walker, S. L. (2010) Initial colloid deposition on bare and zeolite-coated stainless steel and aluminum: Influence of surface roughness. Langmuir, 26, 12605−12613.

(11) **Cleaver**, J. W., B. Yates (1973), Mechanism of detachment of colloid particles from a flat substrate in turbulent flow. J. Colloid Interface Sci., 44, 464-474.

(12) **Cushing**, R. S., and D. F. Lawler (1998), Depth filtration: Fundamental investigation through three-dimensional trajectory analysis, Environ. Sci. Technol., 32, 3793-3801, doi: 10.1021/es9707567.

(13) **Derjaguin**, B. V., Landau, L. D. (1941), Theory of the stability of strongly charged lyophobic sols and of the adhesion of strongly charged particles in solutions of electrolytes. Acta Physicochim. USSR, 14, 733-762.

(14) **Du**, Y., C. Shen, H. Zhang, and Y. Huang (2013), Effects of flow velocity and nonionic surfactant on colloid straining in saturated porous media under unfavorable conditions. Transp Porous Med, 98, doi: 10.1007/s11242-013-0140-3.

(15) **Gregory**, J. (1981), Approximate expressions for retarded van der Waals interaction, J. Colloid Interface Sci., 83, 138–145.

(16) **Goldman**, A.J., R.G. Cox, and H. Brenner. (1967), Slow viscous motion of a sphere parallel to a plane wall: I. Motion through a quiescent fl uid. Chem. Eng. Sci. 22:637–651.

(17) **Hoek**, E.M.V., S. Bhattacharjee, M. Elimelech (2003), Effect of membrane surface roughness on colloid-membrane DLVO interactions. Langmuir, 19, 4836-4847.

(18) **Hoek**, E. M. V.; Agarwal, G. K. (2006), Extended DLVO interactions between spherical particles and rough surfaces. J. Colloid Interface Sci., 298, 50−58.

(19) **Israelachvili**, J.N. (1992), Intermolecular and surface forces, 2nd ed. Academic Press, London.

(20) **Johnson**, W. P.; Tong, M. (2006), Simulated and experimental influence of hetero-domain size on colloid deposition efficiencies on overall like-charged surfaces. Environ. Sci. Technol., 40 (16), 5015–502, doi: 110.1021/es060450c.

(21) **Johnson**, W. P.; Pazmino, E.; Ma, H. (2010), Direct observations of colloid retention in granular media in the presence of energy barriers and pitfalls of

inferring mechanisms from indirect observations. Water Res., 44 (4), 1158–116910.1016/j.watres.2009.12.014.

(22) **Johnson**, W.P., H. Ma, and E. Pazmino (2011), Straining credibility: a general comment regarding common arguments used to infer straining as the mechanism of colloid retention in porous media. Environ. Sci. Technol., 45:3831-3832.

(23) **Karadimitriou**, N.K. (2013), Two-phase flow experimental studies in micro-models. Ph.D thesis, Department of Earth Sciences, Utrecht University, the Netherlands.

(24) **Kohne**, J., S. Schluter, H. Vogel (2011), Predicting solute transport in structured soil using pore network models. Vadose Zone J. 10 (3), 1082.

(25) **Li**, X., W.P. Johnson (2005), Nonmonotonic variations in deposition rate coefficients of microspheres in porous media under unfavorable deposition conditions. Environ. Sci. Technol., 39, 1658-1665.

(26) **Li**, X., C.L. Lin, J.L. Miller, W.P. Johnson (2006), Role of grain-to-grain contacts on profiles of retained colloids in porous media in the presence of an energy barrier to deposition. Environ. Sci. Technol., 40, 3769-3774.

(27) **Li**, L., Peters, C., Celia, M., (2006). Upscaling geochemical reaction rates using pore-scale network modeling? Advances in Water Resources 29 (9), 1351–1370.

(28) **Norde**, W., and J. Lyklema (1989), Protein adsorption and bacterial adhesion to solid surfaces -A colloid chemical approach, Colloids Surf. 38:1–13.

(29) **O'Neill**, M. E. (1968), A sphere in contact with a plane wall in a slow linear shear flow. Chem. Eng. Sci., 23, 1293-1298.

(30) **Raoof**, A., S. Hassanizadeh, A. Leijnse (2010), Upscaling transport of adsorbing solutes in porous media: pore-network modeling. Vadose Zone J. 9 (3), 624.

(31) **Raoof**, A., Hassanizadeh, S. (2012), A new formulation for pore-network modeling of two-phase flow. Water Resour. Res. 48 (1), W01514.

(32) **Reeves**, P., M. Celia (1996), A functional relationship between capillary pressure, saturation, and interfacial area as revealed by a pore-scale network model. Water Resour. Res. 32 (8), 2345–2358.

(33) **Ryan**, J. N., and M. Elimelech (1996), Colloid mobilization and transport in groundwater, Coll. Surf. A: Physicochem. Eng. Aspects, 107, 1-56.

(34) **Sharma**, M. M., H. Chamoun, D. S. H.Sita Rama Sarma, R. S. Schechter (1992), Factors controlling the hydrodynamic detachment of particles from surfaces. J. Colloid Interface Sci. 149 (1), 121-134.

(35) **Shang**, J., M. Flury, G. Chen, and J. Zhuang (2008), Impact of flow rate, water

content, and capillary forces on in situ colloid mobilization during infiltration in unsaturated sediments. Water Resour. Res. 44, doi: 10.1029/2007WR006516.

(36) **Sharma**, M. S., H. Chamoun, D. S. H. Sita Rama Sarama, and R. S. Schechter. (1992), Factors controlling the hydrodynamic detachment of particles from surfaces, J. Colloid Interface Sci., 149, 121– 134.

(37) **Shen**, C., Huang, Y., Li, B., Jin, Y. (2008), Effects of solution chemistry on straining of colloids in porous media under unfavorable conditions. Water Resour. Res., 44, W05419, doi: 10.1029/2007WR006580.

(38) **Shen**, C., Wang, F., Li, B., Jin, Y., Wang, L.-P., Huang, Y. (2012), Application of DLVO energy map to evaluate interactions between spherical colloids and rough surfaces. Langmuir 28, 14681–14692.

(39) **Sze**, A., D. Erickson, L. Ren, and D. Li (2003), Zeta-potential measurement using the Smoluchowski equation and the slope of the current–time relationship in electro osmotic flow, J. Colloid Interface Sci., 261, 402-410.

(40) **Suresh**, L.; Walz, J. Y. (1996), Effect of surface roughness on the interaction energy between a colloidal sphere and a flat plate. J. Colloid Interface Sci., 183, 199−213.

(41) **Torkzaban**, S., S. A. Bradford, and S. L. Walker (2007), Resolving the coupled effects of hydrodynamics and DLVO forces on colloid attachment to porous media, Langmuir, 23, 9652- 9660, doi:10.1021/la700995e.

(42) **Verwey**, E. J. W., Overbeek, J. T. G. (1948), Theory of the Stability of lyophobic Colloids; Elsevier: Amsterdam.

(43) **X**. Li, S. Assemi (2007), Deposition and re-entrainment dynamics of microbes and non-biological colloids during non-perturbed transport in porous media in the presence of an energy barrier to deposition. Advances in water Resources, 30, 1432-1454.

(44) **Xu**, S., B. Gao, J.E. Saiers (2006), Straining of colloidal particles in saturated porous media. Water Resour. Res., 42, doi: 10.1029/2006WR004948.

(45) **Xu**, S., Q. Liao, J.E. Saiers (2008), Straining of non-spherical colloids in saturated porous media. Environ. Sci. Technol., 42, 771-778.

(46) **Yao**, K. M., M. T. Habibian, and C. R. O'Melia (1971), Water and wastewater filtration: concepts and applications, Environ. Sci. Technol., 5(11), 1105–1112.

(47) **Zhang**, Q.L., N.K. Karadimitriou, S.M. Hassanizadeh, P. J. Kleingeld, and A. Imhof (2013), Study of Colloids Transport during Two-Phase Flow using a Novel Polydimethylsiloxane Micro-model, J. Colloid Interface

Sci.:10.1016/j.jcis.2013.02.041.

Chapter 6

Retention and Remobilization of Colloids during Steady-state and Transient Two-Phase Flow

Abstract

In this work, we study colloid transport through a porous medium under steady-state and transient two-phase flow conditions. The porous medium was a PDMS micro-model and the immiscible fluids were water and fluorinert-FC43. Given the fact that the micro-model was hydrophobic, fluorinert was the wetting phase and water was the non-wetting phase. We used hydrophilic fluorescent microspheres (dispersed in water) with mean diameter of 300nm. We directly observed colloid movement and fluid distribution within pores of the micro-model using a confocal laser scanning microscope. We also obtained concentration breakthrough curves by measuring the fluorescent intensities in the outlet of the micro-model. The breakthrough curves showed that, under steady-state flow at different water saturations, more colloids were retained at lower saturations. Our visualization results
suggested that the enhanced attachment was due to the retention of colloids onto fluorinert-water interfaces (FWIs) and fluorinert-water-solid contact lines (FWSCs). At the end of a steady-state two-phase flow experiment, we changed the micro-model saturation by injecting either water (drainage) or fluorinert (imbibition). We found

Accepted as: Zhang, Q.L., S.M. Hassanizadeh, N.K. Karadimitriou, A. Raoof, B. Liu, P. J. Kleingeld, and A. Imhof "Retention and Remobilization of colloids during steady-state and transient two-phase flow", Water Resources Research, 2013.

remobilization of colloids during imbibition events, but no mobilization was observed during drainage. Visualization showed that colloids deposited on solid-water interfaces (SWIs) were dislodged by moving FWSCs during imbibition. We simulated breakthrough curves by modeling colloids interactions with SWIs and FWIs separately. Remobilization of colloids attached to SWI was modeled as a first-order kinetic process and the rate coefficient was assumed proportional to temporal rate of change of saturation. Colloids attachment to and detachment from FWIs was modeled as equilibrium process. Generally, good agreements between experimental results and simulation were obtained. This is the first study of colloid transport in two phase flow, where pore-scale visualization, breakthrough concentration measurement, and modeling of results are combined. Video images, included as ancillary material, provide insightful images of the movement of colloid in a network of pores occupied by two immiscible liquids.

6.1 Introduction

Over the past few decades, considerable research has been done to understand the behavior of colloidal particles and viruses in partially-saturated porous media, through laboratory works, field studies, and numerical simulations. An important aspect of colloids behavior is the remobilization of attached colloids. Recently, colloids remobilization has drawn significant attention due to its potential for enhancing contaminant transport through the vadose zone to the groundwater [Saiers et al., 2003; Zhuang et al., 2009]. Remobilization of colloids has been found to be sensitive to the following factors: properties of colloids and soils [Bradford and Kim, 2012], solution ionic strength and PH [Torkzaban et al., 2006a; Zevi et al., 2009; Zhuang et al., 2010; Sadeghi et al., 2012], and flow patterns [Saiers and Lenhart, 2003; Torkzaban et al., 2006a, b; Shang et al., 2008; Zhuang et al., 2007, 2009; Cheng and Saiers, 2009].

In particular, it was observed that temporal changes in flow conditions can cause a significant increase of the rate of colloid detachment. For example, Saiers and Lenhart [2003] observed in column experiments that increase in water flow rates and water saturation led to enhanced colloid release, compared to steady-state flow conditions. Similarly, Shang et al. [2008] reported mobilization of colloids due to a step increase in water saturation and flow rates. Not only imbibition, but also drainage is found to cause colloids remobilization, as observed by Zhuang et al. [2007] and Cheng and Saiers [2009]. Transients in chemical conditions can also cause colloids remobilization. Flury

et al. [2003] reported that colloids can be mobilized when low ionic strength pore water displaces high ionic strength pore water. Bradford et al. [2012] also found that decrease in ionic strength can result in colloid remobilization. Virus remobilization was observed by Sadeghi et al. [2013] when reducing the calcium concentration of the inflow solution, keeping the ionic strength constant.

Colloids transport processes in unsaturated media are complex. Generally, enhanced colloid attachment has been observed at lower saturations. Interestingly, different authors have given different reasons for this enhanced attachment. In some studies, increased colloids retention at lower saturation was mainly attributed to irreversible colloids attachment to air-water interfaces (AWIs) [e.g. Wan and Wilson, 1994a, b; Wan and Tokunaga, 2002; Sirivithayapakorn and Keller. 2003; Keller and Sirivithayapakorn, 2004; Torkzaban et al., 2006a]. Some other researches, however, found that colloid attachment to the AWI is reversible [Chen and Flury, 2005; Torkzaban et al., 2006b; Lazouskaya and Jin, 2008]. Another group of researchers, e.g., Crist et al. [2004, 2005] and Zevi et al. [2005, 2006, and 2009], found that air-water-solid (AWS) contact lines are the primary locations for enhanced colloids retention. In addition to attachment to SWI, AWI, and AWS, film straining has been reported as another important mechanism for colloids retention under unsaturated conditions [Wan and Tokunaga, 1997, Veerapaneni et al., 2000]. Apparently, knowledge on mechanisms of colloids transport in unsaturated porous media is still limited.

Recently, in an attempt to achieve a better understanding of the above mechanisms, studies involving direct observations of colloid transport in unsaturated porous media have been conducted. Some experiments were performed in a capillary channel with moving air-water interfaces [Sharma et al., 2008; Aramrak et al., 2011]. Others were performed in a micro-model or in soil [see e.g., Wan and Wilson, 1994; Chen and Flury, 2005; Gao et al., 2006]. All these experiments were performed with air and water as the two immiscible phases. But, it is difficult to control air flow rate in a network of pores. Also, in some visualization experiments, the two fluids must have the same index of refraction; this is not possible with air and water. So, in some experiments, two immiscible liquids have been employed. Moreover, oil–water systems are also important in industry. Hence colloids transport in oil-water system, especially their behavior close to the oil-water interface has been studied [Leunissen et al., 2007]. Zevi et al. [2010] employed water and low-viscosity silicone oil as the wetting and non-wetting phases to study pathogen transport during two-phase flow. Zhang et al. [2013] also used two liquids, namely water and fluorinert, and studied the effect of interfaces on the

distribution of colloids in a PDMS micro-model.

In this work, we report on results of experiments performed in a PDMS micro-model under steady-state and transient two-phase flow conditions. Our aim was to study pore-scale processes that affect the remobilization of attached colloids, when fluid saturation is changed, i.e. when imbibition or drainage occurs. In particular, we were interested in the role of fluid-fluid interfaces in the remobilization. Another objective was to formulate a macro-scale model of colloid transport and remobilization and produce experiment data for verifying it. We directly observed the distribution and movement of colloids by means of a confocal microscope. We also measured the concentrations of colloids as a function of time in the outlet reservoir. We performed transport experiments under steady-state flow (of one of the phases) followed by imbibition or drainage. To simulate the remobilization of colloids, the rate of detachment of adsorbed colloids were modeled to be a linear function of the rate of change of saturation. The remobilization of colloids attached to fluid-fluid interfaces was modeled as a function of the change in interfacial area. This is the first study of colloid transport in two phase flow, where pore-scale visualization, breakthrough concentration measurement, and modeling of results are combined. Video images, included as ancillary material, provide insightful images of the movement of colloid in a network of pores occupied by two immiscible liquids.

6.2 Experimental materials and methods

We have performed experiments on transport of colloids in a micro-model. The details of our experimental set-up can be found in Zhang et al. (2013). A schematic representation of the setup is shown in Figure 6.1. The micro-model pore network covered an area of $1mm \times 10mm$. It contained around 90 pore bodies and 200 pore throats, with mean pore size of 30 microns, and porosity of 40%. The micro-model ended in an outlet channel, leading to an outlet reservoir. Details of micro-model fabrication and construction were described in Karadimitriou et al. (2013a). To make the micro-model uniformly and stably hydrophobic, the micro-model was treated by silanization. Using a confocal microscope, images were acquired of the movement of phases and colloids within the micro-model. The microscope was also used to measure the concentration of colloids in the outlet channel, as explained shortly. A dual-direction syringe pump was used to control the flow rates of liquids and colloids suspension via a three-way valve. The pump could be used to inject water (with or without colloids) and fluorinert through

three different inlets of the micro-model.

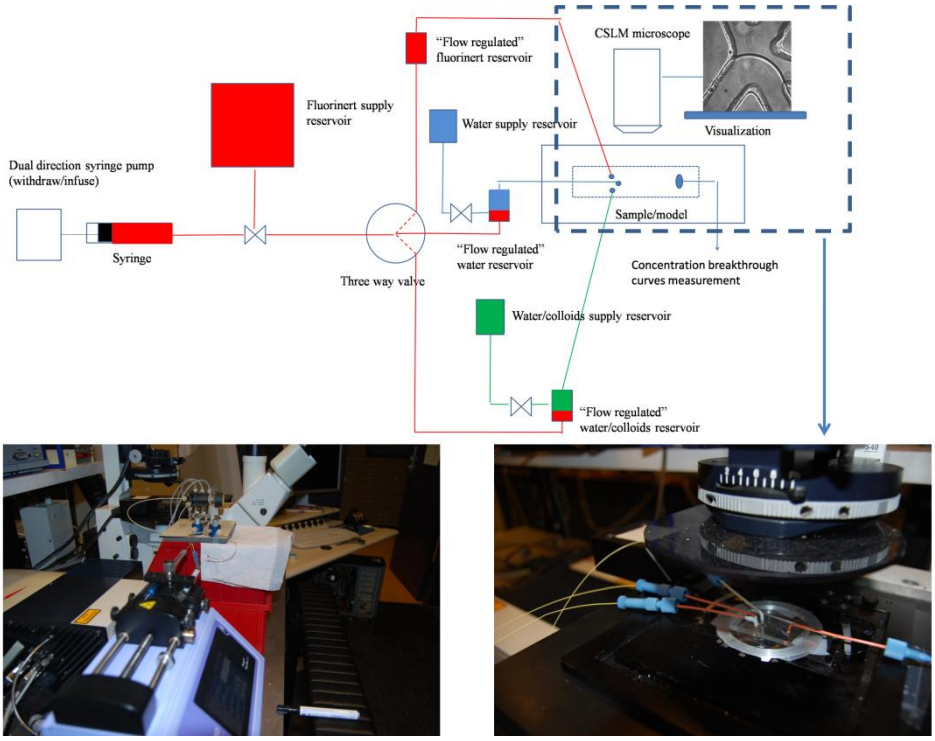

Fig. 6.1 *Schematic representation of the experimental setup.*

As mentioned earlier, the two fluids in our study were fluorinert and water. We chose fluorinert instead of air, mainly because fluorinert and water have almost the same refractive indices. This is necessary for using confocal microscopy and being able to focus at different depths of the micro-model. Given the fact that the micro-model was hydrophobic, fluorinert was the wetting phase and water was the non-wetting phase. The colloids used in this study were carboxylate-modified polystyrene fluorescent microspheres with a mean diameter of 300nm and a particle density of 1055 kg m^{-3}. They were hydrophilic and had weakly negative charged surfaces. The colloid suspensions were prepared by dispersing the microspheres in de-ionized (DI) water to reach a final concentration of around 5.8×10^{10} particles per liter. The pH of the suspension was measured and kept between 6.8 and 7.0 during the experiments. Also, the value of ionic strength was kept constant at 1.2×10^{-3} mM. All experimental conditions are listed in Table 6.1.

Table 6.1. *Experimental conditions of micro-model measurements*

Parameter	Experiment-1	Experiment-2	Experiment-3
Initial water Saturation (%)	100	60 (±2)	40 (±2)
Flow rate during stage 1 (nL/min) –steady-state flow without colloids	150	850	500
Flow rate during stage 2 (nL/min) –steady-state flow with colloids	150	150	150
Final water saturation during imbibition (%)	20 (±2)	15(±2)	20 (±2)
Final saturation during drainage (%)	-	80(±5)	55(±5)
pH (-)	6.8	6.8	6.8

The experiments on colloids transport and remobilization were conducted in three stages. The ***first stage*** of an experiment was designed in order to create steady-state flow conditions at constant water saturation with no colloids. We performed experiments at three different water saturations: 100%, 60%, and 40% denoted as Experiment 1, Experiment 2, and Experiment 3, respectively. In order to achieve 100% water saturation, the model was put vertically and then flushed with carbon dioxide for few minutes to expel the air. After that, the micro-model was put horizontally on the stage of the confocal microscope and connected to the injection tubes. Then, DI water was introduced into the micro-model at the rate of 150nL/min in order to displace and dissolve the carbon dioxide, leading to a fully saturated micro-model. We continued the flow until visualization images showed a stable flow field, where the fluid-fluid interfaces didn't move anymore. For lower-water-saturation experiments, first the micro-model was saturated with fluorinert. Then, water was injected at a rate of either 500nl/min or 850nl/min in order to establish a water saturation of approximately 40% or 60%, respectively. The water distribution was visualized by a set-up developed by Karadimitriou et al. [2012] and its saturation as well as capillary pressure was calculated by image analysis software IDL. Saturation of water was calculated as the ratio of the pixels which corresponded to the non-wetting phase (water dyed with ink), over the total number of pixels of the flow network. Average capillary pressure of the collection of all interfaces within the flow network was calculated as the summation of all local capillary pressures times local interfacial areas, over the total interfacial area. In this way, we obtained the saturation-capillary pressure curve.

In each experiment, the flow rate of water was kept at the above-mentioned rate until

steady-state flow was achieved. In all three experiments, the micro-model was flushed under steady-state flow for approximately five hours. Continuous observation of interfaces showed that no changes were taking place. The ***second stage*** of the experiments involved colloids transport under steady-state flow conditions. In both saturated and unsaturated experiments, the particle suspension was injected into the micro-model at rate of 150 nL/min for 20 minutes. This was followed by the injection of colloids-free DI water for 25 minutes without changing the flow rates. So, the second stage of experiment, i.e. colloids transport under steady-state flow, lasted for 45 minutes. The ***third stage*** of the experiments involved transient two-phase flow and remobilization of attached colloids. This started either with injecting fluorinert (causing imbibition) to displace the water phase and reduce its saturation; or increasing the flow rate of water to increase its saturation (causing drainage).

During the experiments, colloids distribution and their interactions with solid-water interfaces (SWIs), fluorinert-water interfaces (FWIs), and fluorinert-water-solid contact lines (FWSCs) within the flow network were directly observed by confocal microscopy. In addition to still images, real-time images were also taken for subsequent review and analysis of colloids interactions with the moving interfaces and contact lines. The experiments were found to be repeatable. Under the same conditions as visualization experiments done, series of concentration breakthrough curves were measured at the outlet channel with the same visualization system. This was done by measuring the fluorescent intensities of particles at a focus surface (in the horizontal middle plane) of the micro-model outlet channel at a speed of 834ms per frame. Colloids above and below this focus surface were out of confocal focus, but we assumed the colloids distribution was uniform over the depth. First a calibration curve was prepared by injecting a known concentration of water-colloid suspension into the outlet channel of the micro-model via the outlet reservoir. By measuring the fluorescent intensity of various known concentrations, the calibration curve was obtained. The confocal images were all taken at low intensities (<100 μW) to avoid bleaching of the fluorescent dye.

6.3 Mathematical Model

For modeling the experiments, two-phase flow equations as well as colloids transport equations were employed and solved numerically.

6.3.1 Flow equations

We assumed that the solid phase is rigid and the fluid phases are incompressible. Thus, the combination of mass balance equations and Darcy's law led to the following set of governing equations for fluorinert and water:

$$\phi \frac{\partial S_f}{\partial t} + \nabla \cdot (\frac{Kk_{rf}}{\mu_f} \nabla P_f) = 0 \tag{6.1}$$

$$-\phi \frac{\partial S_f}{\partial t} + \nabla \cdot (\frac{Kk_{rw}}{\mu_w} \nabla P_w) = 0 \tag{6.2}$$

where subscripts f and w indicate fluorinert (wetting phase) and water (non-wetting phase) in our experiments, respectively; ϕ is the porosity [-]; S_α is α-phase saturation [-]; K is intrinsic permeability [L^2]; $k_{r\alpha}$ is α-phase relative permeability [L^{-2}]; μ_α is the dynamic viscosity [$ML^{-1}T^{-1}$]; P_α is α-phase pressure [$MT^{-2}L^{-1}$]. Because in our experiment, the micro-model was put horizontally on the stage of the microscope, we did not consider gravity.

We also employed the following constitutive equations for relative permeability and capillary pressure [van Genuchten, 1980]:

$$k_{rf} = S_e [1 - (1 - S_e^{\frac{1}{m}})^m]^2 \tag{6.3}$$

$$k_{rw} = (1 - S_e)^{1/2} (1 - S_e^{1/m})^{2m} \tag{6.4}$$

$$P_w - P_f = P_c(S) = \frac{1}{\alpha} (S_e^{-1/m} - 1)^{1/n} \tag{6.5}$$

where m=1-1/n, the parameter n can be related to the pore size distribution; α [Pa^{-1}] can be interpreted as the inverse of the entry pressure; S_e is the effective saturation, defined as S_e=(S_f -S_{rf})/(1-S_{rf}), where $S_{rf} \leq S_f \leq 1$.

The initial condition for each experiment was set to the specified saturation given in Table 1 and the corresponding pressure. For the inlet boundary condition, we specified the flux of either the non-wetting phase (water) for drainage experiments and the flux of or the wetting phase (fluorinert) was specified related to drainage or imbibition, respectively. The outlet boundary pressure was set equal to zero.

6.3.2 Transport equations

We simulated colloids transport during stages 2 and 3 of the experiments by advection-dispersion-sorption equations. As the colloids were hydrophilic, they were present in the water (i.e. the non-wetting phase) only. The governing equation for colloids transport in the water phase is:

$$\phi \frac{\partial S_w C_w}{\partial t} = \frac{\partial}{\partial x}(\phi S_w D \frac{\partial C_w}{\partial x}) - \frac{\partial q_w C_w}{\partial x} - \gamma_s - \gamma_{fw} \tag{6.6}$$

where C_w [L^{-3}] is the number concentration of colloids in water (number of colloids per unit volume of water); D [L^2T^{-1}] is the dispersion coefficient, q_w [LT^{-1}] is the flow rate; γ_s and γ_{fw} [pfu $L^{-3}T^{-1}$] are net rates of attachment of colloids to SWIs and FWIs, respectively. The net rate of adsorption to FWIs can be expressed as:

$$\gamma_{fw} = \frac{\partial a_{fw} C_{fw}}{\partial t} \tag{6.7}$$

where a_{fw} [L^{-1}] is the specific fluorinert-water interfacial area per unit volume of porous medium; C_{fw} [Number L^{-2}] is the concentration of colloids attached to the FWI given as the number of colloids per unit area of fluorinert-water interface. According to the theory developed by Hassanizadeh and Gray [1993], interfacial area depends not only on saturation but also on capillary pressure. However, for the purpose of this study, we assumed that a_{fw} only depends on saturation. This is certainly justified in the case of imbibition experiments, where the primary imbibition curve was followed, along which there is unique relationship to saturation-capillary pressure. Here, we used the following formula for a_{fw}:

$$a_{fw} = a_0 (1 - S_w)^{1.2} S_w \tag{6.8}$$

where a_0 is the specific interfacial area corresponding to residual saturation of the medium.

In principle, FWI colloid attachment/detachment should be modeled as a kinetic process. But in our preliminary simulations, we found that the kinetic constant is large and an equilibrium description provides satisfactory results. This was in line with our findings when we simulated the experiment results of Torkzaban et al. (2006a, b) [See Zhang et al., 2012].

Next, we assumed linear equilibrium partitioning of colloids between water and

fluorinert-water interface, such that:

$$C_{fw} = K_D^a C_w \tag{6.9}$$

where K_D^a [L] is the equilibrium distribution coefficient for sorption onto the FWI. Note that Equations (6.7) and (6.8) model both attachment of colloids to FWIs and their remobilization. When fluorinert-water interfaces are created (occurs mainly during drainage), more colloids can get attached to them. But, when interfaces are destroyed (occurs mainly during imbibition), attached colloids are released back into the water phase.

The attachment-detachment to/from SWI is described by the following equation [due to Cheng and Saiers, 2009]:

$$\gamma_s = \frac{\partial \rho_b C_s}{\partial t} = \phi S_w k_{att}^s C_w - (1-\phi)\rho_s k_{det}^s C_s - (1-\phi)\rho_s \sum_{i=1}^{N_c} k_{rem}^i(t) C_{si} \tag{6.10}$$

where C_s [M^{-1}] is the number of colloids adsorbed to the SWI per unit mass of solid phase; ρ_s [ML^{-3}] is the mass density of the PDMS solid grain; k_{att}^s and k_{det}^s [T^{-1}] are attachment and detachment rate coefficients of colloids to and from the solid-water interface, respectively. The last term in Equation (6.10) models the colloids remobilization from SWI due to transient flow. The time-dependent coefficient $k_{rem}^i(t)$ and N_c are defined shortly. Note that the last term will be nonzero only in stage 3of the experiments, i.e. during transient conditions.

For stage 2 of the experiment (steady-state flow), the initial conditions were $C_w(x, 0) = 0$ and $C_s(x, 0) = 0$. The inlet boundary conditions were: $C_w(0, t) = C_0$ ($0 < t < t_{seeding}$) and $C_w(0, t) = 0$ ($t_{seeding} < t < t_{end}$), where $t_{seeding}$ represents the final time of colloids seeding, and t_{end} is the final time of steady-state transport. For the outlet boundary, a zero concentration gradient was assumed.

For stage 3 of the experiments, the inlet boundary condition was zero concentration, and for the outlet boundary, a zero dispersion flux was imposed. The initial conditions were $C_w(x, 0) = C_{w0}$ and $C_s(x, 0) = C_{s0}$, where C_{w0} and C_{s0} are given by the profiles of the colloid concentration in water and attached to SWIs, respectively. These profiles obtained from the distribution at the final time of stage 2.

Following Cheng and Saiers (2009), the remobilization coefficient $k_{rem}^i(t)$ is related to the time rate of change of saturation. Cheng and Saiers [2009] hypothesized that remobilization of adsorbed colloids occurs only in pores that are being emptied during

drainage or are filled during imbibition. Based on the variability in pore size, the pores were divided into N_c compartments. Once a compartment i empties or fills as its entry pressure P_{ci} is reached, adsorbed particles are assumed to be removed from the pore walls of that compartment. Thus, the remobilization coefficient for imbibition and drainage are given by the following equations, respectively.

$$k_{rem}^{i}(t) = \begin{cases} 0 & for \;\; P_w - P_f > P_{ci} \\ N_{imb}\left|\dfrac{\partial S_w}{\partial t}\right| & for \;\; P_w - P_f \le P_{ci} \end{cases} \tag{6.11}$$

$$k_{rem}^{i}(t) = \begin{cases} 0 & for \;\; P_w - P_f < P_{ci} \\ N_{dr}\left|\dfrac{\partial S_w}{\partial t}\right| & for \;\; P_w - P_f \ge P_{ci} \end{cases} \tag{6.12}$$

where P_w and P_f are fluid pressures, obtained by solving equations (6.1) and (6.2); P_{ci} is the entry pressure for each compartment i; N_{imb} and N_{dr} are empirical coefficients that quantify colloids remobilization during imbibition and drainage, respectively. The entry pressure for each compartment was determined from the capillary pressure-saturation curve.

The set of equations presented above were solved with the aid of COMSOL code 4.3a. The model was coupled to the genetic algorithm [see Houck et al., 1995] optimization module in MATLAB in order to determine model parameter values. All model parameter values are given in Table 6.2.

6.4 Results

6.4.1 Colloid transport and retention under steady-state flow

As mentioned earlier, colloid transport experiments during steady-state flow were performed at three different water saturations: 100%, 60%, and 40%. The seeding lasted 20 minutes followed by 25 minutes of steady-state colloids-free water flow. The measured breakthrough curves are shown in Fig.2. It is clear that there was significantly more retention at lower water saturations. The peak values of normalized breakthrough concentrations are around 0.95, 0.80, and 0.65 for experiments 1, 2, and 3, respectively. Also, the total mass recovered at the end of stage 2 of our experiments was less at a lower saturation as given in Table 6.3. Pore-scale images with the size of 512μm ×

512μm, taken with confocal microscope from an area at the middle plane of the micro-model (the same depth where the breakthrough concentrations were measured), helped us to see colloid attachment sites. An example is shown in Fig. 6.3. The particles observed in this image are either in water or attached to the FWIs/FWSCs. There are also few colloids attached to SWIs.

Table 6.2. *Parameters determined from fitting the breakthrough curves (average ± standard deviations).*

	Parameter	Experiment-1	Experiment-2	Experiment-3
Steady-state condition	Dispersivity (cm)	0.035	0.052	0.09
	SWI attachment coefficient, k_{att}^{s} (s^{-1})	1.07 (±0.096) x 10^{-3}	1.63(±0.12)x10^{-3}	1.58 (±0.14)x 10^{-3}
	SWI detachment coefficient, $k_{\det}^{s}$ (s^{-1})	0.1117 (±0.006) x 10^{-3}	0.07 (±0.005)x10^{-3}	0.2167 (±0.017)x 10^{-3}
	K_D^a (m)	-	0.55 (±0.1)	0.57 (±0.02)
Transient condition (imbibition and drainage)	N_{imb}	1.53	0.32	0.26
	a_0 (m^{-1})	2500	2500	2500
	α	0.000395	0.000395	0.000395
	n	5.17	5.17	5.17
	N_c	5	5	5
	N_{dr}	-	0	0

6.4.2 Remobilization of colloids during imbibition

As mentioned earlier, the seeding of colloids during steady-state water flow (stage 2) was followed by transient flow, basically changing the saturation (stage 3). In the case of imbibition, this was achieved by stopping the flow of water and injecting fluorinert at a rate of 150nL/min. This resulted in sudden decrease of water saturation to the residual value in all three experiments. When fluorinert was observed coming out of the outlet reservoir, then we stopped the experiments. The imbibition process caused a remobilization of the colloids that were left in the micro-model at the end of stage 2. As mentioned earlier, the majority of colloids were attached to FWIs and FWSCs. The remobilization of colloids resulted in a spike in the breakthrough concentration as can be seen in Fig. 6.2. The peak concentration is highest for experiment 1 and lowest for experiment 3. We have also calculated the ratio of remobilized colloids to the total

injected colloids. These numbers were 1%, 6.4%, and 5.3%, respectively. The strength of this remobilization depends on two main factors: (1) the rate of saturation change (which in the three experiments were from 100% to 20%, from 60% to 15%, and from 40% to 20% in increasingly longer times); (2) the accessibility of emplaced colloids to the displacing fluorinert.

Real-time images of the movement of colloids can be found in the Ancillary Material (see Movie 6.1 and Movie 6.2). Four images from experiment 2 (with initial water saturation of 60%) are shown in Fig.5. The images show that as the imbibition front advanced into the micro-model, FWIs and FWSCs, and colloids attached to them, were pushed towards the outlet. Moreover, the moving FWIs and FWSCs scoured the colloids adsorbed to the solid surface. We know that some of these colloids re-entered the flowing water. This was the case with "interface 1" shown in Fig. 6.5.

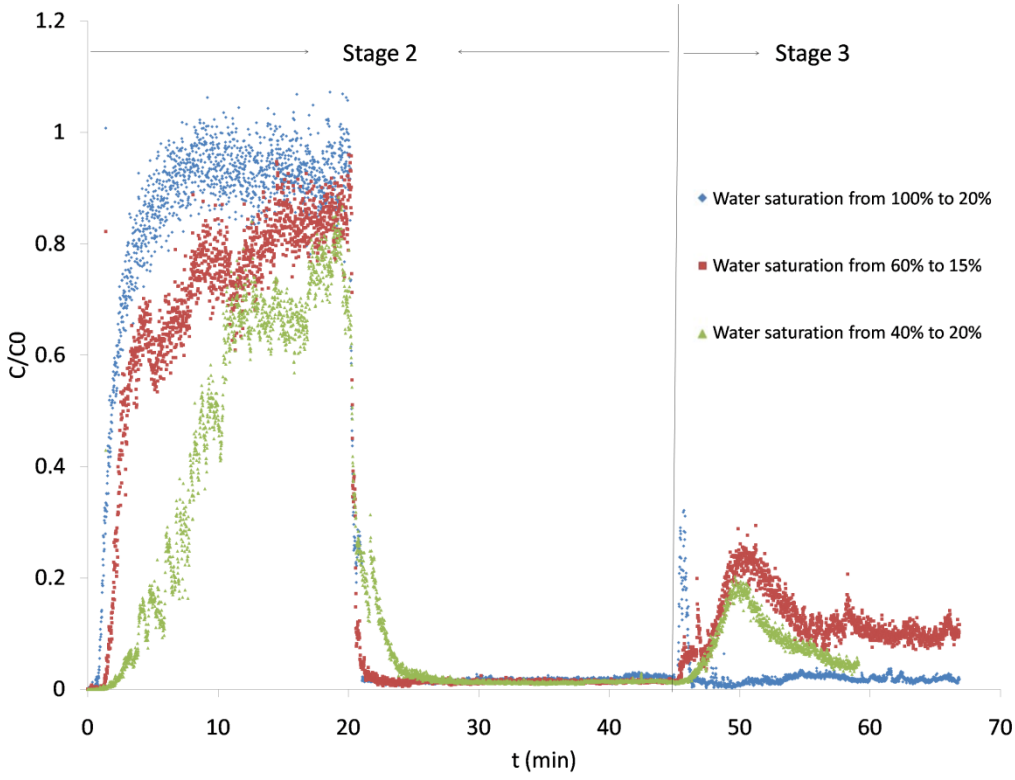

Fig. 6.2 *Impact of saturation on the transport and remobilization of colloids under steady-state and during imbibition of the micro-model.*

During imbibition, we also had local drainage. For example, we can see that water is pushed into large pore B (see Fig. 6.5a) displacing fluorinert. The interface corresponding to this local drainage is Interface 2. Some of the colloids attached to Interface 2 were re-deposited on the SWI in pore B, as visible in areas indicated by white circles in Fig. 6.5c and Fig. 6.5d. Some of the remobilized colloids originated from immobile water blubs that were trapped in the pore network and got re-connected during imbibition and moved out of the network. But due to the limitations of objective lens, we could not capture this phenomenon.

6.4.3 Colloid transport during drainage

In the case of experiments 2 and 3 (with a water saturation of 60% and 40%, respectively), we also performed drainage experiments; i.e. we expelled fluorinert and increased water saturation. This was achieved by increasing the flow rate of fresh water from 150 nL/min to 600 nL/min. The measured breakthrough concentration curves are shown in Fig. 6. Real-time images of parts of micro-model are also shown in Movie 3 and Movie 4 of the Ancillary Material.

Contrary to the case of imbibition, we did not find any peak in the breakthrough curves, which means no remobilization, occurred during drainage. The main reason for the lack of remobilization in our drainage experiments is that FWIs and FWSCs moved very little and the distribution of water and fluorinert did not change much. Because the micro-model was fluorinert-wet, despite the four-fold increase in water injection rate, the water saturation change was small: from 60% to 80% and from 40% to 55% in experiment 2 and 3, respectively. From the real-time images shown in Movie 6.3 and Movie 6.4 of the Ancillary material, we can see that even some FWIs were destroyed as water pockets get reconnected; the released colloids got attached to other FWIs downstream. In fact, drainage (i.e. the increase of water saturation in our case) generally leads to an increase in fluid-fluid interfacial area [see e.g. Karadimitriou et al., 2013a]. So, there is no decrease in the number of attachment sites in our drainage experiment, and therefore no remobilization.

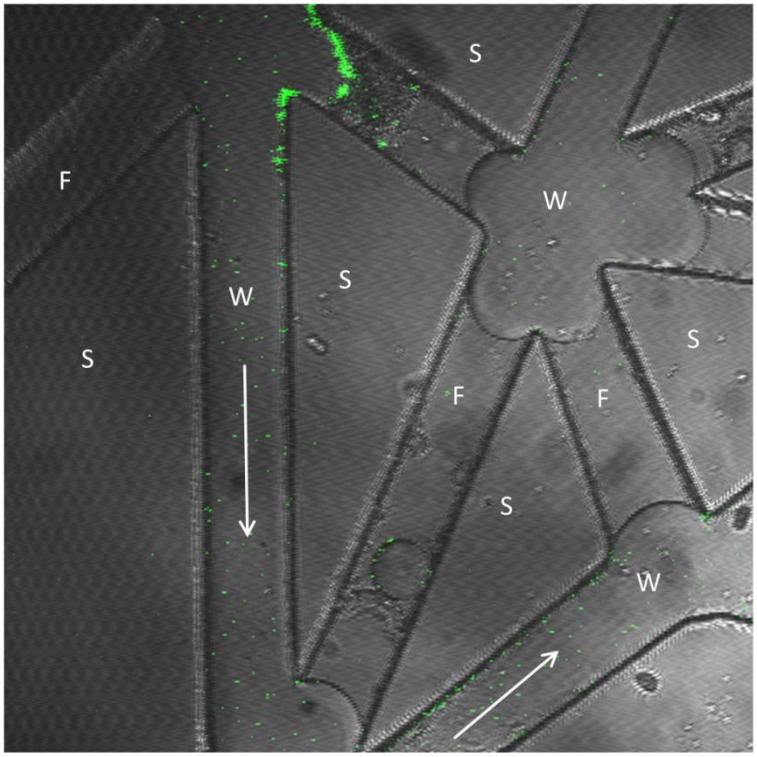

Fig. 6.3 *A confocal microscope image of micro-model (image size 512μm ×512μm) during unsaturated steady-state flow. S, PDMS solid; W, water; F, fluorinert. White arrows indicate the flow path and direction. Green dots are colloidal hydrophilic particles.*

6.4.4 Simulation of breakthrough curves

Experimental results were simulated based on the model presented earlier in this paper. For the stage 2 of experiments, only colloid transport equations had to be solved as the flow velocity was known and constant. Data from the stage 2 were used to determine the values of attachment and detachment coefficients k_{att}^{s} and k_{det}^{s} (for solid phase) as well as the distribution coefficient K_D^a (for FWI). The fitted values are given in Table 6.2. As we can see, the value of attachment coefficient, k_{att}^{s}, is larger for experiments with smaller water saturation. The value of detachment coefficient, k_{det}^{s}, is one order of

magnitude smaller than the attachment coefficient. Also, it does not show a clear correlation with saturation. The value of the FWI distribution coefficient K_D^a is found to be the same for stage 2 and stage 3. This is to be expected as this coefficient accounts for local equilibrium between colloids in water and attached to interfaces; so, it should be independent of saturation.

For stage 3 of experiments (transient flow), flow equations were solved too. Parameter values determined from steady-state experiment were kept unchanged for the transient part. Results of simulation of the three imbibition experiments are shown in Fig. 6.4, and for the two drainage experiments, they are given in Fig. 6.6 (a) and Fig. 6.6 (b). The agreement between simulations and data is very good. In particular, it is encouraging that the remobilization parts of the curves are closely followed by the simulations.

(a)

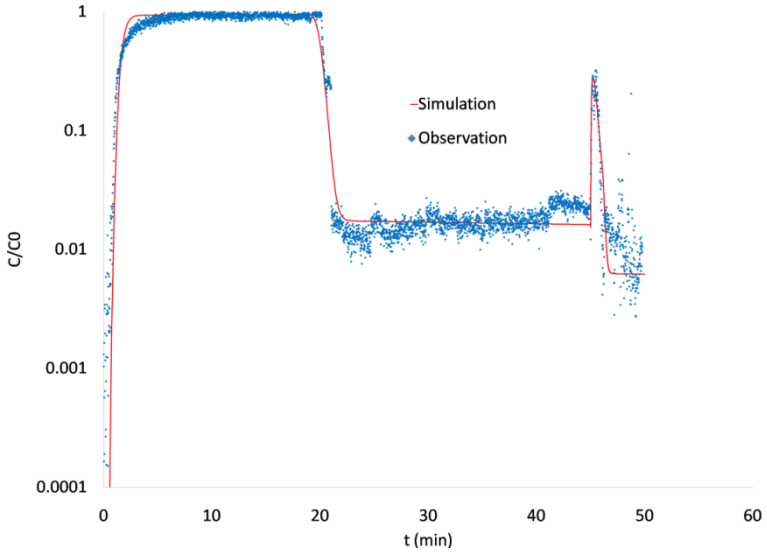

(b)

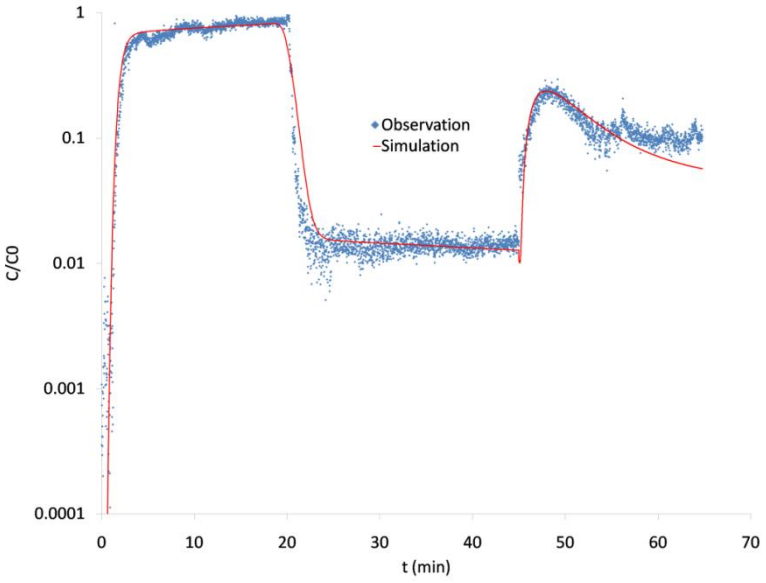

(c)

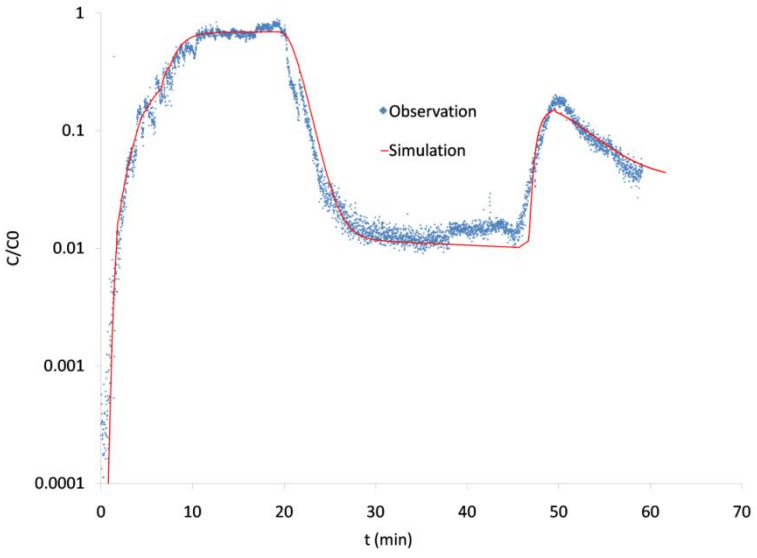

Fig. 6.4 *Measured (dots) and fitted (line) breakthrough curves of a) experiment 1 (from water saturation 100% to 20%), b) experiment 2 (from 60% to 15%), and c) experiment 3 (from 40% to 20%).*

6.5 Discussion and Conclusions

In this study, we employed three approaches to investigate colloids transport and in particular the remobilization of colloids under transient two-phase flow conditions in a porous medium. The first approach was pore-scale visualization using a confocal laser microscope, which allowed direct observation of movement of colloids and fluid-fluid interfaces. Due to the limitation of the objective lens of confocal microscope, we could monitor only a few pores in a single image at any given time. Nevertheless, the visualization gives us valuable insight in attachment as well as remobilization mechanisms as interactions of colloids with fluid-fluid and fluid-solid interfaces can be directly observed. The second approach was the measurement of the effluent concentration, which provided quantitative information on the macro-scale behavior of the colloids transport through the micro-model. Our third approach was the numerical simulation of the breakthrough curves. For describing the remobilization of colloids as a result of saturation change, we adapted the remobilization model of Cheng and Saier's model [2009]. They assumed that the colloid remobilization occurs only in pores where fluid saturation change drastically, for example due to snap-off. This means that the remobilization starts in larger pores during drainage (and then in a hierarchy of smaller and smaller pores), but it starts in smaller pores during imbibition (and then in a hierarchy of larger and larger pores). Cheng and Saiers [2009] did not explicitly model colloid attachment/detachment related to fluid-fluid interfaces. They lumped it together into the attachment/detachment processes at solid-wetting phase interface. We used Cheng and Saier's model to describe colloid release from solid surfaces, but we explicitly accounted for fluid-fluid interfaces and corresponding attachment and remobilization. We do not explicitly account for the movement of contact lines. The corresponding attachment/detachment is lumped with the fluid-fluid interfaces. We did not explicitly model the evolution of interfaces with time. We simply assumed that the fluid-fluid interfacial area is a function of saturation. This assumption is valid during primary imbibition process. Through visualization experiments, we clearly observed colloids attached to the FWSCs. But, in the simulation, we didn't directly consider colloid attached to/detached from FWSC as an individual equation, it was lumped into SWI. It would be nice if people can measure the length of the contact lines and develop a formula for that.

Our micro-model was hydrophobic which means that water was the non-wetting phase and fluorinert was the wetting phase. The colloids were hydrophilic and had

absolutely no affinity for fluorinert. So, our experiments would be similar to the transport of colloids in a hydrophobic soil. Therefore, a direct application of our results to natural soil is not possible. But we can learn about the role of fluid-fluid interfaces and the effect of change in water saturation on colloids behavior.

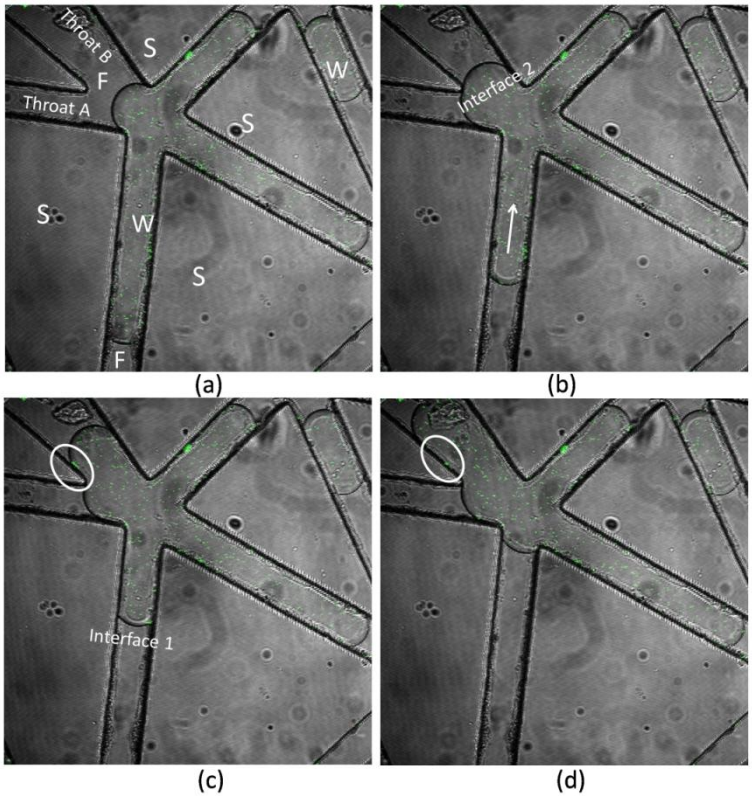

Fig. 6.5 *Real-time images of colloids transport during imbibition in stage 3 of experiment 2 (initial water saturation of 60%). Times are given from the start of stage 2 (see also Fig. 1). (a) Right before the start of imbibition, t=45min; (b) t=45min 16sec; (c) t=45min 31sec; (d) t=46min 22sec. Arrow shows the direction of the flow; S, PDMS matrix; F, fluorinert; W, water.*

Our results clearly show a very significant increase in colloids removal during steady-state flow under unsaturated conditions compared to saturated conditions. It must be noted that the flow rate in all experiments was the same. So, the average pore velocity was higher in unsaturated experiments. Higher velocities should lead to less attachment. Yet, we had more attachment under unsaturated conditions. After injecting a pulse of

colloids, 88% of colloids were found in the effluent of the water-saturated micro-model as opposed to 70% and 53% when the micro-model saturation was 60% and 40%, respectively.

The enhanced removal of colloids under unsaturated conditions has been reported by many researchers. Various authors have mentioned (a combination of) different mechanisms for this enhanced attachment. For example, Torkzaban et al. [2006a] reported that there is enhanced adsorption of viruses to the solid-water interface. The explanation for the occurrence of this mechanism is as follows. Under unsaturated conditions, the thickness of water pathways becomes smaller because the pore space is shared by water and fluorinert. Thus, the colloids have to travel closer to the pore walls and they have a higher chance of getting attached. This mechanism could not occur in our micro-models and we did not find enhanced adsorption to the solid phase. First, when comparing images from saturated to unsaturated experiments, we did not find observable differences in the number of colloids attached to the solid-water interface. In fact, in our micro-model, at any given location, the pore space was not being shared by the two fluids. Any given pore segment was filled either by water or by fluorinert. So, the thickness of water-filled pathways was not different under different saturations. Secondly, our numerical simulation results did not show a significant increase of attachment to the solid phase. The estimated values of attachment and detachment coefficients are given in Table 6.2. We see that the values of the ratio of $k_{att}^{s} / k_{det}^{s}$ for the three experiments are not drastically different. It could be that we did not see a significant increase in attachment because the colloids were dispersed in water, which was the non-wetting phase in our micro-model. Experiments with hydrophobic colloids (to be dispersed in fluorinert) are needed in order to investigate this question.

Another mechanism for enhanced attachment under unsaturated conditions is reported to be attachment to fluid-fluid interfaces [e.g. Wan and Wilson, 1994; Powelson and Mills, 2001; Keller and Sirivithayapakorn, 2004; Torkzaban et al., 2006a, b] and fluid-fluid-solid contact lines [see e.g. Crist et al., 2004, 2005; Zevi et al., 2009]. This seems indeed to be the main mechanism for enhanced attachment according to our experimental results. We certainly observed a large number of colloids attached to FWIs and FWSCs. Also, we clearly had more interfaces and contact lines at lower saturations. So, even if the attachment per surface area of interface was constant, there was more attachment at lower saturations. For a satisfactory simulation of breakthrough curves, we needed to include the attachment of colloids to interfaces and contact lines.

Finally, a third mechanism for enhanced attachment is reported to be the straining of colloids by thin films of water [see e.g. Wan and Tokunaga, 1997; Auset et al., 2005]. We could not investigate this effect in our experiments. First of all, the wetting phase (that could form a film) was fluorinert in our case. But, fluorinert was devoid of colloids. So, colloids could not be trapped in such films. Secondly, wetting phase films are expected to be a few nano-meters and the objective lens of our microscope was not able to see such a thin film.

Table 6.3. *Calculated colloid mass recovered in the micro-model effluent, given as a percentage of injected colloid mass.*

Exp.	Mass balance (%)			
	Recovery at the end of stage 2	Remobilized during imbibition	Remaining at the end of imbibition	Remobilized during drainage
Experiment-1	88 (±2)	1(±0.1)	11	-
Experiment-2	70 (±4)	6.4 (±0.4)	23.6	0
Experiment-3	53 (±5)	5.3 (±0.2)	41.7	0

We also performed transient experiments to investigate the effect of saturation change on remobilization of attached colloids. We performed both imbibition and drainage experiments, starting from different initial saturations. Before transient experiments, a pulse of colloids were injected (during steady-state flow) in order to emplace colloids in the micro-model. Both pore-scale images and breakthrough curves showed a significant remobilization of colloids occurring during imbibition (i.e. fluorinert displacing water, which contained colloids). As can be seen in Movie 6.1 and Movie 6.2, as soon as fluorinert started to displace water, FWI interfaces, with colloids attached to them, were pushed towards the micro-model outlet. Moving interfaces also scoured colloids attached to the solid surface. In the breakthrough curve, we see a distinct spike in concentration. The peak concentration was largest for the experiment 1, where the water saturation dropped from 100% to about 20% in a short time. This was a saturation change of 80%. A lower peak concentration was observed in experiment 2, where the water saturation was reduced from 70% to 15% (giving a saturation change of

55%). The lowest peak concentration was reached in experiment 3, where the water saturation changed only 20% (from 40% to 20%). So, clearly the strength of remobilization depends on the degree of saturation change. At the same time, a reduction of the water saturation leads to the creation of more fluid-fluid interfaces. So, remobilized colloids could re-attach to new FWIs. This is why the percentage of emplaced colloids that were remobilized is lower in the case of experiment 1 (see Table 6.3) as many new interfaces were created in that case.

We also performed drainage experiments, where water saturation was increased from an initial value of 60% to 80% in experiment 2 and from 40% to 55% in experiment 3. Contrary to imbibition experiments, we found no remobilization of attached colloids. The main reason for this result is that the saturation change, and thus the change in fluids distribution were small. This also meant that there was not much change in amount of interfacial area. So, the water flow field did not change much before and after drainage. Another reason is that there were no colloids available in the fluorinert to be remobilized.

Apart from saturation change, another concept should be considered is colloid attachment to and release from interfaces due to force/torque balance on the colloid. Based on DLVO (Derjaguin-Landau-Verwey-Overbeek) theory, colloids can only attached to the SWI due to attractive forces. Non-DLVO forces such as hydrodynamic force and capillary force are likely play significant role under unsaturated condition [Bradford et al., 2008]. Capillary forces were reported to be several orders of magnitude bigger than DLVO force and hydrodynamic force. The capillary forces help pin the colloid at the FWSC and FWI. Under transient unsaturated conditions, the colloids pinned at the solid interfaces contacted with a moving FWI/ FWSC and the repulsive capillary force started acting on them, leading to colloid remobilization. The evidence is described by Shang et al. [2008, 2009] in detail, which calculated and directly measured forces exerting on colloids, and suggested that capillary forces play the dominant role in controlling colloid release.

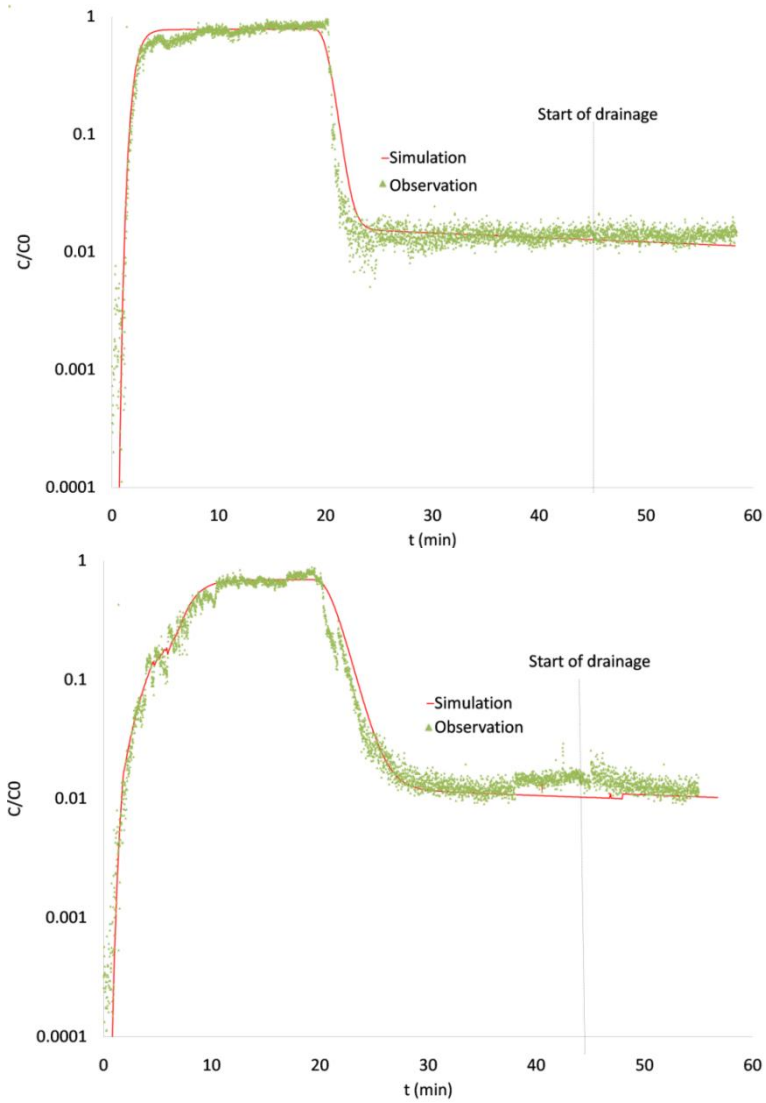

Fig. 6.6 *Breakthrough curves of (a) experiment 2 (drainage causing increase of water saturation from 60% to 80%) and (b) experiment 3 (drainage causing increase of water saturation from 40% to 55%). Measured data are shown as dots and simulation results are shown as solid lines. Note that the steady-state flow parts of the curves are identical to the results shown in Fig. 6.2.*

Our results are only partially comparable to the studies reported in the literature. Some studies have shown that remobilization occurs during both drainage and imbibition [Saiers et al., 2003; Zhuang et al., 2007; Cheng and Saiers, 2009], even with a

stronger remobilization during drainage [Cheng and Saiers, 2009]. But, these drainage experiments involved displacement of the wetting phase (which was water) containing colloids by air (the non-wetting phase). In our case, drainage means the displacement of fluorinert (which has no colloids) by water (injected without colloids). So, if the injected fresh water does not disturb the residual water much, we should not find remobilization, as observed in our experiments.

In summary, micro-model experiments combined with confocal laser microscopy provides valuable insights in the behavior of colloids in porous media filled by two fluid phases. Fluid-fluid interfaces and fluid-fluid-solid contact lines play a major role in the retention as well as remobilization of colloids. The behavior of colloids is determined by the combination of porous medium wettability properties, fluids involved and property of colloids.

Acknowledgements

Prof. Jack F. Schijven (National Institute of Public Health and the Environment, the Netherlands) and Dr. Qin Chaozhong are gratefully acknowledged for very helpful discussions. Funding of the first author by the China Scholarship Council is greatly appreciated. The first four authors are members of the International Research Training Group NUPUS, financed by the German Research Foundation (DFG) and Netherlands Organization for Scientific Research (NWO).

References

(1) **Aramrak**, S., M. Flury, and J.B. Harsh (2011), Detachment of deposited colloids by advancing and receding air-water interfaces Langmuir, 27, 9985-9993.

(2) **Auset**, M., A. A. Keller, F. Brissaud, and V. Lazarova (2005), Intermittent filtration of bacteria and colloids in porous media, Water Resour. Res., 41, W09408, doi: 10.1029/2004WR003611.

(3) **Bradford**, S. A., and H. Kim (2012), Causes and implications of colloid and microorganisms retention hysteresis, J. Contam. Hydrol., 138-139, 83–92, doi:10.1016/j.jconhyd.2012.06.007.

(4) **Bradford**, S.A., S. Torkzaban, H. Kim, and J. Simunek (2012), Modeling colloid and microorganism transport and release with transients in solution ionic strength, 2012, Water Resour. Res., 48, doi: 10.1029/2012WR012468.

(5) **Chen**, G., and M. Flury (2005), Retention of mineral colloids in unsaturated porous

media as related to their surface properties, Colloids and Surfaces A: Physicochem. Eng. Aspects, 256, 207-216.

(6) **Cheng** T., and J.E. Saiers (2009), Mobilization and transport of in situ colloids during drainage and imbibition of partially saturated porous media. Water Resour. Res. 45, W08414, doi: 10.1029/2008WR007494.

(7) **Flury**, M., J.B. Harsh, and J.B. Mathison (2003), Miscible displacement of salinity fronts: Implications for colloid mobilization, Water Resour. Res.39 (12): doi:10.1029/2003WR002491.

(8) **Gao**, B., J.E. Saiers, and J. N. Ryan (2006), Pore-scale mechanisms of colloid deposition and mobilization during steady and transient flow through unsaturated granular media, Water Resour. Res. 42, W01410, doi: 10.1029/ 2005WR004233.

(9) **Hassanizadeh**, S.M., and W.G. Gray (1993), Thermodynamic basis of capillary pressure in porous media, Water Resour. Res., 29: 3389-3405, doi: 0043-1397/93/93WR-01495.

(10) **Houck**, C.R., J.A. Joines, and M.G. Kay. 1995. A genetic algorithm for function optimization: A Matlab implementation. Tech. Rep. NCSU-IE-TR-95–09. North Carolina State Univ., Raleigh.

(11) **Karadimitriou**, N.K., M. Musterd, P.J. Kleingeld, M.T. Kreutzer, S.M. Hassanizadeh, and V. Joekar-Niasar (2013a), On the fabrication of PDMS micro-models by rapid prototyping, and their use in two-phase flow studies, Water Resour. Res., 49: 2056-2067, doi: 10.1002/wrcr.20196.

(12) **Karadimitriou**, N.K., V. Joekar-Niasar, S.M. Hassanizadeh, P.J. Kleingeld, and L.J. Pyrak-Nolte (2012), A new micro-model experimental approach for two-phase flow studies; comparison with a pore-network model, Lab on a Chip, Vol. 12, pp. 3413-3418, doi: 10.1039/C2LC40530J.

(13) **Keller**, A. A., and S. Sirivithayapakorn (2004), Transport of colloids in unsaturated porous media: Explaining large-scale behavior based on pore-scale mechanisms, Water Resour. Res., 40, W12403, doi:10.1029/ 2004WR003315.

(14) **Lazouskaya**, V., and Y. Jin (2008), Colloid retention at air-water interface in a capillary channel, Colloids Surf. A, 325, 141– 151.

(15) **Lazouskaya**, V., L-P. Zhang, H.Gao, X. Shi, K. Czymmek, and Y. Jin (2011), Pore-Scale Investigation of Colloid Retention and Mobilization in the Presence of a Moving Air–Water Interface ,Vadose Zone J., 10, 1250-1260.

(16) **Leunissen** M. E., A. van Blaaderen, A.D. Hollingsworth, M.T. Sullivan, and P. M. Chaikin (2007), Electrostatics at the oil–water interface, stability, and order in

emulsions and colloids, PNAS, 8, 2585-2590, Doi: www.pnas.org_cgi_doi_10.1073_pnas.0610589104.

(17) **Powelson**, D. K., and A. L. Mills (2001), Transport of Escherichia coli in sand columns with constant and changing water content water saturations, J. Environ. Qual., 30(1), 238–245.

(18) **Saiers**, J. E., and J.J. Lenhart (2003), Colloid mobilization and transport within unsaturated porous media under transient-flow conditions, Water Resour. Res., 39(1): 10-19, doi: 10.1029/2002WR001370.

(19) **Sadeghi**, G., J.F. Schijven, T. Behrends, S.M. Hassanizadeh, J. Gerritse, and P.J. Kleingeld (2011), Systematic study of effects of pH and ionic strength on attachment of phage PRD1. Ground Water 49:12–19. doi:10.1111/j.1745-6584.2010.00767.x

(20) **Sadeghi**, G., T. Behrends, J.F. Schijven, and S.M. Hassanizadeh (2013), Effect of dissolved calcium on the removal of bacteriophage PRD1 during soil passage: the role of double-layer interactions, J. Contam. Hydrol., 144(1):78-87. doi: 10.1016/j.jconhyd.2012.10.006.

(21) **Sharma** P., M. Flury, and J. Zhou (2008), Detachment of colloids from a solid surface by a moving air-water interface, J. Colloid Interface Sci., 326, 143-150.

(22) **Shang**, J., M. Flury, G. Chen, and J. Zhuang (2008), Impact of flow rate, water content, and capillary forces on in situ colloid mobilization during infiltration in unsaturated sediments. Water Resour. Res. 44, doi: 10.1029/2007WR006516.

(23) **Shang**, J., M. Flury, and Y. Deng (2009), Force measurements between particles and the air-water interface: Implications for particle mobilization in unsaturated porous media, Water Resour. Res., 45, W06420, doi: 10.1029/2008WR007384.

(24) **Sirivithayapakorn**, S., and A. Keller (2003), Transport of colloids in unsaturated porous media: A pore-scale observation of processes during the dissolution of air-water interface, Water Resour. Res., 39(12), 1346, doi: 10.1029/2003WR002487.

(25) **Torkzaban**, S., S.M. Hassanizadeh, J.F. Schijven, A.M. de Bruin, and A.M. de Roda Husman (2006a), Virus transport in saturated and unsaturated sand columns. Vadose Zone J. 5: 877-885.

(26) **Torkzaban**, S., S.M. Hassanizadeh, J.F. Schijven, and H.H.J.L. van den Berg (2006b), Role of air-water interfaces on retention of viruses under unsaturated conditions. Water Resour. Res., 42, W12S14, doi: 10.1029/2006WR004904.

(27) **Van Genuchten**, M. (1980), A closed-form equation for predicting the hydraulic conductivity of unsaturated soils, Soil Sci. Soc. Am.J., 44.

(28) **Veerapaneni**, S., J. Wan, and T. K. Tokunaga (2000), Motion of particles in film

flow, Environ. Sci. Technol., 34, 2465-2471.

(29) **Wan**, J., and J. L. Wilson (1994a), Visualization of the role of the gas-water interface on the fate and transport of colloids in porous media, Water Resour. Res., 30, 11– 23, doi: 10.1029/93WR02403.

(30) **Wan**, J., and J. L. Wilson (1994b), Colloid transport in unsaturated porous media, Water Resour. Res., 30, 857– 864, doi: 10.1029/93WR03017.

(31) **Wan**, J. M., and T. K. Tokunaga (1997), Film straining of colloids in unsaturated porous media: Conceptual model and experimental testing, Environ. Sci. Technol., 31, 2413– 2420.

(32) **Wan**, J., and T. K. Tokunaga (2002), Partitioning of clay colloids at air water interfaces, J. Colloid Interface Sci., 247, 54 –61, doi: 10.1006/jcis.2001.8132.

(33) **Zevi**, Y., A. Dathe, J. F. McCarthy, B. K. Richards, and T. S. Steenhuis (2005), Distribution of colloid particles onto interfaces in partially saturated sand, Environ. Sci. Technol., 39(18), 7055 – 7064, doi: 10.1021/es048595b.

(34) **Zevi**, Y., A. Dathe, B. Gao, B. K. Richards, and T. S. Steenhuis (2006), Quantifying colloid retention in partially saturated porous media, Water Resour. Res., 42, W12S03, doi: 10.1029/2006WR004929.

(35) **Zevi**, Y., A. Dathe, B. Gao, W. Zhang, B.K. Richards, and T.S. Steenhuis (2009), Transport and retention of colloidal particles in partially saturated porous media: Effect of ionic strength, Water Resour. Res., 45, doi: 10.1029/2008WR007322.

(36) **Zevi**, Y., J. Yan, Elena Rodriguez, Masa Provanovic and Steven Bryant (2010), Micromodel Investigation of Model Pathogen Transport during Two-Phase Flow, 2010 Land Grant and Sea Grant National Water Conference.

(37) **Zhuang**, J., J.F. McCarthy, J.S. Tyner, E. Perfect, and M. Flury (2007), In situ colloid mobilization in Hanford sediments under unsaturated transient flow conditions: Effect of irrigation pattern. Environ. Sci. Technol., 41: 3199- 3204, doi: 10.1021/es062757h.

(38) **Zhuang**, J., J.S. Tyner, E. Perfect (2009), Colloid transport and remobilization in porous media during infiltration and drainage. J. Hydrol. 377:112-119.

(39) **Zhuang**, J., N. Goeppert, C. Tu, J. McCarthy, E. Perfect, and L. McKay (2010), Colloid transport with wetting fronts: Interactive effects of solution surface tension and ionic strength, Water Research, 44, 1 2 7 0-1 2 7 8. doi:10.1016/j.watres.2009.12.012.

(40) **Zhang**, Q.L., S.M. Hassanizadeh, A. Raoof, M.Th. van Genuchten, and S.M. Roels (2012), Modeling virus transport and remobilization during partially saturated flow. Vadose Zone J. 11. doi:10.2136/vzj2011.0090

(41) **Zhang**, Q.L., N.K. Karadimitriou, S.M. Hassanizadeh, P. J. Kleingeld, and A. Imhof (2013), Study of Colloids Transport during Two-Phase Flow using a Novel Polydimethylsiloxane Micro-model. J. Colloid Interface Sci. 141-147. doi:10.1016/j.jcis.2013.02.041.

Appendix materials:

Movie 6.1: Colloid remobilization during imbibition of the micro-model-1

Movie 6.2: Colloid remobilization during imbibition of the micro-model-2

Movie 6.3: Colloid transport during drainage of the micro-model-1

Movie 6.4: Colloid transport during drainage of the micro-model-2

Chapter 7

Effect of Hydrophobicity on Colloid Transport during Two-phase Flow in a Hydrophobic Porous Medium

Abstract

The goal of this research was to investigate the difference in behavior of hydrophilic and hydrophobic colloids during transport in two-phase flow and their attachment and remobilization characters. The effect of hydrophobicity on colloid transport, retention, and remobilization during two-phase flow was studied in a hydrophobic Polydimethylsiloxane (PDMS) micro-model. Water and fluorinert-FC43 were used as the two immiscible liquids. Given the fact that the micro-model was hydrophobic, fluorinert was the wetting phase and water was the non-wetting phase. As model colloids, we used hydrophilic polystyrene carboxylate-modified microspheres (dispersible in water) and hydrophobic fluorous-modified silica microspheres (dispersible in fluorinert) in separate experiments. Using a confocal laser scanning microscope, we directly observed colloid movement and fluid distribution within pores of the micro-model. We also obtained concentration breakthrough curves by measuring the fluorescent intensities in the outlet of the micro-model.

The breakthrough curves during steady-state flow showed that the colloids attachment rate is inversely related to the background saturation of the fluid in which the colloid

Zhang Q.L., S.M. Hassanizadeh, B. Liu, N.K. Karadimitriou, and J.F. Schijven "Effect of hydrophobicity and capillarity on colloid transport during two-phase flow", modified and submitted to Water Resources Research.

were dispersed. Our visualization results showed that the enhanced attachment of hydrophilic colloids at lower water saturations was due to the retention at the fluorinert-water interface and fluorinert-water-solid contact lines. This effect was observed to be much less in the case of hydrophobic colloids (dispersed in fluorinert). In order to explain the colloids behavior, we calculated interaction potential energies of colloids with PDMS surfaces, fluid-fluid interfaces and fluid-fluid-solid contact lines. Also, capillary forces were included in considering forces that control colloid transport. Our calculations showed that there is a stronger repulsive energy barrier between hydrophobic colloids and fluorinert-water interface and solid-fluid interface, compared with the hydrophilic colloids. Moreover, hydrophobic colloids were seen to aggregate due to the strong attractive forces among them. These aggregates had even less tendency to attach to various interfaces, due to an increase in the corresponding energy barrier. For the colloid retention at fluid-fluid-solid contact lines, we found that the role of DLVO interactions was less important than capillary forces.

During transient events, we found that attached colloids become remobilized. The colloids deposited on the solid-fluid interface were detached by the moving fluid-fluid-solid contact lines. But, this happened only when the liquid containing colloids was displaced by the other liquid. Very good agreements were obtained among measured breakthrough curves, visualization results, and numerical modeling.

7.1 Introduction

The behavior of colloids in groundwater and the vadose zone has been an active research area in recent decades (McCarthy and Zachara, 1989; Saiers and Ryan, 2006). Also, the issue of colloid remobilization has attracted much interest in both saturated and unsaturated porous media. Many studies have involved viruses and bacteria, but results usually pertain to colloids in general.

There have been many studies on the factors that affect colloid transport, retention, and remobilization. One set of factors related to hydraulic conditions, such as flow rate (see e.g. Shang et al., 2008), water content (*cf.* Gao et al., 2006), and temporal variations in flow (Saiers and Lenhart, 2003a; Cheng and Saiers, 2009). Also, solution chemistry, such as pH (see e.g. Sadeghi et al., 2011) and ionic strength (*cf.* Saiers and Lenhart, 2003b; Zevi et al., 2009; Sadeghi et al., 2011; Bradford et al., 2012; Sang et al., 2013), and fluid properties like surface tension (Zhuang et al., 2010) are important. There has been much work on the role of porous medium properties such as solid wettablity (Crist

et al., 2005; Torkzaban et al., 2008; Geobel et al. 2013) as well as characteristics of colloids like size, shape, and concentration (Zhuang et al., 2005; Bradford et al., 2011; Aramrak et al., 2013).

Interaction potential energies have been used to explain colloid attachment to the solid-liquid interfaces, fluid-fluid interfaces, and colloid-colloid interactions (Schäfer et al., 1998a; Sirivithayapakorn and Keller, 2003; Crist et al., 2005; Auset and Keller, 2006; Sharma et al., 2008; Zevi et al., 2009; Geobel et al., 2013). The extended Derjaguin-Landau-Verwey-Overbeek (DLVO) theory, which describes the interaction energy as a sum of electrostatic, hydrophobic forces, and van der Waals interactions, is normally used to calculate the interactions among colloids and their interactions with interfaces.

As reported in the literatures, fluid-fluid-solid contact lines could be sites of significant colloid retention (Crist et al., 2004, 2005; Zevi et al., 2005, 2006, 2009). This cannot be explained by the extended DLVO theory only. We need to account for capillary forces to explain colloid attachment at contact lines (Gao et al., 2008; Shang et al., 2008, 2009). Sharma et al. (2008), Shang et al. (2009), and Aramrak et al. (2011) considered DLVO force, hydrodynamic force, as well as capillary force to explain the remobilization of colloids by the moving air-water interfaces and/or contact lines.

Recently, Zhang et al. (2013) conducted experiments on transport of hydrophilic particles (dispersed in water) during two-phase flow in order to investigate how saturation change affects colloids retention and remobilization. The experiments were performed in a micro-model made of Polydimethylsiloxane (PDMS) filled by water and fluorinert. Given the fact that PDMS is hydrophobic, water was the non-wetting phase and fluorinert was the wetting phase. That study raised the question whether hydrophobic colloids (dispersed in fluorinert) would behave differently.

Thus, in this work, we performed two different series of experiments with hydrophilic colloids dispersed in water (which is the non-wetting phase) and with hydrophobic colloids dispersed in fluorinert (which is the wetting phase). Based on concentration breakthrough curves and visualization results, we discuss the attachment behaviors and the remobilization of colloids by the moving fluid-fluid interfaces. Theoretical calculation of the interaction potential energy is used to explain the interactions among colloids and between colloids and fluid-fluid interfaces and solid-fluid interfaces. Our results show very significant differences in the behaviors of hydrophobic and hydrophilic colloids.

7.2 Description of Experiments

We performed colloid transport experiments during steady-state flow of the liquid carrying colloids followed by transient two-phase flow conditions. Experiments were done with either hydrophobic or hydrophilic colloids. Pore-scale visualization of colloids attachment and remobilization and measurement of concentration breakthrough curves was performed.

Porous medium: The porous medium was a two-dimensional micro-model made of Polydimethylsiloxane (PDMS). The flow network covered an area of 1mm×10mm. It contained around 90 pore bodies and 200 pore throats, with mean pore size of 30 microns, and porosity of 40%. The micro-model ended in an outlet channel, leading to an outlet reservoir. Details of micro-model fabrication and construction were described by Karadimitriou [2013]. To make the micro-model uniformly and stably hydrophobic, the micro-model was treated by silanization [see Karadimitriou., 2013].

Fluids and colloids: As the two immiscible liquids, we selected de-ionized (DI) water and 3M fluorinert^{TM} FC-43. Given the fact that our PDMS micro-model was hydrophobic, water was the non-wetting phase and fluorinert was the wetting phase. During two-phase flow experiments, three interfaces were formed: water-fluorinert, denoted by FWI, water-solid, denoted by SWI, and fluorinert-solid, denoted by SFI. Also, contact line between three phases was formed, designated by FWSC.

Two types of synthetic microspheres were used as the model colloids. Hydrophilic colloids, which could be suspended in water, were carboxylate-modified polystyrene microspheres (Polysciences Inc. GmbH). The colloids have green color both optically and under laser microscope. The hydrophobic colloids, which could be suspended in fluorinert, were fluorous-modified silica microspheres (optically in orange and show green under laser microscope). Both types of colloids had a mean diameter of 300nm. The hydrophobic colloids were custom made in Debye Institute of Utrecht University, following a procedure briefly described below.

(1) First, a dye solution was prepared by dissolving 10 mg of fluorescein isothiocyanade (FITC) in 2mL of ethanol, and then adding 20 μL of (3-Aminopropyl) trimethoxysilane. The mixture was stirred overnight in the dark. Then, 50mL of ethanol, 4.2mL of ammonia, and 1.3mL of water were added to the above mentioned mixture in a 100-mL flask.

(2) After 15 min of stirring, 2.6mL of tetraethoxysilane (TEOS) and the above prepared dye solution were mixed. The mixture was left at room temperature to react for

12h. Afterwards, TEOS was added at time intervals of 6 h, each time 2 mL to the mixture.

(3) Silica particles were separated by centrifugation at 6000 rpm for 10 min and washed repeatedly with ethanol and water in turn until the supernatant was clearly transparent. Using SEM, the particles size was established to be 300 nm of dynamic diameter.

(4) A given amount of the above-treated silica particles was dried with nitrogen gas flow and then we immersed them in saturated perfluorotetradecanoic acid. Finally, we sonicated the mixture for 10 minutes, and the mixture was diluted with fluorinert and sonicated to obtain well distributed fluorous-modified silica colloids suspension.

Visualization system: The visualization system employed was an inverted confocal laser scan microscope with oil immersion objective lens of 40× magnification and a numerical aperture of 1.25 (Leica TCS SP2, Heidelberg GmbH). We used the 488nm argon laser source of the microscope for excitation of the fluorescent hydrophilic and hydrophobic particles.

Visualization and breakthrough experiments

The same experimental set-up described by Zhang et al. (2013) was employed. The PDMS micro-model was put horizontally on the stage of the confocal microscope. A dual-direction syringe pump (Harvard Apparatus GmbH) was used to inject one of the liquids at a pre-specified constant rate. Both saturated and unsaturated colloid transport experiments for each colloid were conducted. The schematic of the experimental set-up can be found in Zhang et al. (2013).

Each experiment consisted of three stages. During stage 1, we established a steady-state flow of the liquid that would carry the colloids of interest (the other phase was stagnant). Stage 2 involved colloids transport under steady-state flow conditions. We first introduced a slug of colloids, without changing the flow conditions. This led to the emplacement of colloids, followed by injecting colloids-free liquid, still with the same flow rates. At the end of this stage, a large fraction of colloids were still attached to solid-liquid and/or fluid-fluid interfaces. An overview of various experiments and fraction of recovered colloids is shown in Table 7.1.

In experiments with hydrophilic particles, the steady-state flow of water was established (for stages 1 and 2) at two different water saturations: 100% and 60%. We refer to these experiments as **W100-lic** and **W60-lic**, respectively. In experiments with hydrophobic particles, the steady-state flow of fluorinert was established (for stages 1 and 2) at two different fluorinert saturations: 100% and 70%. These are designated as

experiments **F100-bic** and **F70-bic**, respectively.

Stage 3 involved transient two-phase flow and remobilization of attached colloids. For W100-lic, fluorinert was introduced to displace water (causing imbibition). For F100-bic, water was injected to displace fluorinert (causing drainage). For the experiments under unsaturated flow conditions, both drainage and imbibition were conducted. So, for **W60-lic**, in one experiment, we injected fluorinert (causing imbibition) to displace the water phase and reduce its saturation; in another experiment, we increased the flow rate of water to increase its saturation (causing drainage). For **F70-bic**, in one case, we injected water (causing drainage), and in another case, we increased the flow rate of fluorinert to cause imbibition. An overview of various experiments and fractions of recovered colloids are given in Table 7.1.

During the experiments, colloid distributions and their interactions with solid-fluid interfaces, FWIs, and FWSCs within the flow network were directly observed by confocal microscopy. Simultaneously, the distribution of fluids and position of interfaces and contact lines was observed and recorded by optical microscopy. The fluids distribution was visualized by a set-up developed by Karadimitriou et al. [2012] and their saturation as well as capillary pressure was calculated by image analysis software IDL. Saturation of water was calculated as the ratio of the pixels which corresponded to the non-wetting phase (water dyed with ink), over the total number of pixels of the flow network. Average capillary pressure of the collection of interfaces within the flow network was calculated as the summation of product of all local capillary pressures times local interfacial areas, dived by the total interfacial area. In this way, we obtained the saturation-capillary pressure curve.

In addition to still images, real-time images were also taken for subsequent review and analysis of colloids interactions with the moving interfaces and FWSCs. The experiments were found to be repeatable. Under the same conditions as visualization experiments done, series of concentration breakthrough curves were measured at the outlet channel with the same visualization system. This was done by measuring the fluorescent intensities of particles at a focus surface (in the horizontal middle plane) of the micro-model outlet channel at a speed of 834ms per frame. Colloids above and below this focus surface were out of confocal focus, but we assumed the colloids distribution was uniform over the depth. First, a calibration curve was prepared by injecting a known concentration of water-colloid or fluorinert-colloid suspension into the outlet channel of the micro-model via the outlet reservoir. By measuring the fluorescent intensity of various known concentrations, the calibration curve was obtained. The

confocal images were all taken at low intensities (<100 μW) to avoid bleaching of the fluorescent dye.

7.3 Calculation of Interaction Potential Energies

The interaction energies among colloids (hydrophilic or hydrophobic) and between colloids and FWIs or fluid-solid interfaces were estimated by DLVO theory. The total potential energy was calculated as the sum of electrostatic energy ΔG_{el}, van der Waals interaction energy ΔG_{vdw} (Derjaguin and Landau, 1941; Verwey and Overbeek, 1948):

$$\Delta G_{tot}{}^{I}(h) = \Delta G_{el}{}^{I}(h) + \Delta G_{vdw}{}^{I}(h) \tag{7.1}$$

where h is the separation distance between the colloids and the surface or interface of interest, denoted by I. The calculations of various energies for different surfaces are explained below.

The van der Waals interaction energy between a colloid dispersed in a liquid and the solid surface or an interface can be calculated as (Gregory, 1981):

$$\Delta G_{vdw}{}^{I} = -\frac{A_{123}{}^{I} R}{6h}\left[1 - \frac{5.32h}{\lambda_0}\ln(1 + \frac{\lambda_0}{5.32h})\right] \tag{7.2}$$

where R is radius of the colloid; λ_0 is a characteristic length, set equal to 100nm (Gregory, 1981) ; $A_{123}{}^{I}$ is the effective Hamaker constant of the combination of colloid and surface of interest. It is expressed as (Israelachvili, 1992):

$$A_{123} = (\sqrt{A_{11}} - \sqrt{A_{33}})(\sqrt{A_{22}} - \sqrt{A_{33}}) \tag{7.3}$$

where A_{11} is the Hamaker constant of the colloid, A_{22} is the Hamaker constant for the solid surface, and A_{33} is the Hamaker constant for water. The values of the Hamaker constant for polystyrene microspheres, silica microspheres, PDMS, and water are reported to be 6.6 × 10^{-20}, 1.9 × 10^{-20}, 6.4 × 10^{-20}, and 3.7 × 10^{-20} J, respectively (Israelachvili, 1992). The value of Hamaker constant for the fluorinert solution that we used (Fluorinert™-FC43) was not found. So, we used the value reported for Fluorinert ™ FC-75, namely, a value between -0.4× 10^{-20} J and -4× 10^{-20} J (Lee et al., 2002), the Hamaker constant of PDMS-silica-fluorinert was calculated according to Lee et al.

The electrostatic energies involved in the interaction of two colloids with each other, the electrostatic energies were expressed as (Hogg et al., 1966):

$$\Delta G_{el}^{\ c} = \frac{2\pi\varepsilon\varepsilon_0 R R_c}{2R + R_c}\{2\phi_{0c}^2 \ln[\frac{1+\exp(-\kappa h)}{1-\exp(-\kappa h)}] + (2\phi_{0c}^2)\ln[1-\exp(-2\kappa h)]\} \tag{7.4}$$

where ε is the dielectric constant of the medium, ε_0 is the permittivity in vacuum, R_c is the radius of the second colloid; κ is the inverse Debye-Hückel length, and ϕ_{0c} is the surface potential for the colloid.

The electrostatic interaction of colloids with the solid surface or with the fluid-fluid interface was approximated by (Norde and Lyklema, 1989):

$$\Delta G_{el}^{\ I} = \pi\varepsilon\varepsilon_0 R(\phi_{0c}^2 + \phi_{0I}^2)\{\frac{2\phi_{0c}\phi_{0I}}{\phi_{0c}^2 + \phi_{0I}^2}\ln[\frac{1+\exp(-\kappa h)}{1-\exp(-\kappa h)}] + \ln[1-\exp(-2\kappa h)]\} \tag{7.5}$$

ϕ_{0I} is the surface potential for the colloid and the interfaces of interest. it is related to the zeta potential by

$$\phi_{0I} = \zeta(1+\frac{z}{R})\exp(-\kappa z) \tag{7.6}$$

where z is the distance between the charged particle and the slipping plane; it was taken to be 0.5nm [Geobel et al., 2013]. The ζ-potential of the colloids in the electrolyte solution used in the experiments was measured using a Zetasizer (Malvern Instruments, UK) and was found to be -36.6 and -44.9 mV for the hydrophilic colloids (dispersed in water) and hydrophobic colloids (dispersed in fluorinert), respectively. The ζ-potential of the PDMS surface was taken to be -80 mV [Sze et al., 2003].

The total potential of colloid interaction with the fluids-solid contact line ($\Delta G_{tot}^{\ FWSC}$) was calculated as the algebraic sum of the total potential of colloid interaction with solid-fluid interface ($\Delta G_{tot}^{\ SFI}$) and fluid-fluid interface ($\Delta G_{tot}^{\ FWI}$):

$$\Delta G_{tot}^{\ FWSC} = \Delta G_{tot}^{\ SFI}(h) + \Delta G_{tot}^{\ FWI}(h') \tag{7.7}$$

where h is the separation distance between colloid and solid-fluid interface and h' is the separation distance between colloid and fluid-fluid interface. According to the schematic shown in Fig. 7.1, the relationship between h an h' can be expressed as:

$$h' = \frac{h+R}{\sin\alpha}\sin(\varphi-\alpha) - R \tag{7.8}$$

where φ is the contact angle between fluid-fluid interface and solid-fluid interface, α is an angle that relates to the position of the colloid at the contact line area. In our case, for colloids dispersed in wetting phase, α is between 0° and 4°, and for colloids dispersed in

non-wetting phase, α is between 4° and 176°.

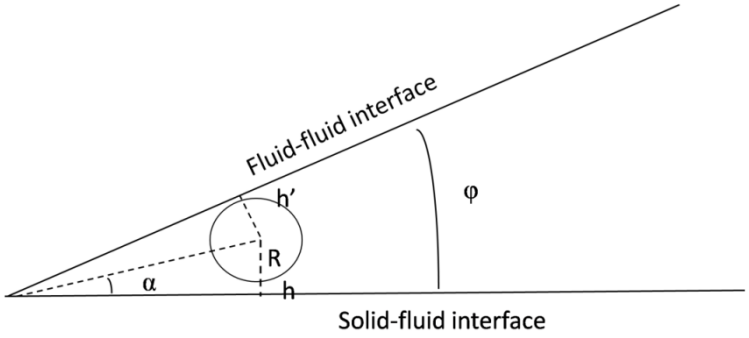

Fig. 7.1. *Schematic of an individual colloid interacts with the fluid-fluid-solid contact line.*

The values of total interaction energy, calculated from the above equations, were used to investigate colloids interaction with the interfaces. Plots of the total interaction energy as a function of separation distance, for hydrophilic and hydrophobic colloids, are given in Fig. 7.2A and Fig. 7.2B, respectively. As can be seen, a repulsive energy barrier exists for interaction of hydrophilic colloids with each other. However, there is no repulsive energy barrier among hydrophobic colloids. These results predict that hydrophilic colloids can be transported through the porous media easier than hydrophobic colloids. The latter may aggregate, due to the strong attractive potential energy at a relatively small separation distance, and therefore have difficulty in moving through small pores. The interaction of both hydrophilic colloids and hydrophobic colloids with the solid-fluid interface shows a repulsive energy barrier, which could hamper attachment of colloids to the solid surface. In particular, for hydrophobic colloids, there is a substantial repulsive energy at larger separation distance, which could prevent them from attaching to the solid surface. Also, there is repulsive energy barrier between fluid-fluid interfaces and hydrophobic colloids, which will hamper colloid attachment to the fluid-fluid interface too.

Aggregated hydrophobic particles behave as a relatively large "particle". From pore-scale images, we observed clusters of about 10 hydrophobic particles. So, in Fig. 2B, we have also plotted the potential energy between interfaces and colloids with effective size of 3μm. We find even stronger repulsive energy barrier between big size particles and the solid-fluid surface and fluid-fluid interfaces.

(A)

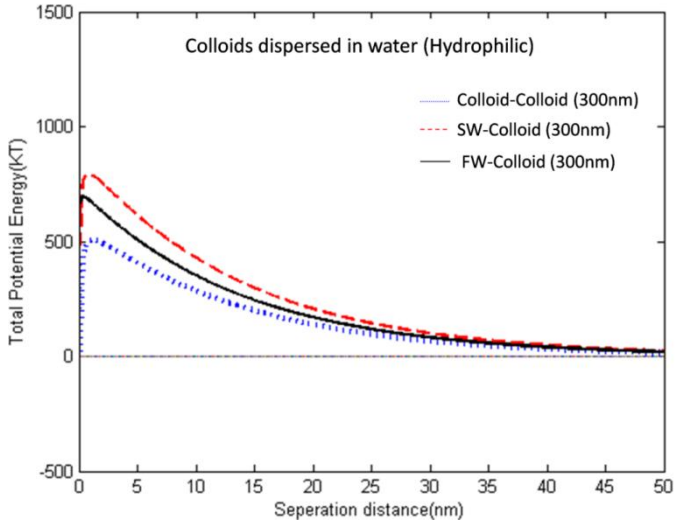

(B)

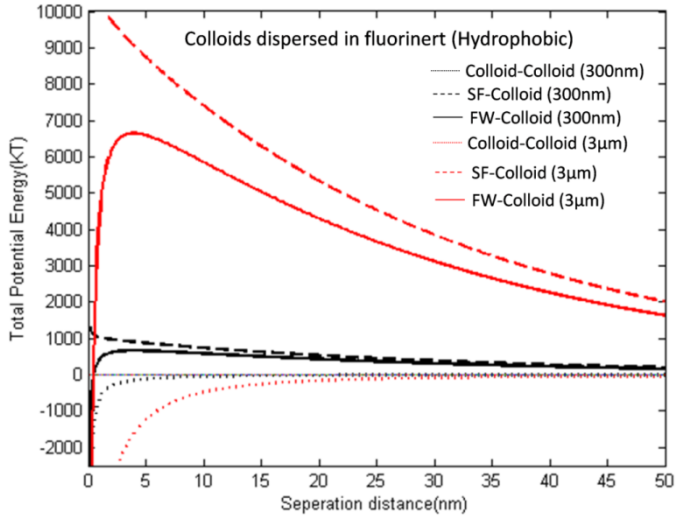

Fig. 7.2 *Total interaction potential energies for a colloid with the solid-fluid surface (SWI, SFI), fluorinert-water interface (FWI), and another colloid (colloid-colloid), as a function of separation distance.*

In Fig. 7.3(A) and (B), total interaction potential energies of hydrophilic colloids and hydrophobic colloids, respectively, with the fluid-fluid-solid contact line is plotted as a

function of separation distance and position angle α (see Fig. 7.1). The calculations suggest that there is a repulsive energy barrier under all conditions. The repulsive energy barrier between colloids and the contact line is 10 times bigger for hydrophobic colloids than for the hydrophilic ones.

(A)

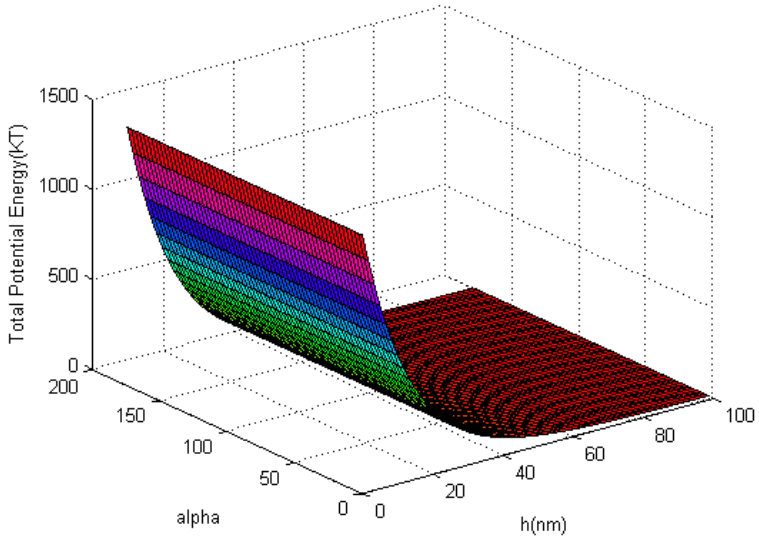

(B)

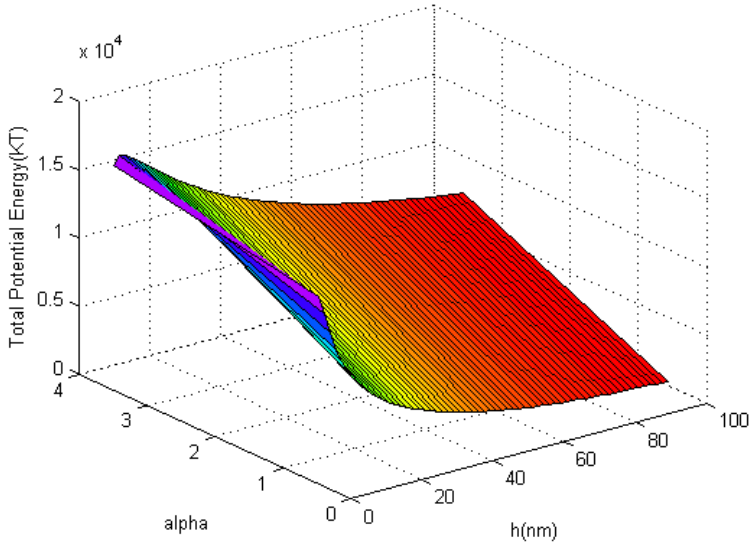

Fig. 7.3 *Total potential energies for interactions between fluid-fluid-solid contact lines and (A) Hydrophilic colloids; and (B) Hydrophobic colloids.*

7.4 Results and discussion

7.4.1 Breakthrough curves

Breakthrough curves of hydrophilic and hydrophobic colloids are shown in Fig. 7.4A and 4B, respectively. In each graph, the upper curve is from saturated experiments and the lower curve is from unsaturated experiments. From saturated curves, we can see that the average peak concentration of hydrophilic colloids was around C/C0=0.90, whereas for hydrophobic colloids was around 0.98. Also, as can be seen in Table 7.1 that, at the end of steady-state stage in saturated experiments, approximately 88% of hydrophilic colloids were recovered in the effluent, whereas the recovery of hydrophobic colloids was only about 95%. As all other conditions were the same, these results suggest that hydrophilic colloids attached more strongly to the PDMS surface than hydrophobic colloids. This was unexpected as PDMS is hydrophobic. But, we found justification for it from the potential energy calculations presented earlier. There we found that there is a stronger repulsive energy barrier between the solid surface and hydrophobic colloids than the hydrophilic colloids. Indeed, in pore-scale images we saw more hydrophilic particles attached to PDMS surface than hydrophobic particles (Fig. 7.5 and Fig. 7.8).

A similar trend was found in unsaturated experiments. That is, retention of hydrophilic colloids (dispersed in water) was larger than the hydrophobic colloids (dispersed in fluorinert). In general, comparing unsaturated experiments with saturated experiments, we found that both hydrophobic and hydrophilic colloids are removed much more under unsaturated conditions. This can be noticed from Table 1, where mass recoveries are inversely correlated to the background fluid saturations.

In transient experiments (see Table 7.1 for an overview), fast imbibition was performed in the case of hydrophilic colloids, and the water saturation was reduced from 100% to 20% (Exp. W100-lic) and from 60% to 15% (Exp. W60-lic). In the case of hydrophobic colloids, fluorinert was drained from 100% saturation to 45% (Exp. F100-bic) or from 70% to 42% (Exp. F70-bic).

(A)

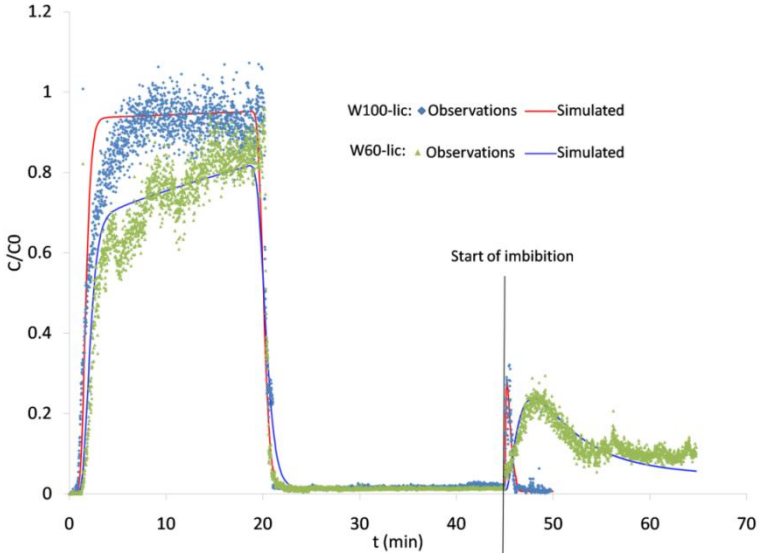

(B)

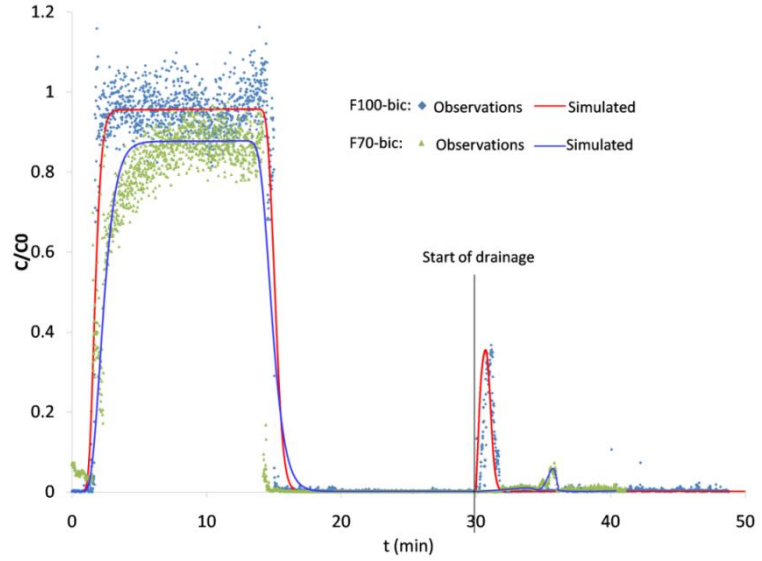

Fig. 7.4 *Measured (symbols) and simulated (lines) breakthrough curves for hydrophilic colloids (A) and hydrophobic colloids (B) at different steady-state saturations.*

Under transient conditions, remobilization of colloids occurred as indicated by a peak in the breakthrough curves. In the case of saturated experiments, much more water and

fluorinert (and thus colloids) were displaced during imbibition stage and drainage process, respectively, than in the unsaturated experiments. That is why the peak in W100-lic and F100-bic was the highest. For hydrophilic colloids, the ratios of remobilized colloids to the colloids remaining in the micro-model at the start of stage 3 were 8.3% and 21.3% during W100-lic and W60-lic, respectively (see Table 1). These ratios for hydrophobic colloids were 42.8% and 25.7% during F100-bic and F70-bic, respectively.

Table 7.1. *Colloid mass recovered in the micro-model effluent.*

Colloids property	Exp.	Saturation change (%)		Mass balance (%)		
		Steady-state saturation	Final transient saturation	Remaining at the end of stage 2 % of injected	Remobilized during stage 3 % of injected	Ratio of remobilized mass to the mass of colloids remaining in the micro-model at the end of stage 2
Hydrophilic colloids	W100-lic	100*	20 (±2)*	12 (±2)	1 (±0.1)	8.3%
	W60-lic	60 (±2)*	15 (±5)*	30 (±4)	6.4 (±0.4)	21.3%
Hydrophobic colloids	F100-bic	100+	45 (±5)+	5 (±2)	2.14 (±0.1)	42.8%
	F70-bic	70 (±2)+	42 (±2)+	18.8 (±4)	4.84 (±0.4)	25.7%

**These are fluorinert saturation values*

+These are water saturation values

7.4.2 Modeling of breakthrough curves

The mathematical model described by Zhang et al. (2013) was employed to simulate the breakthrough curves (during steady-state as well as transient flow) for both hydrophilic and hydrophobic colloids. The model is based on a coupled system of equations for two-phase flow, advection-dispersion of colloids, adsorption to and desorption from fluid-fluid interfaces and fluid-solid interfaces. The remobilization of colloids from fluid-solid interface was modeled as a kinetic process, with rate coefficient assumed to be a linear function of the rate of change of saturation. Also, the remobilization of colloids from the fluid-fluid interfaces was modeled. The rate was assumed to depend on the change of the specific fluid-fluid interfacial area. We assumed there is linear equilibrium partitioning occurring between colloids in the flowing phase and fluid-fluid interfaces. In principle, fluid-fluid interface colloid attachment/detachment should be modeled as a kinetic process. But in our preliminary simulations, we found that an equilibrium description provided satisfactory results. This was in line with our findings when we simulated the experimental results of Torkzaban et al. (2006a, b) [See Zhang et al., 2012].

Values of attachment/detachment rate coefficients for solid-fluid interfaces and equilibrium adsorption coefficient for fluid-fluid interfaces were estimated by fitting our model to measured breakthrough curves. Resulting curves are shown in Fig. 7.4A and 4B. The estimated parameter values are given in Table 7.2.

Table 7.2 *Simulated transport parameters.*

Parameters	Hydrophilic colloids		Hydrophobic colloids	
	W100-lic	W60-lic	F100-bic	F70-bic
Solid-fluid interface attachment coefficient, k_{att}^{s} (s^{-1})	1.07(±0.096) x 10^{-3}	1.63(±0.12)x10^{-3}	0.44(±0.05)x10^{-3}	0.89(±0.095)x10^{-3}
Solid-fluid interface detachment coefficient, k_{det}^{s} (s^{-1})	0.1117(±0.006)x10^{-3}	0.17(±0.005)x10^{-3}	0.1267(±)x10^{-3}	0.18267(±)x10^{-3}
K_D^i (m) Equlibirum adsorption coefficient to fluid-fluid interface	-	0.85 (±0.1)	-	0.08 (±0.03)

7.5 Discussion of Results

Still and video images provided valuable information on understanding the mechanisms of colloids transport. Two selected video images of hydrophilic colloids distribution during imbibition process (introducing fluorinert) and hydrophobic colloids distribution during drainage process (introducing water) are provided in the supplemental material, named Movie 7.1 and Movie 7.2, respectively. Based on the results of breakthrough

curves and the video and still images, the mechanisms transport, retention, and remobilization for both types of colloids are discussed below.

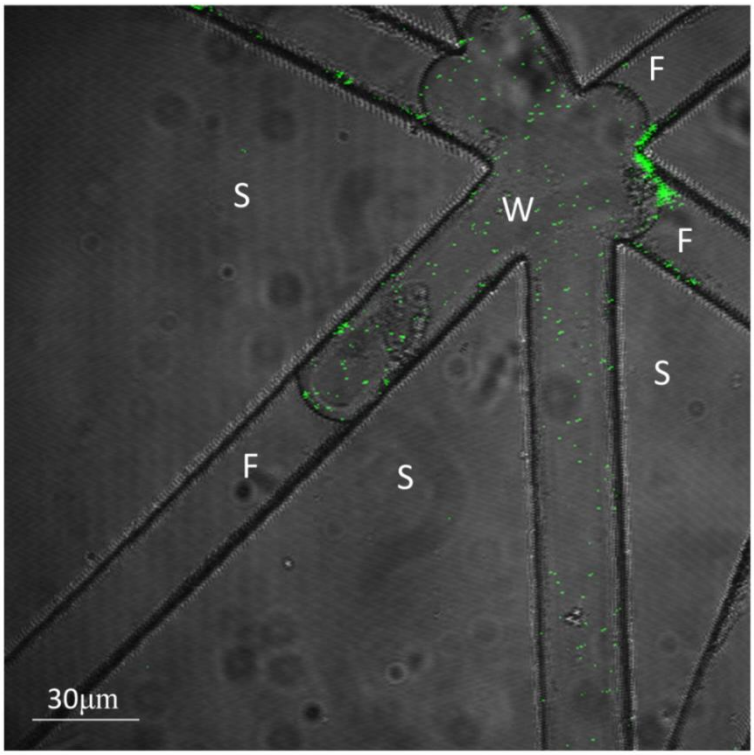

Fig. 7.5 *Image taken from a given area of a PDMS micro-model for Exp. W60-lic of hydrophilic colloids during imbibition (fluorinert displacing water). In the image, S stands for solid, F represents fluorinert, and W indicates water.*

7.5.1 Retention of hydrophilic colloids

Fig. 7.5 shows the distribution of hydrophilic colloids under unsaturated condition during the process of imbibition (water displaced by fluorinert). They were observed to be dispersed in water as well as attached to the SWIs, FWIs, and FWSCs. Based on the calculation of interaction potential energy (Fig. 7.2), there exists an energy barrier between the solid surface and the colloids. So, the attachment of colloids to the solid surface (SWI) should not occur. But, we did observe some attachment of colloids to the solid surface. This discrepancy is probably due to the fact that the calculation of interaction potential energy was made for a bare, unmodified, and smooth PDMS surface.

But, we know that PDMS surface has nano-scale roughness (in our case, around 50nm), that may result in small surface fractions being favorable for colloid attachment. Also, Shen et al. (2011) and Bradford et al. (2013) modified and calculated the interaction energies between colloids and a rough surface, indicating that the sharp asperities on the solid surface can facilitate colloid deposition by reducing energy barrier. Also, the presence of the nano-scale depressions on the solid surfaces can shield colloids from hydrodynamic shear. Therefore, the local roughness of the PDMS surface of the micro-model should also provide localized spots for the colloid attachment.

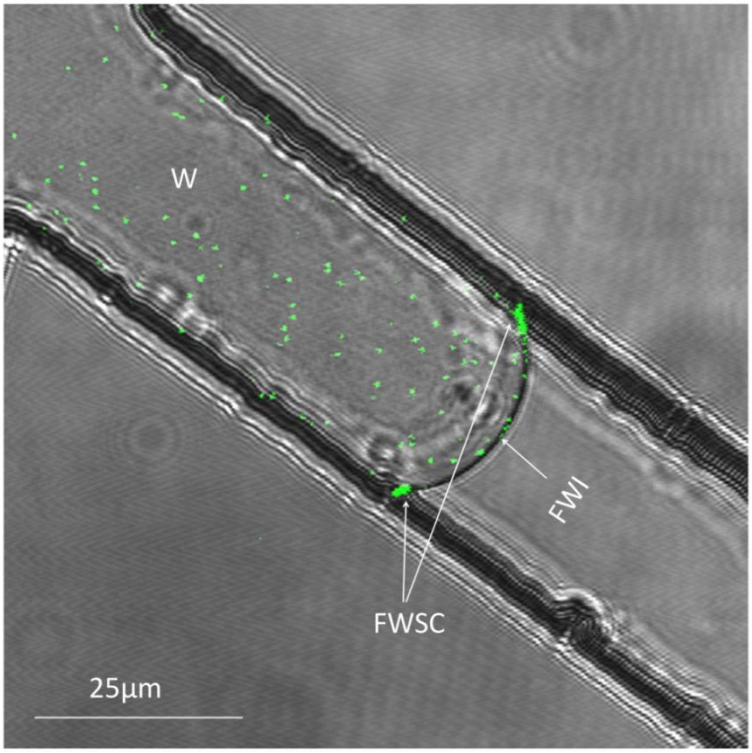

Fig. 7.6 *Accumulation of hydrophilic colloids at the FWSCs during steady-state flow. The interface is stationary. W stands for water, F represents fluorinert, FWSC indicates fluorinert-water-solid contact line, and FWI stands for fluorinert-water interface.*

The interaction potential energy calculations also show a repulsive energy barrier between hydrophilic colloids and the FWSCs (as shown in Fig. 7.3A). But as can be seen from Fig. 7.6, we did observe hydrophilic colloids attached to the FWSCs. This is because under unsaturated conditions, apart from DLVO force and hydrodynamic force,

the capillary force needs to be taken into account too. According to Gao et al. (2008) and Shang et al. (2008) capillary forces are at least two orders of magnitude greater than DLVO force. The capillary force exerting on colloids plays the dominant role and act to pin the colloids to the FWSCs as shown in Fig. 7.7.

Van der Waals and electrostatic forces can be calculated from the derivatives of corresponding interaction energies:

$$F_{el} = d(\Delta G_{el}^{FWSC})/dh \tag{7.8}$$

and

$$F_{vdw} = d(\Delta G_{vdw}^{FWSC})/dh \tag{7.9}$$

The capillary force F_{cap} is the resultant of surface tensions acting by FWI on the colloid and can be expressed as (Chateau et al., 2002):

$$F_{cap} = 2\pi R\gamma sin(\varphi)sin(\theta+\varphi) + \Delta p\pi R^2 sin^2\varphi \tag{7.10}$$

where γ is the fluid-fluid interfacial tension; θ is the contact angle between the surface of the particle and the liquid-liquid interface; ΔP is the capillary pressure defined as the pressure jump across the fluid-fluid interface.

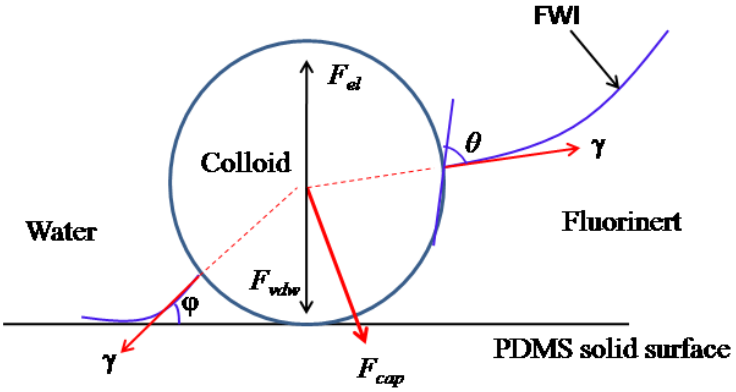

Fig. 7.7 *Schematic presentation of forces acting on a hydrophilic colloid captured at a stationary contact line.*

7.5.2 Retention of hydrophobic colloids

Fig. 7.8 shows the hydrophobic colloids distribution during the process of drainage (i.e. water displacing fluorinert). The hydrophobic colloids were found to remain dispersed in fluorinert and only a few were attached to the FWIs. Aggregation of hydrophobic

colloids was also observed.

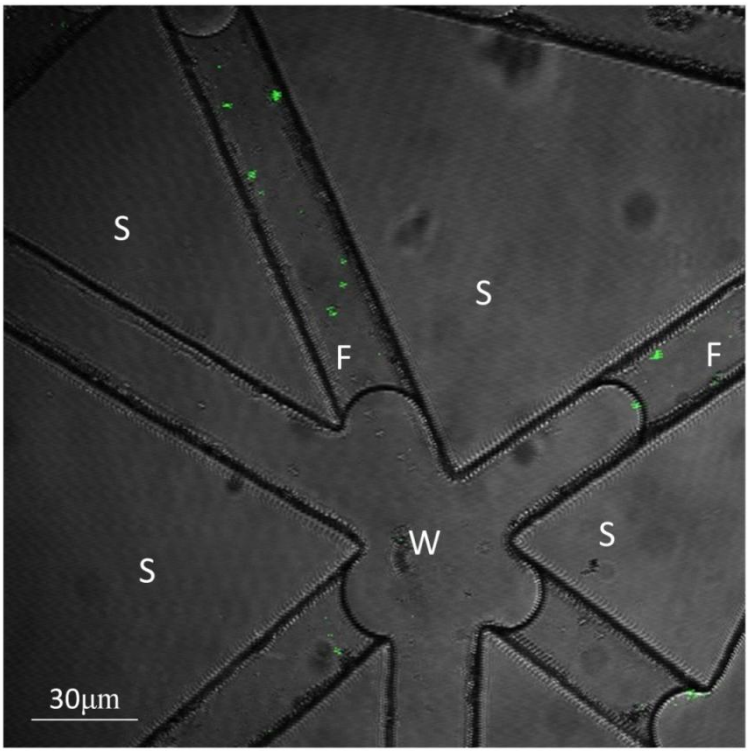

Fig. 7.8 *Exp. F70-bic for hydrophobic colloids during drainage (water displacing fluorinert).*

Our observations showed that the overall retention of the hydrophobic colloids was much less compared with the retention of hydrophilic colloids. Also, the estimated values for rate coefficients of attachment of hydrophobic colloids to the solid phase were much smaller than those for hydrophilic colloids (see Table 7.2). Similarly, the value of portion coefficient for equilibrium attachment to the FWI was one order of magnitude smaller than for hydrophilic colloids. These results were in agreement with the calculated interaction potential energies (see Fig. 7.2), where there is a larger repulsive energy barrier between hydrophobic colloids and solid-fluid interface and FWIs (Fig. 7.2). With regard to the colloids in the vicinity of contact line area, apart from the strong repulsive energy barrier (Fig. 7.3B), the capillary force also opposes the attachment of colloids to the FWSC (this is the resultant force in Fig. 7.9).

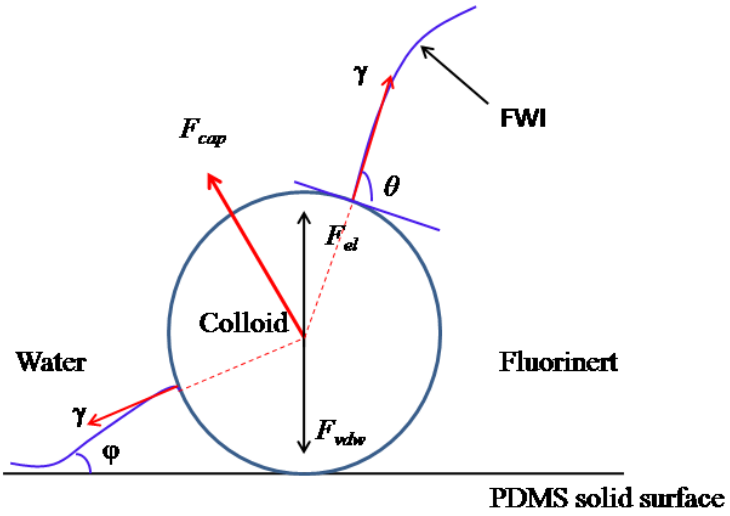

Fig. 7.9 *Schematic presentation of forces acting on a hydrophobic colloid captured at a stationary contact line.*

Due to the strong attractive interactions of hydrophobic colloids (as indicated in Fig. 7.2), colloids aggregation occurred. This can be seen in Fig. 7.8 and Movie 7.2, where colloid clusters of different sizes are visible. As the injected solution contained colloids of nearly uniform size, aggregation of colloids must have occurred during the transport. One would expect that colloidal aggregated to be strained as they move through the pore network. This was indeed observed by Wan et al. (1994), Schäfer et al. (1998b), and Crist et al. (2005), who reported stronger retention of hydrophobic colloids than hydrophilic colloids. They attributed it to the aggregation of colloids, due to the strong attractive force among them. Thus, colloidal aggregates could be strained at the relatively narrow pore spaces where the grains are touching. However, we did not observe any straining of colloidal aggregates in our experiments. The reason is that, as can be seen in Fig. 5, the pores of our micro-model had parallel walls and there were no pore constrictions. Even the smallest pore sizes were much larger than colloidal aggregates. Therefore, straining of colloids did not occur in our experiments. Another difference with the works of Wan et al. (1994) and Crist et al. (2005) is that, in their studies, water was the wetting phase and hydrophobic colloids were dispersed in water. Therefore, the colloids had very low affinity for staying in water. However, in our experiments, the hydrophobic colloids were dispersed in the fluorinert and had a very high affinity for staying in that fluid and they would be carried out of the micro-model

with the flowing fluorinert.
Another important mechanism for colloids attachment is reported to be film straining (Wan and Tokunaga, 1997; Veerapaneni et al., 2000). In our experiments, given the fact that PDMS micro-model was fluorinert-wet; only a fluorinert film could exist (in a pore filled by water). Thus, the film straining can only occur for the hydrophobic colloids dispersed in fluorinert. But, the resolution of confocal microscope was not sufficient for showing the presence of a fluorinert film. So, we could not confirm whether film straining was absent or present.

7.5.3 Remobilization of colloids

The remobilization of colloids during stage 3 of experiments was characterized by the appearance of a peak in the tailing part of the breakthrough curves (see e.g. Fig. 7.4). For both types of colloids, a concentration spike was observed in the initially fully-saturated experiments W100-lic and F100-bic. However, a slower rise in concentration and a lower peak was observed in initially unsaturated experiments W60-lic and F70-bic, but remobilization lasted longer. Our calculations showed that, in the case of 100% saturation, the remobilization time was almost equal to one pore volume; the moving front moved with the flow speed. But, under unsaturated conditions, as there were already fluid-fluid interfaces existing, when the saturation was changed, the fluid-fluid interfaces were destroyed and new interfaces were created, which resulted in more dynamic of colloids transport. Therefore, more transport time was needed. But the total mass of remobilized colloids during W60-lic and F70-bic was more than during W100-lic and F100-bic for both hydrophilic and hydrophobic colloids.
Movies 7.1 and 7.2 in the supplementary material show the video images captured by confocal microscopy for hydrophilic colloids and hydrophobic colloids, respectively, during the passage of fluorinert-water interface. In movie 7.1, with the passage of the moving imbibition front (fluorinert displacing water containing colloids), we observed that the hydrophilic colloids deposited on the solid surface were all detached by the fluid-fluid interfaces and FWS contact lines. In movie 7.2, with water displacing fluorinert containing colloids, no clear detachment of colloids was observed with the drainage front. Colloids attached to the fluid-fluid interface can be transported with it. Some colloids attached to the PDMS surface were released by the moving fluorinert-water interfaces. But, after the passage of the interface, the majority of hydrophobic colloids remained attaching to the solid surface.

Acknowledgements

Financial support was provided by the China Scholarship Council (CSC) to the first author. Qiulan Zhang, S.M. Hassanizadeh, and N.K. Karadimitriou, are members of the International Research Training Group NUPUS, financed by the German Research Foundation (DFG) and Netherlands Organization for Scientific Research (NWO).

References

(1) **Aramrak**, S., M. Flury, and J.B. Harsh (2011), Detachment of deposited colloids by advancing and receding air-water interfaces, Langmuir, 27, 9985-9993.

(2) **Aramrak**, S., M. Flury, J.B. Harsh, R.L. Zollars, and H.P. Davis (2013), How does colloid shape affect detachment of colloids by a moving air-water interface? Langmuir, 29, 5770-5780.

(3) **Auset,** M., and A. A. Keller (2006), Pore-scale visualization of colloid straining and filtration in saturated porous media using micro-models, Water Resour. Res., 42, W12S02, doi: 10.1029/2005WR004639.

(4) **Bradford**, S. A., S. Torkzaban, and J. Simunek (2011), Modeling colloid transport and retention in saturated porous media under unfavourable attachment conditions, Water Resour. Res., 47, W10503, doi: 10.1029/ 2011WR010812.

(5) **Bradford**, S.A., S. Torkzaban, H. Kim, and J. Simunek (2012), Modeling colloid and microorganism transport and release with transients in solution ionic strength, Water Resour. Res., 48, doi: 10.1029/2012WR012468.

(6) **Bradford,** S.A. and S. Torkzaban (2013), Colloid interaction energies for physically and chemically heterogeneous porous media, Langmuir, 29, 3668-3676.

(7) **Chateau,** X., P. Moucheront, and O. Pitois (2002), Micromechanics of unsaturated granular media, J. Eng. Mech., 128, 856–863.

(8) **Cheng** T., and J.E. Saiers (2009), Mobilization and transport of in situ colloids during drainage and imbibition of partially saturated porous media, Water Resour. Res. 45, W08414, doi: 10.1029/2008WR007494.

(9) **Crist**, J. T., J. F. McCarthy, Y. Zevi, P. C. Baveye, J. A. Throop, and T. S. Steenhuis (2004), Pore-scale visualization of colloid transport and retention in partly saturated porous media, Vadose Zone J., 3(2), 444– 450, doi:10.2113/3.2.444.

(10) **Crist**, J. T., Y. Zevi, J. F. McCarthy, J. A. Troop, and T. S. Steenhuis (2005),

Transport and retention mechanisms of colloids in partially saturated porous media, Vadose Zone J., 4, 184– 195.

(11) **Gao**, B., J.E. Saiers, and J. N. Ryan (2006), Pore-scale mechanisms of colloid deposition and mobilization during steady and transient flow through unsaturated granular media, Water Resour. Res. 42, W01410, doi: 10.1029/ 2005WR004233.

(12) **Gao,** B., T. S. Steenhuis, Y. Zevi, V. L. Morales, J. L. Nieber, B. K. Richards, J. F. McCarthy, and J.-Y. Parlange (2008), Capillary retention of colloids in unsaturated porous media, Water Resour. Res., 44, W04504, doi:10.1029/2006WR005332.

(13) **Geobel**, M., S. K. Woche, P.M. Abraham, G.E. Schaumann, and J. Bachmann (2013), Water repellency enhances the deposition of negatively charged hydrophilic colloids in a water-saturated sand matrix, Colloids and Surfaces A: Physicochem. Eng. Aspects, 431, 150-160.

(14) **Gregory**, J. (1975), Interaction of unequal double layers at constant charge, J. Colloid Interface Sci., 51, 44– 51.

(15) **Gregory**, J. (1981), Approximate expressions for retarded van der Waals interaction, J. Colloid Interface Sci., 83, 138–145.

(16) **Gómez Suárez,** C., J. Noordmans, H.C. van der Mei, H.J. Busscher (1999), Detachment of colloidal particles from collector surfaces with different electrostatic charge and hydrophobicity by attachment to air bubbles in a parallel plate flow chamber, Phys. Chem. Chem. Phys., 1, 4423-4427.

(17) **Hogg**, R., D.S. Cahn, T.W. Healy, and D.W. Fuerstenau (1966), Diffusional mixing in an ideal system, Chem. Eng. Sci. 21:1025–1038.

(18) **Israelachvili**, J.N. (1992), Intermolecular and surface forces, 2nd ed. Academic Press, London.

(19) **Karadimitriou,** N.K., V. Joekar-Niasar, S.M. Hassanizadeh, P.J. Kleingeld, and L.J. Pyrak-Nolte (2012), A new micro-model experimental approach for two-phase flow studies; comparison with a pore-network model, Lab on a Chip, Vol. 12, pp. 3413-3418, doi: 10.1039/C2LC40530J.

(20) **Karadimitriou**, N.K. (2013), Two-phase flow experimental studies in micro-models. Ph.D thesis, Department of Earth Sciences, Utrecht University, the Netherlands.

(21) **Lee** S., F. L. Sigmund (2002), AFM study of repulsive van der Waals forces between Teflon AF™ thin film and silica or alumina, Colloids and Surfaces A: Physicochem. Eng. Aspects, 204, 43-50.

(22) **McCarthy**, J.F., and J.M. Zachara (1989), Subsurface transport of

contaminants—Mobile colloids in the subsurface environment may alter the transport of contaminants, Environ. Sci. Technol. 23:496–502.

(23) **Norde**, W., and J. Lyklema (1989), Protein adsorption and bacterial adhesion to solid surfaces -A colloid chemical approach, Colloids Surf. 38:1–13.

(24) **Saiers**, J. E., and J.J. Lenhart (2003a), Colloid mobilization and transport within unsaturated porous media under transient-flow conditions, Water Resour. Res., 39(1): 10-19, doi: 10.1029/2002WR001370.

(25) **Saiers**, J.E., and J.J. Lenhart (2003b), Ionic-strength effects on colloid transport and interfacial reactions in partially saturated porous media, Water Resour. Res. 39(9):12-56. doi:10.1029/2002WR001887.

(26) **Saiers**, J.E., and J.N. Ryan (2006), Introduction to special section on Colloid Transport in Subsurface Environments, Water Resour. Res. 42(12), doi: 10.1029/2006WR005620

(27) **Sadeghi**, G., J.F. Schijven, T. Behrends, S.M. Hassanizadeh, J. Gerritse, and P.J. Kleingeld (2011), Systematic study of effects of pH and ionic strength on attachment of phage PRD1, Ground Water 49:12–19. doi:10.1111/j.1745-6584.2010.00767.x.

(28) **Sang,** W., V.L. Morales, W. Zhang, C. R. Stoof, B. Gao, A. L. Schatz, Y. Zhang, and T.S. Steenhuis (2013), Quantification of Colloid Retention and Release by Straining and Energy Minima in Variably Saturated Porous Media, Environ. Sci. Technol. doi: 10.1021/es400288c.

(29) **Schäfer,** A., H. Harms, and A.J.B. Zehnder (1998a), Bacterial accumulation at the air-water interface, Environ. Sci. Technol. 32(23): 3704–3712.

(30) **Schäfer,** A., P. Ustohal, H. Harms, F. Stauffer, T. Dracos, and A.J.B. Zehnder (1998b), Transport of bacteria in unsaturated porous media, J. Contam. Hydrol. 33:149–169.

(31) **Shang**, J., M. Flury, G. Chen, and J. Zhuang (2008), Impact of flow rate, water content, and capillary forces on in situ colloid mobilization during infiltration in unsaturated sediments, Water Resour. Res. 44, doi: 10.1029/2007WR006516.

(32) **Shang**, J., M. Flury, and Y. Deng (2009), Force measurements between particles and the air-water interface: Implications for particle mobilization in unsaturated porous media, Water Resour. Res., 45, W06420, doi: 10.1029/2008WR007384.

(33) **Sharma** P., M. Flury, and J. Zhou (2008), Detachment of colloids from a solid surface by a moving air-water interface, J. Colloid Interface Sci., 326, 143-150.

(34) **Shen**, C., B. Li, C. Wang, Y. Huang, and Y. Jin (2011), Surface roughness effect on deposition of nano- and micro-sized colloids in saturated columns at different

solution ionic strengths. Vadose Zone J.10, 1071-1081.

(35) **Sirivithayapakorn**, S., and A. Keller (2003), Transport of colloids in unsaturated porous media: A pore-scale observation of processes during the dissolution of the air-water interface, Water Resour. Res., 39(12), 1346, doi: 10.1029/2003WR002487.

(36) **Sze,** A., D. Erickson, L. Ren, and D. Li (2003), Zeta-potential measurement using the Smoluchowski equation and the slope of the current–time relationship in electroosmotic flow, J. Colloid Interface Sci., 261, 402-410.

(37) **Torkzaban**, S., S.A. Bradford, M.T. van Genuchten, and S. L. Walker (2008), Colloid transport in unsaturated porous media: The role of water content and ionic strength on particle straining, J. Contam. Hydrol. 96, 113–127,

(38) **Veerapaneni**, S., J. Wan, and T. K. Tokunaga (2000), Motion of particles in film flow, Environ. Sci. Technol., 34, 2465-2471.

(39) **Wan**, J., J. L. Wilson, and T. L. Kieft (1994), Influence of the gas-water interface on transport of microorganisms through unsaturated porous media, Appl. Environ. Microbio. 60(2), 509-516.

(40) **Wan**, J., and T.K. Tokunaga (1997). Film straining of colloids in unsaturated porous media: Conceptual model and experimental testing, Environ. Sci. Technol. 31:2413–2420.

(41) **Yoon**, R.-H., D.H. Flinn, and Y.I. Rabinovich (1997). Hydrophobic interactions between dissimilar surfaces, J. Colloid Interface Sci. 185:363–370.

(42) **Zevi**, Y., A. Dathe, J. F. McCarthy, B. K. Richards, and T. S. Steenhuis (2005), Distribution of colloid particles onto interfaces in partially saturated sand, Environ. Sci. Technol., 39(18), 7055 – 7064, doi: 10.1021/es048595b.

(43) **Zevi**, Y., A. Dathe, B. Gao, B. K. Richards, and T. S. Steenhuis (2006), Quantifying colloid retention in partially saturated porous media, Water Resour. Res., 42, W12S03, doi: 10.1029/2006WR004929.

(44) **Zevi**, Y., A. Dathe, B. Gao, W. Zhang, B.K. Richards, and T.S. Steenhuis (2009), Transport and retention of colloidal particles in partially saturated porous media: Effect of ionic strength, Water Resour. Res., 45, doi: 10.1029/2008WR007322.

(45) **Zhuang**, J., J. Qi, and Y. Jin (2005), Retention and transport of amphiphilic colloids under unsaturated flow conditions: effect of particle size and surface property, Environ. Sci. Technol.39: 7853-7859.

(46) **Zhuang**, J., N. Goeppert, C. Tu, J. McCarthy, E. Perfect, and L. McKay (2010), Colloid transport with wetting fronts: Interactive effects of solution surface tension and ionic strength, Water Research, 44, 1270-1278. doi:10.1016/j.watres.2009.12.012

(47) **Zhang,** Q.L., S.M. Hassanizadeh, A. Raoof, M.Th. van Genuchten, and S.M. Roels (2012), Modelling virus transport and remobilization during partially saturated flow. Vadose Zone J. 11. doi:10.2136/vzj2011.0090.
(48) **Zhang**, Q.L., N.K. Karadimitriou, S.M. Hassanizadeh, P. J. Kleingeld, and A. Imhof (2013), Study of Colloids Transport during Two-Phase Flow using a Novel Polydimethylsiloxane Micro-model, J. Colloids Inc. Science:10.1016/j.jcis.2013.02.041.

Appendix materials

Movie 7.1: Retention and remobilization of hydrophilic colloids (polystyrene colloids dispersed in water) with the moving fluid-fluid interface.
Movie 7.2: Retention and remobilization of hydrophobic colloids (silica colloids dispersed in fluorinert) with the moving fluid-fluid interface.

Chapter 8

Summary and Recommendations

8.1 Summary

In this study, we designed and fabricated a closed micro-fluidic device made of polydimethylsiloxane (PDMS), with uniform wettability and stable hydrophobic properties; so we employed a PDMS micro-model as the porous medium. The overall flow network dimensions were 1 mm by 10 mm, with 90 pore bodies and roughly 200 pore throats. The mean diameter of pore bodies was 30μm.

The PDMS micro-model that we designed and manufactured had some important properties that are usually lacking in other PDMS models.

- First, the micro-model was made uniformly and stably hydrophobic.
- Second, the model was sealed with a very thin glass plate (120 microns) with a thin PDMS coating. This made it possible for the confocal laser microscope to focus at planes located as deep as 30 microns in the micro-model (the microscope depth of field was around 170 microns).
- Third, the system of injection of fluids, with and without colloids, was constructed such as to avoid mixing of fluid phases at the entrance.
- Fourth, because of the PDMS coating of the glass cover, the inner surfaces of the pores were all PDMS. This made sure that the fluids would experience the same wetting properties everywhere; there was no mixed wettability.
- Fifth, we did experiments with two immiscible liquids (water and fluorinert) and used two different microspheres, one for each liquid.
- Sixth, there is an outlet channel where the effluent concentration breakthrough curves can be measured by confocal laser microscope.

As the visualization system, we employed confocal microscopy; the sample can be tracked spatially in three dimensions by superposing two-dimensional images taken at sequential depth stacks. Furthermore, it allows real-time information about the complex mechanisms under fast transient flow conditions.

We are interested in studies of the fate of adsorbing colloidal particles under transient two-phase flow conditions. So, it is not crucial which phase is the wetting phase and which one is the nonwetting. As the two immiscible fluids, we selected deionized water and Fluorinert FC-43(3M). Given the fact that our PDMS micro-model was hydrophobic, water was the non-wetting phase and fluorinert was the wetting phase. The fluorinert liquid type was chosen such that it had nearly the same index of refraction as water (1.291 and 1.332, respectively, at 20℃).

As model colloids, we used hydrophilic polystyrene carboxylate-modified microspheres (dispersible in water) and hydrophobic fluorous-modified silica microspheres (dispersible in fluorinert) in separate experiments.

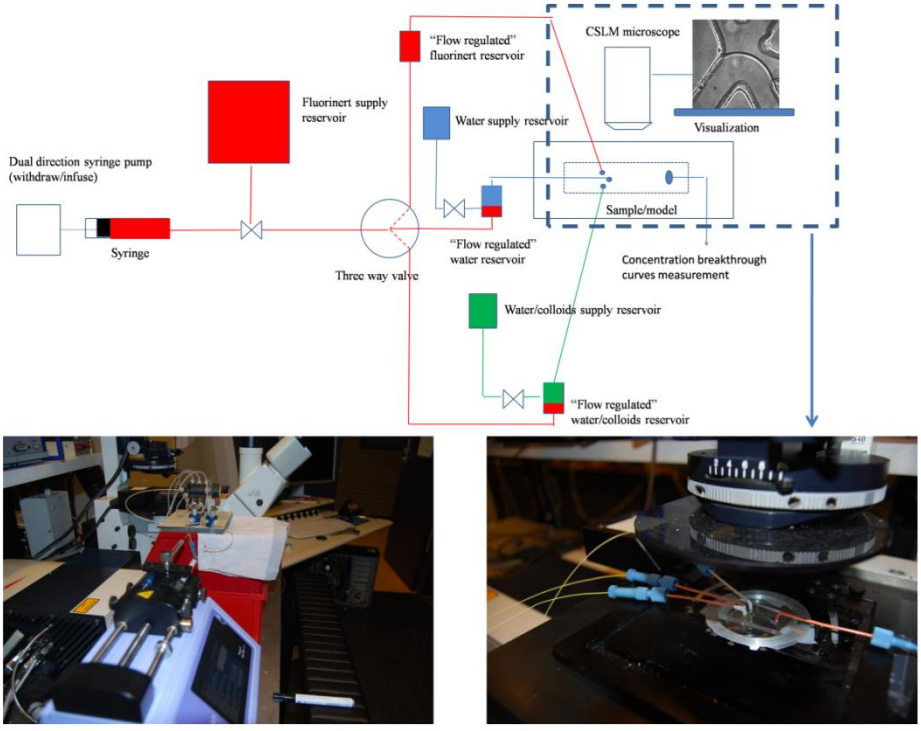

Fig. 8.1 *Schematic of the experimental set-up.*

Using this set-up (as shown in Fig. 8.1), we conducted series of experiments under steady-state and transient two phase flow conditions, to investigate the effect of flow rate, colloidal surface property, saturation and saturation change on colloids transport and remobilization. During the experiments, colloids distribution and their interactions with solid-water interfaces (SWIs), fluorinert-water interfaces (FWIs), and fluorinert-water-solid contact lines (FWSCs) within the flow network were directly observed by confocal microscopy. In addition to still images, real-time images (showing the movement of colloids) were also taken for subsequent review and analysis of colloids interactions with the moving interfaces and contact lines. Co-currently, series of concentration breakthrough curves were measured at the outlet channel with the same visualization system. This was done by measuring the fluorescent intensities of particles at a focus surface (in the horizontal middle plane) of the micro-model outlet channel at a speed of 834ms per frame. Colloids above and below this focus surface were out of confocal focus, but we assumed the colloids distribution was uniform over the depth. First a calibration curve was prepared by injecting a known concentration of water-colloid suspension into the outlet channel of the micro-model via the outlet reservoir. By measuring the fluorescent intensity of various known concentrations, the calibration curve was obtained. The confocal images were all taken at low intensities (<100 μW) to avoid bleaching of the fluorescent dye.

Effect of flow rate on colloid transport

The effect of flow rate (and flow rate change) was studied by conducting colloids transport experiments in single-phase flow (of either water or fluorinert), as well as performing pore-scale computational studies. We performed experiments and simulations at different flow rate. In some experiments, we increased or decreased the flow rate suddenly (by many folds).

Under saturated conditions, results of column experiments have shown that increasing flow rate decreases colloid straining at, e.g. grain junctions, under unfavorable conditions (Bradford et al., 2002, 2003, 2005; Shen et al., 2008; Du et al., 2013). In agreement with those findings, the measurement of micro-model effluent concentrations indicated more attachment at lower flow rates. But, we argued that the colloids are retained not because of straining but due to the presence of surface charge heterogeneity and surface roughness. In addition, through both visualization and measured breakthrough curves, we found that during the flushing colloids-deposited

micro-model, dramatic increase of the flow rate results in remobilization of colloids.

We developed a pore-network model exactly representing the micro-model pore structure. By performing many pore-network simulations to the measured breakthrough curves, we developed new relationships for the dependence of attachment and detachment coefficients on flow rate.

Effect of saturation on colloid transport

We conducted series of experiments under steady-state flow at three different water saturations: 100%, 60%, and 40%. The measured breakthrough curves showed that there was significantly more retention at lower water saturations. As observed in the images (shown in Fig. 8.2), the enhanced retention of colloids under unsaturated conditions was mainly due to the colloids attached to the fluid-fluid interfaces and fluid-fluid-solid contact lines.

Effect of saturation change on colloid remobilization

Following the steady-state flow, we either drained or imbibed the system. This resulted in sudden increase or decrease of water saturation (increase to a higher water saturation or decrease to the residual value). The imbibition process also caused a remobilization of colloids (Fig. 8.2). During the moving of fluid-fluid interface, the majority of colloids attached to fluid-fluid interfaces and fluid-fluid-solid contact lines. The remobilization of colloids resulted in a spike in the breakthrough concentration.

During imbibition, we also had local drainage. For example, we can see that water is pushed into large pore B (see Fig. 8.2a) displacing fluorinert. The interface corresponding to this local drainage is Interface 2. Some of the colloids attached to Interface 2 were re-deposited on the SWI in pore B, as highlighted in white circle in Fig. 8.2c and Fig. 8.2d.

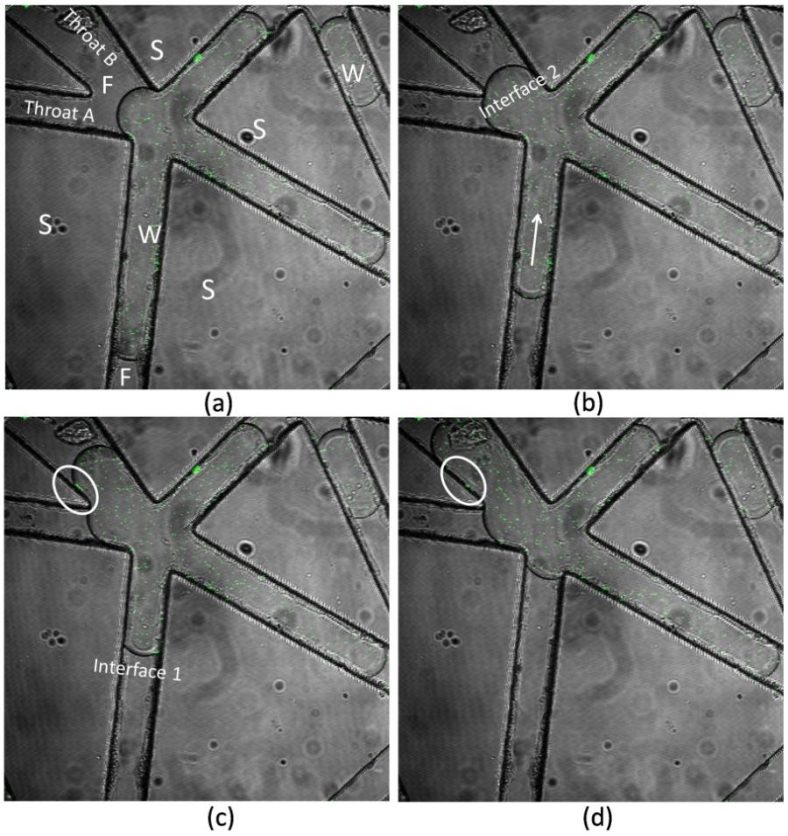

Fig. 8.2 *Images of colloids transport during imbibition of the micro-model.*

Effect of colloid surface property on colloids transport

The effect of surface property on colloid transport, retention, and remobilization during two-phase flow was studied in our hydrophobic Polydimethylsiloxane (PDMS) micro-models. Our results showed that hydrophobic colloids attached much less to the solid-fluid interface, fluid-fluid interface, and fluid-fluid-solid contact lines than hydrophilic colloids. According to our theoretical calculation of interaction energy potentials, this was mainly because of the presence of a strong energy barrier between hydrophobic colloids and solid-fluid and fluid-fluid interfaces.

Modeling of colloids transport and remobilization

Three different modeling approaches were employed to simulate virus remobilization caused during fast drainage or imbibition process. First, we used a

constant-detachment-coefficient model, where we simply increased the value of steady-state detachment coefficient by a constant factor for transient conditions. In a second approach, we modified the model of Cheng and Saiers (2009), who related the rate of remobilization of colloids to the time rate of change of saturation. We kept this assumption for the detachment from the solid-fluid interface. Moreover, we modeled attachment–detachment on the fluid-fluid interfaces separately, also as a kinetic process. We related the corresponding remobilization to the time rate of change of saturation as well. In the third approach, virus/colloid sorption on the fluid-fluid interface was modeled as an apparent linear equilibrium partitioning process; and the corresponding detachment rate was assumed to depend on the available fluid-fluid interfacial area. The three approaches were employed to simulate column experiments performed by Torkzaban et al. (2006a, b). The best agreement was obtained with the third approach.

Therefore, we use the third approach to simulate steady-state and transient breakthrough curves obtained in our own experiments conducted through the PDMS micro-model. The agreement between simulations and observations is very good. In particular, it is encouraging that the remobilization parts of the curves are closely followed by the simulations. One example is given in Fig. 8.3.

8.2 Recommendations for future work

Visualization experiments have provided clear evidence that colloids can be significantly retained at fluid-fluid interfaces and fluid-fluid-solid contact lines under unsaturated conditions. The moving contact lines can detach deposited colloids from the fluid-solid interfaces. In our experiments, we employed fluorinert and water as the two fluid phases, which were the wetting and non-wetting phases, respectively. In the nature, water is normally the wetting phase. Also, the pore shapes of the micro-model were rectangular in cross sections, whereas normally in soil very irregular shapers are encountered. Further understanding of colloids transport mechanisms in the subsurface will require more research by performing visualization experiments using water and air in sphere-packed porous media. This would be of value for understanding and designing methodologies for protecting soil and water resources.

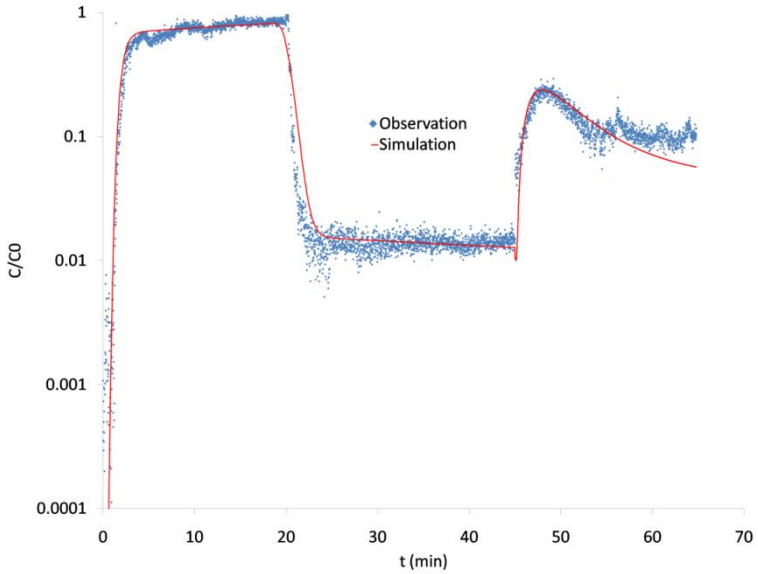

Fig. 8.3 *Measured (symbols) and simulated (line) breakthrough curve of colloid transport during steady-state and transient flow conditions.*

The colloids are usually in various shapes. More recently, Aramrak et al. (2013), Seymour et al. (2013), and Chatterjee and Flury (2013) have worked on how the colloidal shape affects the transport, retention, and remobilization of colloids. More research related to this issue is needed.

It would be of great challenge to investigate the above-mentioned issues at the field scale. But, it will be very helpful if field experiments can be performed, to study the relevance and ramification of our experimental observations at the large scale.

References

(1) **Aramrak** S., M. Flury, J.B., Harsh, R.L. Zollars, and H.P. Davis (2013), Does colloid shape affect detachment of colloids by a moving air-water interface? Langmuir, 29(19): 5770-80, doi: 10.1021/la400252q.

(2) **Bradford**, S.A., S.R. Yates, M. Bettahar, J. Simunek (2002), Physical factors affecting the transport and fate of colloids in saturated porous media. Water Resour. Res. 38(12), doi: 10.2029/2002WR001340.

(3) **Bradford**, S.A., J. Simunek, M. Bettahar, M.T. van Genuchten, S.R. Yates (2003), Modeling colloid attachment, straining, and exclusion in saturated porous media.

Environ. Sci. Technol., 37:2242-2250.

(4) **Bradford**, S.A., J. Simunek, M. Bettahar, Y.F. Tadassa, M.T. van Genuchten, S.R. Yates (2005), Straining of colloids at textural interfaces. Water Resour. Res. 41, doi: 10.2029/2004WR003675.

(5) **Chatterjee** N., and M. Flury (2013), Effect of Particle Shape on Capillary Forces Acting on Particles at the Air–Water Interface, Langmuir, 29 (25): 7903-7911, doi: 10.1021/la4017504.

(6) **Cheng** T., and J.E. Saiers (2009), Mobilization and transport of in situ colloids during drainage and imbibition of partially saturated porous media. Water Resour. Res. 45, W08414, doi: 10.1029/2008WR007494.

(7) **Torkzaban**, S., S.M. Hassanizadeh, J.F. Schijven, A.M. de Bruin, and A.M. de Roda Husman (2006a), Virus transport in saturated and unsaturated sand columns. Vadose Zone J. 5: 877-885.

(8) **Torkzaban**, S., S.M. Hassanizadeh, J.F. Schijven, and H.H.J.L. van den Berg (2006b), Role of air-water interfaces on retention of viruses under unsaturated conditions. Water Resour. Res., 42, W12S14, doi: 10.1029/2006WR004904.

(9) **Seymour** M.B., G. Chen, C. Su, and Y. Li (2013), Transport and Retention of Colloids in Porous Media: Does Shape Really Matter? Environ. Sci. Technol., 47(15):8391-8398, doi: 10.1021/es4016124.

(10) **Shen**, C., Huang, Y., Li, B., Jin, Y. (2008), Effects of solution chemistry on straining of colloids in porous media under unfavorable conditions. Water Resour. Res., 44, W05419, doi: 10.1029/2007WR006580.

(11) **Du**, Y., C. Shen, H. Zhang, and Y. Huang (2013), Effects of flow velocity and nonionic surfactant on colloid straining in saturated porous media under unfavorable conditions. Transp Porous Med, 98, doi: 10.1007/s11242-013-0140-3.

Samenvatting en aanbevelingen

Samenvatting

In dit onderzoek de transport van colloïde in twee fasen stroming is onderzocht. Met name, de effecten zijn onderzocht op het grensvlak tussen twee niet-mengbare vloeistoffen in een micro-poreuze netwerk, in statische en dynamische omstandigheden.

De experimentele opstelling bestaat uit een micro-poreuze netwerk, een vloeistof doserings systeem en een optische detectie systeem. Een Confocal Laser Microscope was gebruikt voor detectie. De micro-poreuze netwerken zijn gemaakt met gebruik van geëtst glas in een flexibele plastic materiaal (PDMS). De netwerken zijn bedekt met een dunne glas plaat (0.120mm) waarover een PDMS coating is geplaatst (0.020mm). Het netwerk bestaat uit 90 poriën van 30 µm, waarvan het oppervlak homogeen en hydrofoob is. Door gefocuste laser, konden beelden worden gemaakt van de 30 µm poriën. De volgende twee vloeistoffen waren gebruikt: Fluorinert-FC43 en water. Daarnaast hebben we Polystyrene (hydrophobic) en Silica micro-colloïden (hydrophilic) gebruikt. De vloeistoffen werden geinjecteerd met behulp van een accurate spuit pomp, die lage stroomsnelheden genereerde. The colloïden concentratie kon gemeten worden in de uitlaat van het systeem.

Meerdere experimenten werden uitgevoerd voor verschillende stroomsnelheden, verzadigingen, oppervlakte eigenschappen van de colloïdes en voor drainge en imbibition. Resultaten waren vertegenwoordigd in beelden die een tijdsserie vormde met een frequentie van twee beeld per seconde. Daarnaast waren de concetraties bij de uitlaat van het systeem gemeten en vormde zogenaamde breakthrough curves. De resultaten suggereerde dat de eigenschappen van het oppervlak van de colloïden van belang zijn. The hydrofobe colloïden plakken meer aan het grensvlak tussen twee vloeistoffen dan de hydrofiele colloïden. Dit komt overeen met de berekeningen, waarbij dit fenomeen is toegeschreven aan de grote energie barriere. Colloïden die aan de netwerk oppervlak vast zaten werden geremobiliseerd door de bewegende grensvlak en contactlijnen, tijdens de stroom experimenten.

Naast de experimenten, waren de breakthrough curves gemodelleerd op basis van drie aannames. (1) Een constante detachement; (2) een aanpassing op het model van

Cheng and Saiers (2009), waarin de attachement en detachement apart gemodelleerd worden als zijnde een kinetisch process; (3) een model equivalent aan model 2, waarin adsorptie als een evenwichts process wordt beschouwd. Door het fitten van de resultaten van kolom experiment van Torkzaban et al. (2006a,b) en de gemeten breakthrough curves, kan er geconcludeerd worden dat model 3 de beste resultaten geeft.

Aanbevelingen voor verder werk

Vizualisatie experimenten hebben aangetoond dat colloïden zich vooral bevinden op vloeistof-vloeistof grensvlakken en vloeistof-vloeistof-vaste stof contact lijnen. Door beweging worden deze colloïden geremobiliseerd. In onze experimenten hebben we alleen fluorinert en water gebruikt als wetting en non-wetting fase. Daarnaast hebben we alleen gekeken naar rechthoekige porie doorsnedes. Daarom zou vervolg onderzoek zich moeten richten op natuurlijkere vormen in poriën en op een water-lucht systeem. Het zou een geweldige uitdaging zijn om de eerder genoemde effecten te onderzoeken op veld schaal.